Journal of Medicinal Chemistry

pubs.acs.org/jmc Article

Lead Optimization of a Pyrrole-Based Dihydroorotate Dehydrogenase Inhibitor Series for the Treatment of Malaria

Sreekanth Kokkonda, Xiaoyi Deng, Karen L. White, Farah El Mazouni, John White, David M. Shackleford, Kasiram Katneni, Francis C. K. Chiu, Helena Barker, Jenna McLaren, Elly Crighton, Gong Chen, Inigo Angulo-Barturen, Maria Belen Jimenez-Diaz, Santiago Ferrer, Leticia Huertas-Valentin, Maria Santos Martinez-Martinez, Maria Jose Lafuente-Monasterio, Rajesh Chittimalla, Shatrughan P. Shahi, Sergio Wittlin, David Waterson, Jeremy N. Burrows, Dave Matthews, Diana Tomchick, Pradipsinh K. Rathod, Michael J. Palmer, Susan A. Charman, and Margaret A. Phillips*

Cite This: *J. Med. Chem.* 2020, 63, 4929–4956 Read Online

ACCESS | Metrics & More | Article Recommendations | Supporting Information

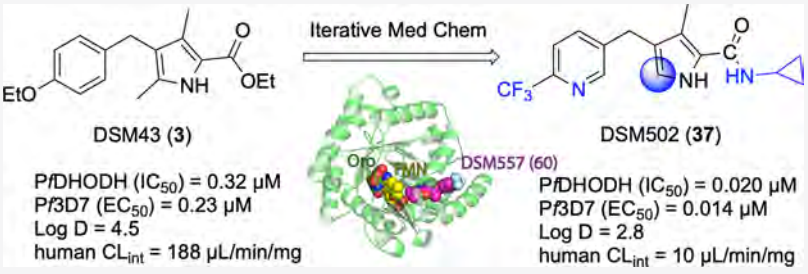

ABSTRACT: Malaria puts at risk nearly half the world's population and causes high mortality in sub-Saharan Africa, while drug resistance threatens current therapies. The pyrimidine biosynthetic enzyme dihydroorotate dehydrogenase (DHODH) is a validated target for malaria treatment based on our finding that triazolopyrimidine DSM265 (**1**) showed efficacy in clinical studies. Herein, we describe optimization of a pyrrole-based series identified using a target-based DHODH screen. Compounds with nanomolar potency versus *Plasmodium* DHODH and *Plasmodium* parasites were identified with good pharmacological properties. X-ray studies showed that the pyrroles bind an alternative enzyme conformation from **1** leading to improved species selectivity versus mammalian enzymes and equivalent activity on *Plasmodium falciparum* and *Plasmodium vivax* DHODH. The best lead DSM502 (**37**) showed *in vivo* efficacy at similar levels of blood exposure to **1**, although metabolic stability was reduced. Overall, the pyrrole-based DHODH inhibitors provide an attractive alternative scaffold for the development of new antimalarial compounds.

INTRODUCTION

Infectious diseases cause the majority of deaths in low-income countries, primarily the result of respiratory infections, diarrheal diseases, human immunodeficiency virus (HIV), malaria, and tuberculosis (TB).[1] Malaria alone is responsible for 0.4 million deaths per year, mostly among young children in sub-Saharan Africa.[2] Most deaths are caused by *Plasmodium falciparum* (*Pf*) malaria, however, nearly 90 countries are endemic with malaria, and *Plasmodium vivax* (*Pv*), while less lethal, has the greater global reach.[3−5] Although a vaccine for the prevention of malaria has recently been recommended for large-scale pilot implementation in Africa, its efficacy is suboptimal, resulting in <50% protection.[6,7] Therefore, both prevention and treatment programs continue to rely on chemotherapy. Although a number of effective compounds have been employed, drug resistance has led to decreased efficacy in most cases (e.g., chloroquine),[8] a challenge that is shared with other infectious diseases such as HIV and TB.[9] The current standard of care treatments for malaria, artemisinin combination therapies (ACTs),[10,11] is safe, effective, and credited with declining cases of malaria worldwide. However, parasites showing delayed clearance times to artemisinin derivatives have been identified in Southeast Asia, and combined with increasing resistance to partner compounds, these issues underlie treatment failures in patients in this region.[8,10,12]

Received: February 27, 2020
Published: April 6, 2020

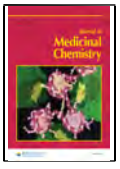

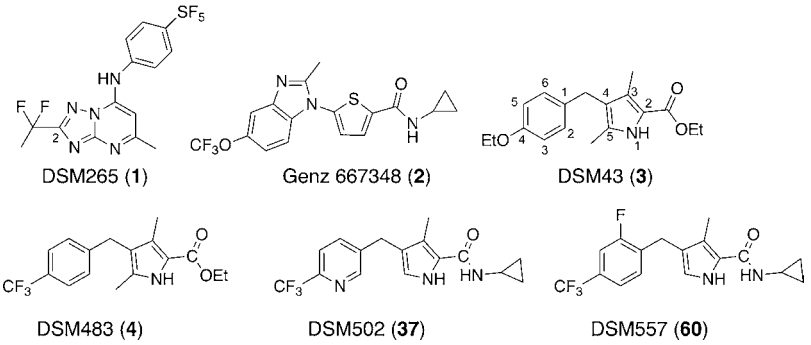

Figure 1. Structures of selected DHODH inhibitors.

Table 1[a]

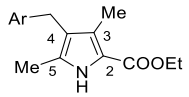

Cmpd	Cmpd ID	Ar	IC_{50} (μM)			EC_{50} (μM)
			*Pf*DHODH	*Pv*DHODH	*h*DHODH	*Pf*3D7 cells[a]
1	DSM265	NA	0.030 ±0.014 (12)	0.072±0.028 (11)	>100 (4)	0.0060 ± 0.0019 (9)
2	Genz-667348 *	NA	0.022	0.042	>30	0.007
3	DSM43		0.27 ±0.092 (3)	0.045 (0.04 – 0.050)	>100 (2)	0.23, 0.25
4	DSM483		0.10±0.033 (3)	0.014 (0.013-0.016)	>100	0.061, 0.071
5	DSM484		0.83 (0.74-0.92)	0.021 (0.018-0.025)	>100	0.53 (0.28-0.78)
6	DSM485		0.52 (0.46-0.60)	0.055 (0.036-0.084)	>100	0.59 (0.47-0.75)
7	DSM486		2.3 (2.0-2.7)	0.47±0.065 (3)	>100	10 (6.7 – 15)
8	DSM487		0.57 (0.46-0.71)	0.040 (0.03-0.054)	>100	0.47 (0.2-1.1)
9	DSM491		0.018 (0.016-0.020)	0.0094 (0.0077-0.011)	>100	0.0092 (0.0076-0.011)
10	DSM520		0.3 (0.25-0.37)	0.06 (0.05-0.072)	>100	0.10 (0.090-0.11)
11	DSM490**		>100	16 (11-21)	nd	nd

[a]*Pf, P. falciparum*; *Pv, P. vivax*; and *h*, human. For each experiment, triplicate data were collected at each inhibitor concentration. A threefold dilution series was used to determine IC_{50}'s, and either a threefold or fourfold dilution series was used to determine the EC_{50}'s. Values in parentheses represent the 95% confidence interval. For key active compounds, multiple independent experiments were performed and for these compounds, data represent mean ± standard deviation with the number of independent experiments in parentheses. If only 2 biological replicates were collected, then both values are shown. *Data taken from ref 28. **The compound has an *N*-methyl, as shown in Scheme 1.

Concerns that ACTs may fail on a global scale are driving drug discovery efforts to find new therapies for the treatment of malaria.[4,13] A number of new chemical entities have reached clinical development, including three that are currently in phase IIb human studies (the peroxide OZ439[14,15] combined with ferroquine, KAF156[16,17] combined with lumefantrine, and spiroindolone KAE609[18,19] as a single agent for severe malaria). Combination therapy is considered a key to reduce the potential for resistance to develop toward any new treatment, increasing the pressure on the malaria drug portfolio to identify a larger number of clinical candidates. Although most of the current clinical candidates were identified by asexual blood stage screens, target-based approaches have also been successful.[4] Notably, dihydroorotate dehydrogenase (DHODH) was validated as a new target by our group through the identification of a clinical development candidate, the triazolopyrimidine DSM265 (**1**) (Figure 1), targeting DHODH.[20−25] A second triazolopyrimidine (DSM421; 2-(1,1-difluoroethyl)-5-methyl-*N*-(6-(trifluoromethyl)pyridin-3-yl)-[1,2,4]triazolo[1,5-*a*]pyrimidin-7-amine) reached preclinical development but was not progressed because of unexpected off-target toxicity[26,27] and a thiophene analogue **2**[28] (Figure 1) developed by Genzyme reached late lead development but was not advanced beyond this stage.

DHODH is a mitochondrial enzyme that is localized to the inner mitochondrial membrane where it catalyzes a key step in the *de novo* synthesis of pyrimidines, the flavin-dependent conversion of dihydroorotate (DHO) to orotic acid.[29,30] Ubiquinone serves as the final oxidant in the reaction. Because *Plasmodium* parasites lack salvage enzymes, the *de novo* pathway is essential to the formation of pyrimidines for DNA and RNA synthesis. As a consequence, inhibitors of

https://dx.doi.org/10.1021/acs.jmedchem.0c00311
J. Med. Chem. 2020, 63, 4929−4956

Scheme 1[a]

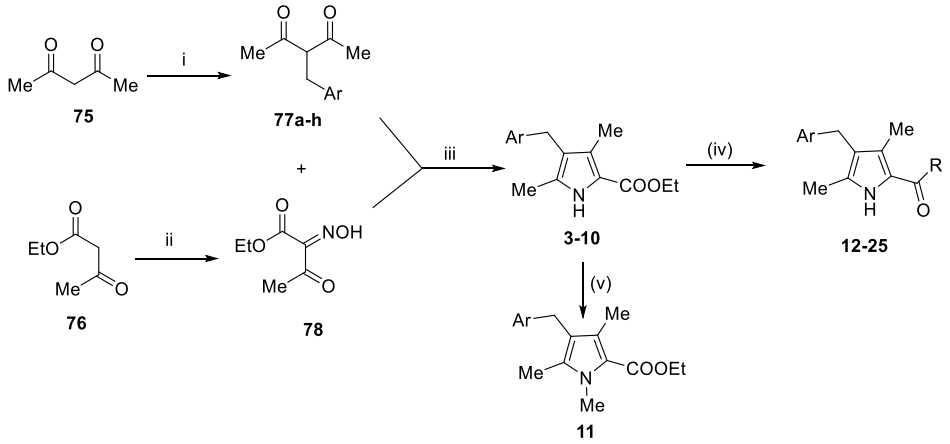

[a]Reagents and conditions: (i) $ArCH_2Br$, acetone, K_2CO_3, 60 °C, 12 h; (ii) $NaNO_2$, AcOH, 0 °C—RT, 3 h; (iii) Zn, AcOH, 80 °C, 6−8 h; (iv) (a) NaOH, EtOH, 80 °C, 2−4 h and (b) EDC, TEA, DMF, RT, 4−6 h; and (v) **4** → **11**, MeI, KOtBu, 18crown6, benzene, 6 h.

Scheme 2[a]

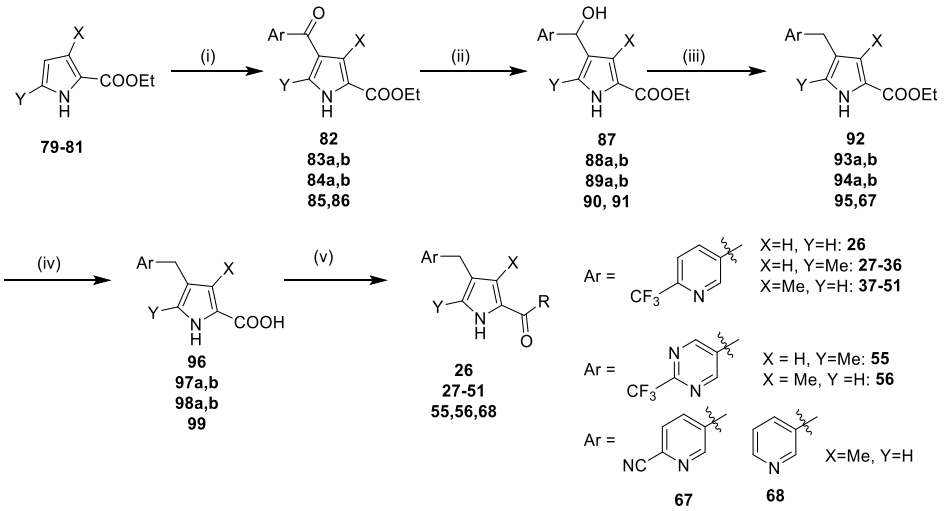

[a]Reagents and conditions: (i) $AlCl_3$, CH_2Cl_2, 0 °C—RT, 16 h; (ii) $NaBH_4$, EtOH, 1 h, RT; (iii) TFA, triethylsilane, CH_2Cl_2, 85 °C, 1 h; (iv) NaOH, H_2O, MeOH, 80 °C, 2 h; and (vi) cyclopropyl amine, HATU, TEA, CH_2Cl_2, RT, 4 h.

*Pf*DHODH (*Pf*DHODH) block parasite replication at the early trophozoite stage prior to the burst of replication required to form the schizont.[22] A key advantage of the target is that it is required for both blood and liver stage development, and thus, DHODH inhibitors meet the product profile for either malaria treatment or chemoprevention.[22,31] **1** has been clinically validated for the treatment of *Pf* infections during phase I and IIa studies to test safety and efficacy in volunteers and patients (phase I[24,25] and phase IIa[23]) and in human challenge studies to assess its potential for chemoprevention.[32,33] **1** showed considerable strengths in the clinic, including good safety and a long human half-life (∼100 h), providing a single dose (400 mg dose) cure of *Pf* malaria in human studies in patients in Peru.[23,25] Additionally, a single dose (400 mg) given 1 day before human volunteers were challenged with the infectious mosquito stage of *Pf* (sporozoites) prevented infection, a result that likely supports once weekly dosing for chemoprevention.[32,33] Two potential liabilities have been the identification of resistance mutations from both *in vitro* selections and in patients experiencing recrudescence[23,34] and the finding that in comparison to *Pf*, **1** showed reduced activity on *Pv* in both *ex vivo* studies and in a human phase IIa clinical trial.[23,26]

To position additional DHODH inhibitors from a chemical series distinct from **1**, we undertook lead optimization of a pyrrole-based series that we identified in our original target-based high throughput screen[35] but did not publish. Our identified hit (DSM43 (**3**); Figure 1) was subsequently published by Genzyme[36] but was not advanced into lead optimization. Herein, we describe a structure-guided lead optimization program around the pyrrole scaffold leading to the identification of potent *Pf*DHODH inhibitors with *in vitro* antimalarial activity and with good *in vivo* pharmacokinetic (PK) properties, supporting *in vivo* efficacy in the severe combined immunodeficiency disease (SCID) mouse model of *Pf* malaria.

RESULTS

Chemistry and Structure−Activity Relationships of the Pyrrole Series on DHODH and *Pf* 3D7. The initial hit compound **3** was used as a starting point for a hit-to-lead optimization program to identify *Pf*DHODH inhibitors that

https://dx.doi.org/10.1021/acs.jmedchem.0c00311
J. Med. Chem. 2020, 63, 4929−4956

Scheme 3[a]

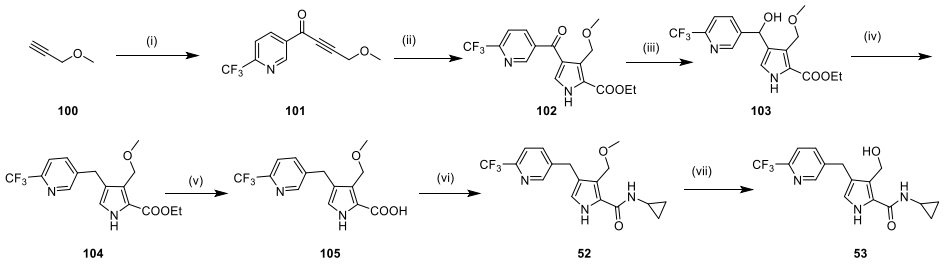

[a]Reagents and conditions: (i) *N*-methoxy-*N*-methyl-6-(trifluoromethyl)nicotinamide, *n*-BuLi, THF, −78 °C, 2 h; (ii) ethyl isocyanoacetate, Ag_2CO_3, NMP, 85 °C, 2 h; (iii) $NaBH_4$, EtOH, 0 °C—RT, 1 h; (iv) TFA, triethylsilane, CH_2Cl_2, 85 °C, 1 h; (v) NaOH, EtOH/H_2O, 80 °C, 2 h; (vi) cyclopropyl amine, HATU, Et_3N, CH_2Cl_2, 4−8 h; and (vii) BBr_3, CH_2Cl_2, 0 °C, 1 h.

Scheme 4[a]

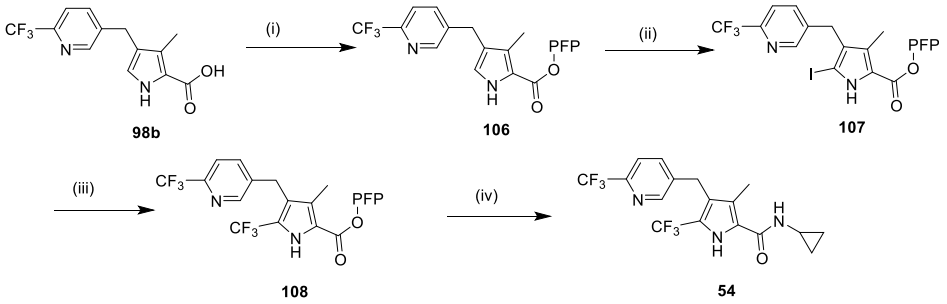

[a]Reagents and conditions: (i) pentafluorophenol (PFP−OH), DCC, THF, RT, 1 h; (ii) NIS, DMF, RT, 1 h; (iii) methyl 2,2-difluoro-2-(fluorosulfonyl)acetate, CuI, NMP, MW, 120 °C, 2 h; and (iv) THF, RT, 30 min.

Scheme 5[a]

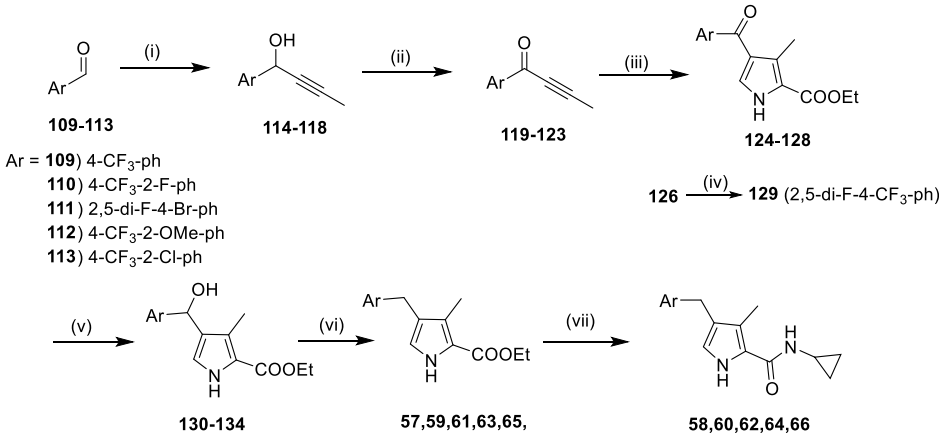

[a]Reagents and conditions: (i) 1-propynylmagnesium bromide, THF, 0 °C—RT, 2 h; (ii) Dess−Martin, CH_2Cl_2, RT, 2 h; (iii) ethyl isocyanoacetate, Ag_2CO_3, NMP, 80 °C, 2 h; (iv) methyl 2,2-difluoro-2-(fluorosulfonyl)acetate, KI, CuI, NMP, 120 °C, 16 h; (v) $NaBH_4$, EtOH, 0 °C—RT, 1 h; (vi) TFA, triethylsilane, CH_2Cl_2, 85 °C, 1 h; and (vii) (a) NaOH, EtOH/H_2O, 80 °C, 2 h and (b) amine, HATU, Et_3N, CH_2Cl_2, 4−8 h.

were differentiated from the current clinical candidate **1** (Figure 1). Notably, our goals were to identify compounds that improved on the known liabilities of **1**, including the development of compounds with equivalent activity on *Pf* and *Pv* parasites. We also sought to identify a series that maintained selectivity against human DHODH but also showed better selectivity versus the common toxicology species (e.g., rat, mouse, and dog). Although **1** is not a significant inhibitor of human DHODH, inhibition of the mouse and rat enzyme complicated its preclinical development.[22] Finally, we also had the objective of identifying compounds with improved solubility to simplify formulation development. The initial hit **3** was a sub-micromolar inhibitor of both *Pf*DHODH and *P. falciparum* 3D7 (*Pf*3D7) parasites in culture, it showed complete selectivity against human DHODH and was more potent on *Pv* DHODH (*Pv*DHODH) than *Pf*DHODH (Table 1). These data suggested that the pyrrole series might meet our objective of improved *Pv* activity.

We systematically explored the structure−activity relationship (SAR) of the series by modifying each of the moieties attached to the pyrrole ring, including the aryl group attached at the position 4, the two methyl groups attached at positions 3

https://dx.doi.org/10.1021/acs.jmedchem.0c00311
J. Med. Chem. 2020, 63, 4929−4956

Scheme 6[a]

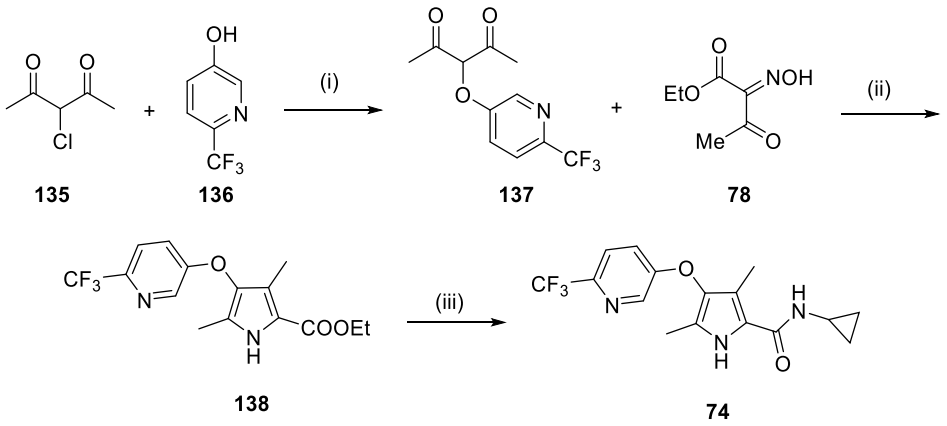

[a]Reagents and conditions: (i) Cs_2CO_3, acetone; (ii) Zn, AcOH, reflux, 6 h; and (iii) (a) NaOH, EtOH/H_2O, 80 °C and (b) amine, HATU, Et_3N, CH_2Cl_2, 4 h.

Table 2. Inhibitory Activity on Mammalian DHODHs[a]

cmpd	*h*DHODH	*m*DHODH	*r*DHODH	*d*DHODH
teriflunomide*	0.30 ± 0.052 (6)	0.11, 0.14	0.017 ± 0.0046 (3)	0.20, 0.27
1	>50 (10)	2.1 ± 0.62 (6)	4.4 ± 2.7 (8)	14 ± 6.7 (5)
4	>100 (1)	>100 (1)	>100 (1)	>100 (1)
6	>100 (1)	>100 (1)	>100 (1)	>100 (1)
9	>100 (1)	>100 (1)	>100 (1)	>100 (1)
37	>100 (2)	>100 (2)	>100 (2)	>100 (2)
45	>100 (3)	>100 (1)	>100 (1)	>100 (1)
60	>100 (3)	nd	nd	nd

[a]*h*, human; *m*, mouse; *r*, rat; and *d*, dog. The number of independent experiments is given in parentheses. nd, not determined. *Human DHODH inhibitor teriflunomide ((*Z*)-2-cyano-3-hydroxy-*N*-(4-(trifluoromethyl)phenyl)but-2-enamide) is an approved drug for the treatment of rheumatoid arthritis and multiple sclerosis; data similar to previous reports.[40]

and 5, and the ester group at position 2 (Table 1). The reported pyrrole derivatives **3**–**74** were synthesized, as shown in Schemes 1–6 and S1 and S2. We utilized various protocols for the preparation of the pyrrole motif with different substitutions. Knorr condensation of α-amino β-keto ester with aryl-substituted 2,4-pentanedione gave the aryl-substituted dimethyl pyrroles (Scheme 1). Mono methyl-substituted pyrroles were prepared by Friedel–Crafts acylation on the corresponding pyrrole, followed by step-wise reduction of the carbonyl group, resulting in pyrrole ester intermediates (Scheme 2). 3-Methoxymethyl- and 3-hydroxymethyl-substituted pyrroles were obtained *via* silver-catalyzed isocyanide-alkyne cycloaddition (Scheme 3).[37] The 5-CF_3-substituted pyrrole ester precursor **108** was prepared from the pentafluorophenyl ester **106**, and subsequent iodination and trifluoromethylation[38] afforded the precursor **108** leading to derivative **54** (Scheme 4). Friedel–Crafts arylation with some of the substituted aryl acid chlorides on the pyrrole proved difficult and gave poor yields. These phenyl substitutions were therefore prepared in a similar manner *via* the α,β alkynyl ketone, as described in Scheme 3, starting from aryl aldehydes (Scheme 5).[39] Similar reaction conditions were used to synthesize other pyrrole scaffolds, as shown in Scheme 6 and Supporting Information schemes, from the appropriate starting materials. Finally, hydrolysis of pyrrole esters obtained in the various protocols/methods followed by coupling with a variety of amines yielded pyrrole amides. Our initial analysis of the resultant compounds included determination of their inhibitory activity versus *Pf*DHODH and *Pv*DHODH, their selectivity versus human DHODH, and their potency against *Pf*3D7 parasites in whole cell assays (Tables 1 and 2, 4–7). Compounds that showed good potency and selectivity in these assays were then profiled further.

Optimization of the Aryl Group. To first further validate the series before beginning a full-scale hit-to-lead program, a handful of additional ester analogues (**4**–**11**) were synthesized that explored different benzyl groups at the 4 position of the pyrrole with varied para, ortho, and meta substituents (Scheme 1 and Tables 1 and 2). The data showed that para-substituted benzyl analogues yielded the most potent activity on both *Plasmodium* DHODHs and on *Pf*3D7. Substitution of the benzyl moiety with a *para*-CF_3 benzyl (**4**) led to a 4-fold increase in potency against *Pf*DHODH and *Pf*3D7, whereas replacement with *para*-CF_3-pyridin-3-yl (**9**) led to a 15–25-fold improvement in enzyme and parasite activity over **3** and also to better activity than *para*-OMe (**6**) or *para*-iPr (**8**) (Table 1). Meta-substituted benzyl rings were less active (**5**, **7**), as was the *para*-CF_3-pyridin-2-yl analogue (**10**). Methylation of the pyrrole nitrogen led to complete loss of activity (**11**). Both **4** and **9** retained good activity on *Pv*DHODH while showing complete selectivity versus the human enzyme. We next tested a panel of mammalian DHODH enzymes from common species used in toxicological studies (mouse, rat, and dog) and again found that both **4** and **9** retained complete selectivity, while neither compound inhibited any of these mammalian enzymes up to the top concentration tested (100 μM) (Table 2). This contrasts with **1**, which showed low to mid μM activity on the mouse, rat, and dog enzymes while not

https://dx.doi.org/10.1021/acs.jmedchem.0c00311
J. Med. Chem. 2020, 63, 4929–4956

Table 3. *Pf*DHODH Co-Inhibitor X-ray Diffraction Data Collection and Refinement Statistics

	Data Collection	
crystal	*Pf*DHODH$_{\Delta 384-413}$-**4**	*Pf*DHODH$_{\Delta 384-413}$-**60**
space group	$P2_12_12_1$	$P6_4$
wavelength (Å)	0.97924	0.97926
resolution (Å)	42.03−1.78 (1.81−1.78)	42.38−2.25 (2.29−2.25)
unique reflections	161,464 (8016)	26,640 (1344)
multiplicity	9.8 (9.0)	11.3 (10.2)
data completeness (%)	100.0 (100.0)	100.0 (100.0)
R_{merge} (%)[a]	8.3 (100)	5.1 (100)
R_{pim} (%)[b]	3.0 (65.6)	1.9 (71.9)
$I/\sigma(I)$	26.2 (1.1)	37.9 (1.0)
Wilson *B*-value (Å^2)	19.0	29.4
	Refinement	
resolution range (Å)	42.02−1.78 (1.82−1.78)	42.38−2.25 (2.33−2.25)
no. of reflections R_{work}/R_{free}	148,953/2002 (4308/57)	21,071/1482 (453/31)
data completeness (%)	92.2 (38.3)	79.2 (18.9)
no. of atoms/water	12,086/897	2958/72
R_{work}/R_{free} (%)	15.14/19.39 (23.85/30.16)	20.24/21.87 (23.72/39.70)
rmsd bond length (Å)	0.020	0.004
rmsd bond angle (deg)	1.497	0.609
mean B (protein/ligand, Å^2)	28.9/20.4	45.4/23.3
Ramachandran plot (%) (favored/additional)[c]	97.96/2.04	98.12/1.82

[a] $R_{merge} = 100\ \Sigma_h\Sigma_i|I_{h,i} - \langle I_h\rangle|/\Sigma_h\Sigma_i\langle I_{h,i}\rangle$, where the outer sum ($h$) is over the unique reflections and the inner sum (i) is over the set of independent observations of each unique reflection. [b] $R_{pim} = 100\Sigma_h\Sigma_i[1/(n_h - 1)]^{1/2}|I_{h,i} - \langle I_h\rangle|/\Sigma_h\Sigma_i\langle I_{h,i}\rangle$, where n_h is the number of observations of reflections **h**. [c] As defined by the validation suite MolProbity.[41]

significantly inhibiting *h*DHODH. Thus, these data confirmed that the pyrrole series could deliver both improved *Pv* DHODH activity and reduced mammalian DHODH inhibitory activity, meeting a key objective for a backup series for **1**. Having met these objectives, we committed to a full-scale hit-to-lead medicinal chemistry program on this series.

X-ray Structure of 4 Bound to *Pf*DHODH. To allow incorporation of a structure-based approach to optimize for good binding to *Pf*DHODH, we solved the X-ray structure of the enzyme bound to **4** (Figure 1) to a resolution of 1.78 Å with an R_{free} and R_{work} of 0.194 and 0.151, respectively (Figure 2 and Table 3). **4** bound adjacent to the flavin mononucleotide (FMN) cofactor in a binding pocket that overlaps the **1**-binding pocket in the region between R265 and H185 (Figure 2A) but which differs significantly in the position of the respective substituted phenyl rings (Figure 2B). The different binding modes arise from the differing conformation of F188, which is rotated 180° to the "up" position in the **4** structure compared to the "down" position observed when bound to **1**.[22] The **4** binding configuration is similar to that observed for the thiophene-based inhibitor **2**[28] (Figures 1 and 2C). The pyrrole nitrogen of **4** forms a hydrogen bond with H185 (replacing the interaction with the bridging NH in **1**), while the carbonyl forms an interaction with R265 (replacing the interaction with the pyridine nitrogen in **1**). The ethyl ester linkage of **4** is bound in a hydrophobic pocket near the FMN cofactor formed by V532, I272, I263, E182, and G181, overlapping the binding site of the C2−CF_2CH_3 of **1**. The benzyl-CF_3 of **4** forms interactions that are completely distinct from the aniline-SF_5 of **1**, as noted above. The **4** benzyl-binding pocket sits between the N-terminal α helices α1 and α2. These helices are composed of mostly hydrophobic amino acids that are thought to pack up against the mitochondrial membrane. The benzyl-CF_3 of **4** instead makes close contacts (<5 Å) with L187, L191, C175, F171, Y168, F188, and M536.

Replacement of Ethyl Ester with Amides. The ester linkage in compounds **3**−**11** is metabolically unstable and thus was replaced to advance the series toward *in vivo* activity. Based on the small size of the ethyl ester pocket (Figure 2), as well as by analogy to previously identified moieties that bound well to this site in either the triazolopyrimidine (e.g., **1**)[21] or in the thiophene series (e.g., **3**),[28] a library of small cyclic and linear chain amides (**12**−**25**) was synthesized to replace the ester, as described in Scheme 1 and Table 4. These modifications were made in the context of 4-CF_3-benzyl, 4-CF_3-3-pyridinyl, and 4-CF_3-2-pyridinyl groups at C4 of the pyrrole ring. The acid **12** was inactive but several amide replacements were well-tolerated. Within a series, *Pf*DHODH inhibitory activity was the best for the smaller substituents with ethyl amines **13** and **16** showing better activity than propyl amines **14** and **17** and with activity dropping off significantly for butyl amine **15**. Cyclopropyl amine **18** showed the best potency of the tested derivatives with cyclobutyl amine **19** a close second. Azetidines **20** and **24** were tolerated with a fivefold reduction in activity compared to the cyclopropyl amine **18**, but dimethyl **22** or diethyl **21** amines showed poor to no activity. Activity was the best for 4-CF_3-3-pyridinyl, with the order of preference 4-CF_3-3-pyridinyl **16**−**19** > 4-CF_3-2-pyridinyl **23**−**25** > 4-CF_3-benzyl **13**−**14**. Activity against *Pv*DHODH and against *Pf*3D7 parasites paralleled the activity observed for *Pf*DHODH, with the best compounds **16** and **18** showing sub-50 nM activity on all three (Table 4). Complete species selectivity was also maintained in the amide series for all tested compounds, with no observed inhibition of mammalian enzymes (Table 4).

Replacement and Modification of the Pyrrole Ring Methyl Substituents. The importance of the methyl substituents on the pyrrole ring was next assessed by either removal or by replacement with alcohols, methoxy ether, or CF_3 and these variations were made within the context of a wider range of amides compared to those in Table 4. Pyrrole derivatives (**26**−**55**) were synthesized by Friedel−Crafts acetylation of the corresponding pyrrole with aryl acid chloride in the presence of Lewis acid ($AlCl_3$) or *via* the alkynyl ketone (Schemes 2−4, Supporting Information Scheme S1 and Table 5). Removal of both pyrrole methyl groups **26** led to a 50-fold drop in potency against the *Plasmodium* enzymes and *Pf*3D7 when compared to the matched cyclopropyl compound **18** containing both methyls (Tables 4 and 5). Methyl at C5 was detrimental to activity, leading to a further fourfold drop in *Pf*DHODH activity relative to the compound lacking both methyls (**27** vs **26**). The best activity was observed for compounds containing methyl at C3 (**37**−**41**, **43**−**45**, **47**, **49**, and **51**) in the absence of the C5 methyl, with those linked to cyclopropyl **37** or cyclobutyl amine **51** showing the highest potency on *Plasmodium* DHODH and *Pf*3D7 (Table 5). Amides linked to carbon rings with >4 atoms showed poor to no activity (**28**, **29**, **32**, **33**, **34**, and **42**) regardless of the position of the pyrrole methyl. Branched chain alkyl groups including dimethyl **40**, *tert*-butyl **41**, −CH_2CF_3 **39**, and

https://dx.doi.org/10.1021/acs.jmedchem.0c00311
J. Med. Chem. 2020, 63, 4929−4956

Table 4. Replacement of the C2 Pyrrole Ester with Amides[a]

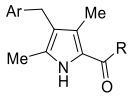

Cmpd	Cmpd ID	Ar	R	IC_{50} (μM)			EC_{50} (μM)
				*Pf*DHODH	*Pv*DHODH	*h*DHODH	*Pf*3D7 cells[a]
12	DSM489			>100	>100	nd	>10
13	DSM496			0.14 (0.12-0.17)	0.031 (0.023-0.041)	>100	0.051 (0.014-0.11)
14	DSM495			0.3 (0.27-0.34)	0.059 (0.05-0.069)	>100	0.11 (0.059-0.22)
15	DSM494			9.9±1.7 (3)	1.8, 0.54	>100	0.71 (0.57-0.90)
16	DSM497			0.054 (0.049-0.06)	0.036 (0.03-0.043)	>100	0.033 (0.018-0.059)
17	DSM498			0.072 (0.066-0.078)	0.038 (0.034-0.044)	>100	0.047 (0.014-0.16)
18	DSM499			0.050 ±0.013 (3)	0.022 (0.019-0.026)	>100	0.036±0.0046 (3)
19	DSM500			0.072, 0.042	0.036 (0.028-0.045)	>100	0.066 (0.057-0.077)
20	DSM508			0.14±0.035 (3)	nd	nd	0.13 ± 0.023 (3)
21	DSM509			13 (11 – 15)	nd	nd	>10
22	DSM517			>30	nd	nd	>10
23	DSM519			0.44 (0.38-0.49)	nd	nd	0.34 (0.31-0.38)
24	DSM521			1.8 (1.5-2.0)	0.6 (0.52-0.7)	>100	1.0 (0.99-1.1)
25	DSM522			0.41 (0.26-0.65)	0.22 (0.18-0.27)	>100	0.47, 0.68

[a]See Table 1 footnote. nd, not determined.

azetidine **38**, including rings with fluorine substitutions (**45** and **47**) all provided sub-100 nM activity, with **45** showing similar activity to the cyclobutyl analogue **51**. Fluorination of cyclobutyl amine led to reduced activity versus **51** with the difluoro analogue **48** showing less activity than the monofluoro **49** analogue. Substitution of the C3 methyl with an alcohol **53** or ether **52** led to a 200-fold and 20-fold reduction in potency, respectively, against *Pf*DHODH relative to **37**. Within the context of Me at C3, replacement of the C5 methyl with CF_3 **54** reduced activity 80-fold, as did analogues of **27** and **37** with pyrimidinyl-CF_3 (**55** and **56**) capping the pyrrole 4 position. A strong correlation between potency on *Pf*DHODH and *Pf*3D7 was observed for this set, and equivalent to better potency was maintained for these compounds on *Pv*DHODH. No inhibition of the human enzyme was observed for any of the tested compounds.

Modification of the 4-Position Benzylic Substitutions. To further explore the potential for the benzyl group to yield potent compounds, we synthesized additional analogues (**57**–**68**) in the context of either cyclopropyl amide or ethyl ester (Scheme 5 and Table 6). 4-CF_3-benzyl (**57** and **58**), or this ring with a single ortho fluoro (**59** and **60**), or ortho chloro (**65** and **66**) all showed similar activity to 4-CF_3-pyridinyl **37**, with the cyclopropyl amide showing better activity than the ethyl ester. There was a significant drop in activity upon adding a second ortho-fluoro to the ring (**61** and **62**), with this substitution leading to complete loss of activity for the ethyl ester. The addition of a single ortho O-methyl to the 4-CF_3 benzyl ring led to ∼10-fold drop in potency (**63** and **64**). Replacement of the 4-CF_3 with CN in the context of the pyridinyl ring **67** led to a potency drop of 30-fold, whereas removal of the 4-CF_3 led to complete loss in activity (**68**).

Comparison of the X-ray Structure of *Pf*DHODH Bound to Cyclopropyl Amide 60 Versus Ethyl Ester 4. Having identified several potent pyrrole analogues containing amide replacements for the original ester, we solved the X-ray structure of *Pf*DHODH bound to cyclopropyl amide derivative **60** (Figure 1 and Table 6). The structure of *Pf*DHODH bound to **60** was solved to be 2.3 Å in a space group of $P6_4$ with the cell dimension of $a = b = 84.8$, $c = 138.0$, and one molecule of *Pf*DHODH in the asymmetric unit binding modes (Table 3 and Figure 2D). The structures of *Pf*DHODH bound to **60** superimposed with the **4**-bound structure with an rmsd = 0.26 over 1199 atoms. The positions of **60** and **4** in the inhibitor binding site were similar, although **60** formed an additional H bond between the amide NH and H185, and as a consequence, **60** was shifted closer to H185 than **4** (Figure 2D). H bonds between the pyrrole NH and H185 and the carbonyl oxygen and R265 were observed for both **60** and **4**. Thus, interestingly for **60**, H185 is involved in a bifurcated H-bonding interaction. Differences in the binding mode between the ester and the amide may explain why benzyl modifications had differential impact depending on which was present (Table 6).

Replacement or Modification of the Bridging Methyl. Finally, the impact of replacing or modifying the bridging methyl was explored (Schemes 6 and S2; Table 7). Oxidation to a ketone (**69** and **71**) led to almost complete loss of activity, whereas replacement with oxygen (**74**) led to a ∼40-fold drop in potency against *Pf*DHODH. In contrast, modification of the bridging carbon with hydroxyl (**73**) caused only a 4-fold drop in potency, demonstrating that hydroxyl modification of this position is tolerated. Additionally, because **73** is racemic, it is likely that the active enantiomer will be 2-fold more potent than what is observed for the racemic mixture. Attempts to replace the bridging carbon with NH were made, but this compound was not synthetically feasible in our hands.

https://dx.doi.org/10.1021/acs.jmedchem.0c00311
J. Med. Chem. 2020, 63, 4929−4956

Table 5. Replacement or Modification of the Pyrrole Ring Methyl Groups[a]

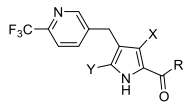

26-54

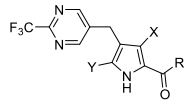

55,56

Cmpd	Cmpd ID	X	Y	R	IC$_{50}$ (μM)			EC$_{50}$ (μM)
					*Pf*DHODH	PvDHODH	*h*DHODH	*Pf*3D7 cells[a]
26	DSM501	H	H		2.5 (1.9-3.2)	1.2 (0.94-1.5)	>100	1.7, 0.50
27	DSM503	H	Me		10 ± 0.96 (3)	2.3 (1.5-3.6)	>100	3.6 (3.1-4.2)
28	DSM506	H	Me		>100 (2)	nd	nd	>10
29	DSM507	H	Me		>100	nd	nd	>20
30	DSM511	H	Me		2.8 (2.1-3.8)	nd	nd	1.9 (1.2-3.0)
31	DSM512	H	Me		5.7 (4.4-7.4)	nd	nd	3.5 (2.5 – 4.9)
32	DSM513	H	Me		>100	nd	nd	>10
33	DSM514	H	Me		>100	nd	nd	>10
34	DSM515	H	Me		>100	nd	nd	>10
35	DSM518	H	Me		>100	nd	nd	>20
36	DSM524	H	Me		>100	nd	nd	>20
37	DSM502	Me	H		0.020 ± 0.0054 (7)	0.014 ± 0.0046 (3)	>100 (3)	0.014 ± 0.0055 (6)
38	DSM525	Me	H		0.17 (0.15-0.2)	0.21 (0.17-0.26)	>100	0.082 (0.073-0.093)
39	DSM528	Me	H		0.21 (0.16-0.27)	0.051 (0.043-0.061)	>100	0.044, 0.059
40	DSM529	Me	H		0.080 (0.062-0.1)	0.018 (0.015-0.021)	>100	0.013 (0.011-0.016)
41	DSM530	Me	H		0.11 (0.084-0.15)	0.064 (0.051-0.082)	>100	0.051 (0.029-0.090)
42	DSM531	Me	H		9.8 (7.4-12.8)	nd	nd	4.8 (3.5 – 6.5)
43	DSM532	Me	H		0.098 (0.077-0.12)	0.041 (0.034-0.049)	>100	0.065 ± 0.029 (4)
44	DSM536	Me	H		0.018±0.0021 (3)	0.0075± 0.0031 (3)	>100 (3)	0.0099 ±0.0020 (3)
45	DSM538	Me	H		0.033±0.0079 (3)	0.018 ±0.0025 (3)	>100 (3)	0.029 ± 0.0079 (4)
46	DSM539	Me	H		>100	nd	nd	>100
47	DSM546	Me	H		0.12 (0.11-0.14)	0.2 (0.17-0.25)	>100	0.051 (0.036-0.072)
48	DSM552	Me	H		3.6 (4.0-5.4)	nd	nd	1.3 (0.86-2.0)
49	DSM553	Me	H		0.32 (0.40 – 0.90)	nd	nd	0.17 (0.16-0.19)
50	DSM559	Me	H		9.3 (6.3-12)	nd	nd	3.9 (3.3 – 6.9)
51	DSM560	Me	H		0.044 ±0.19 (3)	0.019 ± 0.0058 (3)	>100 (3)	0.027 (0.023-0.032)
52	DSM534		H		0.45 (0.34-0.6)	0.07 (0.05-0.096)	>100	0.24±0.046 (3)
53	DSM535		H		4.3 (2.5-7.4)	nd	nd	1.2±0.64 (3)
54	DSM526	Me	CF_3		1.6 (1.4-1.9)	nd	nd	0.77 (0.60 - 1.0)
55	DSM527	H	Me		>100 (2)	nd	nd	>10
56	DSM533	Me	H		0.88 (0.78-1.0)	0.21 (0.17-0.26)	>100	0.39±0.085 (3)

[a]See Table 1 footnote. nd, not determined.

SAR Summary. We identified a number of compounds (**37**, **45**, **51**, **60**, and **66**) with sub-30 nM potency on *Pf*DHODH and *Pf*3D7 parasites that were of interest for potential follow up. Overall, we observed a strong correlation between *Pf*DHODH and activity on *Pf*3D7 throughout the series and across the full dose response range of measured values (Figure 3). Good activity on *Pv*DHODH was also observed, with a tendency for greater potency on *Pv*DHODH than *Pf*DHODH. No inhibition of the mammalian enzymes was observed for compounds in the series.

In Vitro Absorption, Distribution, Metabolism, and Excretion. A subset of compounds was evaluated to assess their physicochemical properties and to determine their propensity to be metabolized using *in vitro* human and mouse liver microsome assays (Table 8). Compounds were typically selected based on having demonstrated good potency in the *Pf*DHODH and *Pf*3D7 assays; however, some compounds were chosen to explore the SAR around this subset of absorption, distribution, metabolism, and excretion (ADME) properties. The log $D_{7.4}$ for compounds containing an amide was generally in good physicochemical space (range 1.7−4.1). Kinetic solubility (phosphate-buffered saline pH 6.5) ranged from poor to quite good, with compounds that contained azetidine attached to the carbonyl bond, showing the best solubility (**20**, **38**, **45**, and **47**). The azetidine contains a tertiary nitrogen that is unable to act as a H-bond donor, in contrast to the amide secondary nitrogen observed in most of the other nonester compounds. Thus, the poorer solubility of

https://dx.doi.org/10.1021/acs.jmedchem.0c00311
J. Med. Chem. 2020, 63, 4929−4956

Table 6. Modification of the 4-Position Benzylic Substitutions[a]

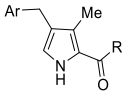

Cmpd	Cmpd ID	Ar	R	IC$_{50}$ (μM)			EC$_{50}$ (μM)
				*Pf*DHODH	*Pv*DHODH	*h*DHODH	*Pf*3D7 cells[a]
57	DSM561			0.13 (0.11-0.15)	0.019 (0.014-0.027)	>100	0.060 (0.05-0.07)
58	DSM562			0.048 ±0.019 (3)	0.0067 ±0.017 (3)	>100 (3)	0.018 ±0.0038 (3)
59	DSM556			0.035 (0.029-0.043)	0.024 (0.018-0.03)	>100	0.028 (0.024-0.031)
60	DSM557			0.044 ±0.19 (3)	0.015 ± 0.0080 (3)	>100 (3)	0.016 ±0.0056 (5)
61	DSM563			>30	nd	nd	>10
62	DSM564			1.2 (1.1-1.4)	nd	nd	0.42 (0.26-0.67)
63	DSM566			1.1 (0.66-1.8)	nd	nd	0.81 (0.4-1.6)
64	DSM567			0.11 (0.093-0.14)	0.092 (0.064-0.13)	>100	0.26 (0.18-0.39)
65	DSM570			0.042 (0.036-0.048)	0.059 (0.049-0.072)	>100	0.029 (0.025-0.033)
66	DSM571			0.017 ±0.0061 (3)	0.014 ±0.0050 (3)	>100 (3)	0.020 ± 0.00086 (5)
67	DSM584			0.63 (0.51-0.77)	nd	nd	0.20± 0.017 (3)
68	DSM585			>100	nd	nd	>10

[a]See Table 1 footnote. nd, not determined.

Table 7. Bridge Modifications[a]

Cmpd	CmpdID	Structure	IC$_{50}$ (μM)			EC$_{50}$ (μM)
			*Pf*DHODH	*Pv*DHODH	*h*DHODH	*Pf*3D7 cells[a]
69	DSM504	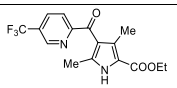	21 (17-25)	nd	nd	6.5 (6.0-7.0)
71	DSM505	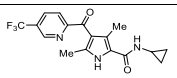	>100 (2)	nd	nd	>10, >20
73	DSM558	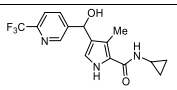	0.074 (0.059-0.092)	0.23 (0.18-0.29)	>100	0.044 (0.038-0.052)
74	DSM537	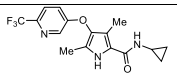	0.8 (0.68-0.94)	0.16 (0.10-0.25)	>100	0.29 (0.24-0.36)

[a]See Table 1 footnote.

the amides may potentially result from intramolecular H-bonding within the crystal lattice. Within the amide series, compounds containing a cyclopropyl amide (**27**, **37**, **55**, and **71**) were more soluble than those with other amide substituents, while replacement of the pyridinyl-CF_3 with a pyrimidinyl-CF_3 improved solubility (**55** vs **27**). Compounds with benzyl-CF_3 were predictably less-soluble (**58** vs **37**) and the addition of an *ortho*-chloro led to further reductions (**66**). Variation in the number of methyl groups on the pyrrole ring (0−2) had little impact on solubility, although those with a single methyl were improved over the others (**27** and **37** vs **18** and **26**).

Metabolic stability ranged from good to poor across the series, but for many compounds, species differences were also observed between human and mouse microsomes (Table 8). Cyclopropyl amides with either *para*-CF_3-pyridine or *para*-CF_3-pyrimidine (**18**, **27**, **37**, **55**, **56**, **71**, **73**, and **74**) showed the best stability with compounds containing pyrimidine performing the best (**55** and **56**). The difluoroazetidine **38** showed excellent stability in human liver microsomes but was much more rapidly metabolized in mouse microsomes, and this was likewise a problem for three potentially interesting compounds with good potency **51**, **60**, and **66**. This issue would likely make the development of these compounds difficult as it suggests that there will be poor plasma exposure in the mouse efficacy model. Replacement or modification of the bridging carbon did not significantly alter stability, for example, hydroxylation (**73** vs **37**), oxidation to a carbonyl (**71** vs **18**), or replacement with oxygen (**74** vs **18**). Not surprisingly, esters (**3** and **9**) showed poor solubility and were very rapidly metabolized.

The estimated extent of protein binding (using an albumin-based column and chromatographic method) ranged from ∼43% (**74**) to 98% (**66**) and the extent of binding strongly correlated with log *D* across the series.

https://dx.doi.org/10.1021/acs.jmedchem.0c00311
J. Med. Chem. 2020, 63, 4929−4956

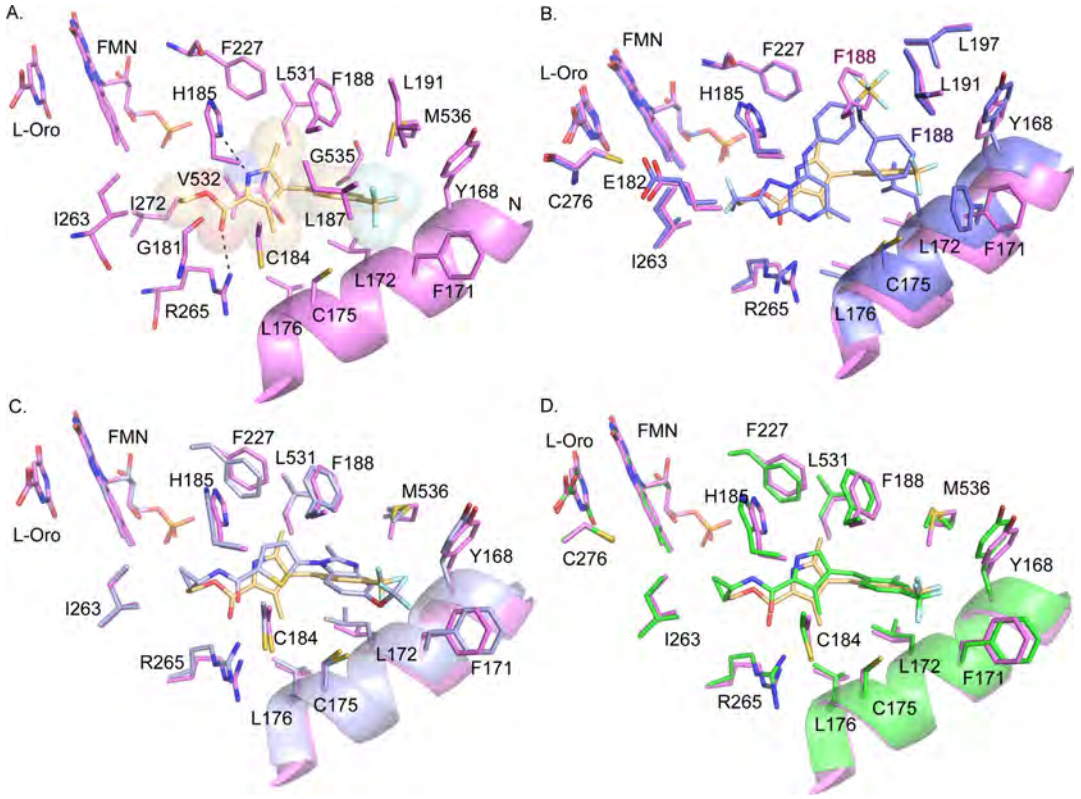

Figure 2. X-ray structures of *Pf*DHODH bound to **4** and **60**. (A) **4** bound to *Pf*DHODH showing amino acid residues within 4 Å of the inhibitor. Dashed lines indicate H-bond interactions. Protein is displayed in pink and **4** is displayed in tan as sticks within shaded spheres. (B) Comparison of the binding mode of **4** [colored as in (A)] with **1** (purple) (PDB 4RX0).[22] (C) Comparison of the binding mode of **4** [colored as in (A)] with **2** (light purple) (PDB 3O8A).[28] (D) Overlay of the binding modes of **4** [colored as in (A)] and **60** (green) showing residues within 4 Å of the inhibitors. The coordinates for the structure of *Pf*DHODH bound to **4** (PDB 6VTY) and **60** (PDB 6VTN) have been submitted to the Protein Data Bank.

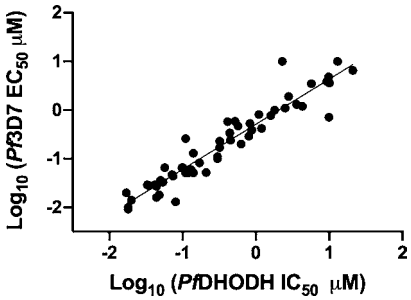

Figure 3. SAR correlation between inhibitory activity on *Pf*DHODH and *Pf*3D7 parasites. Data are taken from Tables 1, 3–6. Compounds where either the *Pf*DHODH IC_{50} or *Pf*3D7 EC_{50} was greater than the top concentration tested in the study (e.g., > 100 μM) were not included.

Identification of 37 as a Lead Compound. Taking into consideration both the potency data against *Pf*3D7 parasites and key parasite enzymes (*Pf*DHODH and *Pv*DHODH) and *in vitro* pharmacology, we selected **37** for additional biological, ADME, and PK profiling. It was the only compound with sufficiently strong properties across these criteria to suggest that it could meet development criteria.

Additional Parasitology Profiling of 37. As **37** showed good potency against both *Pf*3D7 and the *Plasmodium* enzymes (Table 5), we undertook additional parasitology studies to further define its profile. Good activity was also observed for *P. falciparum* Dd2 (*Pf*Dd2), which is an isolate that is resistant to multiple clinically used drugs (EC_{50} 0.016 vs 0.014 μM on Dd2 vs 3D7, respectively) (Tables 5 and 9), thus demonstrating that like other DHODH inhibitors (e.g., **1**), **37** is not cross-resistant with 8-aminoquinolines or dihydrofolate reductase inhibitors. To provide further demonstration that cell killing occurs through DHODH inhibition, we tested **37** against a *Pf* strain that has been transformed with yeast DHODH and is resistant to both *Pf*DHODH and cytochrome bc1 inhibitors.[42,43] Inclusion of proguanil (PG) in this study further allowed us to distinguish between bc1 and DHODH inhibitors, as resistance of the yeast DHODH strain to bc1 inhibitors is rescued in the presence of PG. As expected for a DHODH inhibitor and like **1**, the yeast DHODH strain was resistant to **37**, and this resistance was not rescued by PG, consistent with DHODH inhibition as the mechanism of parasite killing (Table 9).

To assess cross-resistance with **1**, we tested **37** against a panel of **1** resistant cell lines that we previously described[22,34] (Table 9). The cell line containing DHODH gene amplification (1D3) showed a similar fivefold resistance to both **1** and **37**, consistent with their common mechanism of action. Cell lines harboring DHODH point mutations caused a 15–40-fold shift in EC_{50} for **1**, but the effects on **37** were less (range 0.8–6-fold), with the L531F mutation actually leading to slightly improved binding of **37**. The additional data set collected for **1** in this study agreed closely with the previously published results[34] and data are included in Table 9 for comparison. The largest effect (6-fold) for **37** was caused by the C276F mutation, which is the mutation that was observed

https://dx.doi.org/10.1021/acs.jmedchem.0c00311
J. Med. Chem. 2020, 63, 4929–4956

Table 8. Physicochemical Properties and In Vitro Metabolism[d]

compd	log $D_{pH\ 7.4}$	kinetic solubility range in pH 6.5 PBS (μg/mL)	cPPB[a] (% bound)	CL_{int} (H/M)[b] (μL/min/mg protein)
1	3.6	12.5−25	97.4	≪7/8
3	4.5	<1.6	nd	188[c]/470[c]
9	3.7	1.6−3.1	93.6	286/779
16	2.8	12.5−25	77.1	70/54
17	3.2	6.3−12.5	84.5	172/64
18	3	12.5−25	82.8	15/33
20	2.9	>50	77.2	31/53
26	2.6	12.5−25	66.7	31/96
27	2.8	25−50	72.6	36/41
28	3.2	6.3−12.5	81.5	226/138
29	3.5	12.5−25	87.5	173/93
37	2.8	25−50	76.2	10/24
38	2.7	>100	65.9	≪7/192
39	3.3	12.5−25	81.9	15/57
45	3.3	25−50	74.9	21/94
47	Cnd	25−50	cnd	7/145
51	3.2	12.5−25	83.5	29/204
55	2.5	50−100	44.5	≪7/8
56	2.5	12.5−25	nd	≪7/nd
58	3.7	3.1−6.3	97.1	19/173
60	3.8	1.6−3.1	97	15/184
66	4.1	<1.6	98.1	14/264
68	2.6	12.5−25	73.2	19/138
71	2.4	25−50	50.4	8/24
73	3.2	6.3−12.5	89.5	20/40
74	1.7	12.5−25	42.7	8/22

[a]Binding estimated using a chromatographic method with an albumin-based column as described.[21] [b]Human (H) or mouse (M) liver microsomes. [c]Measurable loss of **3** in control incubations without a cofactor suggesting the contribution of non-NADPH-mediated metabolism to the overall degradation rate. [d]cnd, could not determine; nd, not determined.

clinically.[23] However, this mutation caused a significantly smaller shift for **37** than for **1**. Overall, the greatly reduced effects of the **1** selected mutations on efficacy of **37** are consistent with the different binding modes of the triazolopyrimidine and pyrrole series compounds (Figure 2).

Finally, **37** did not show any evidence of cytotoxicity when tested against both human HepG2 cells and mouse L1210 cells (CC_{50} > 50 μM) (Table 9). Preliminary safety pharmacology studies showed that **37** did not inhibit the hERG channel nor a set of additional ion channels that were tested (Table 9).

Advanced ADME Studies on 37. Additional studies were conducted to further profile the physicochemical and ADME properties of **37**. First, solubility studies were conducted in fasted state-simulated gastric fluid (FaSSGF), fasted state- and fed state-simulated intestinal fluid (FaSSIF and FeSSIF, respectively), and pH 7.4 phosphate-buffered saline (PBS). Across these media, solubility was moderate and largely unaffected by differences in pH in FaSSIF, FaSSGF, and PBS (Table 10). The somewhat improved solubility under fed-state intestinal conditions (FeSSIF) most likely occurs through solubilization in mixed micellar colloidal species present under these conditions.

Plasma protein binding and *in vitro* metabolism were also confirmed and extended to additional mammalian species. Protein binding (determined by ultracentrifugation) for **37** ranged from 90% in human plasma to 88% in mouse plasma (Table 10). Binding was also assessed in human liver microsomes, AlbuMAX medium, and Dulbecco's modified Eagle medium (DMEM) containing 10% fetal calf serum (Table 10) where binding was relatively low in each medium (30−50% bound). Metabolic stability was the greatest for human liver microsomes [intrinsic clearance (CL_{int}) of 10 μL/min/mg protein], while the CL_{int} was 1.4- and 2.4-fold higher for rats and mice, respectively (Table 10). Studies using cryopreserved hepatocytes from humans, rats, and mice suggested that there was no additional metabolism by enzymes other than those present in microsomes (e.g., CYPs and FMO).

In vitro metabolite identification studies were also conducted with **37**. Following incubation of **37** (m/z 324.13, Figure 4, panel A) with human liver microsomes, four oxygenated metabolites were detected by high-resolution MS (eluting at 3.08, 3.45, 3.69, and 3.77 min, Figure 4 panel B and C). Metabolites M + 16 (I) to M + 16 (III) had molecular ions at m/z 340.13 (panel B), and M + 16 (IV) was detected as an in-source fragment (panel C). The peak at 3.77 min (panel C) is an in-source fragment of M + 16 (III) (panel B). We hypothesized that the likely sites of oxygenation could include the cyclopropyl ring, the methyl carbon, the methylene carbon, and the pyrrole ring. Based on relative peak areas, metabolite M + 16 (I) appeared to be the predominant product (20% of the total area following a 2 h incubation with 1 mg/mL microsomal protein and 10 μM **37**), followed by M + 16 (III) (6% of the total area) with other metabolites representing minor products only (<3% of the total area).

Authentic metabolites corresponding to oxygenation of the methylene carbon (**74**, Table 7) and oxygenation of the methyl carbon (**53**, Table 5) were then synthesized. Metabolite M + 16 (II) was confirmed to be **74** by comparison of the retention times and collision-induced dissociation (CID) fragmentation patterns (Figure S1). Metabolite **53** was found to be highly susceptible to in-source fragmentation and instead of the expected molecular ion of m/z 340.13, its dehydrated fragment ion was observed at m/z 322.13 (Figure S2). The CID spectrum of M + 16 (IV) was too weak to be used for structure assignment. Instead, the structure of M + 16 (IV) was proposed based on the similarity of the retention time and MS/MS transition at 322.05 > 264.93 compared to the data for **53** (Figure S3).

The identity of the peaks corresponding to M + 16 (I) and M + 16 (III) was proposed based on comparison of their CID fragmentation patterns to that of **37** (Figure 5). For M + 16 (III), the molecular ion at m/z 340.14 was not detected and the peak at m/z 322.13 represents an in-source fragment resulting from loss of water. Below m/z 280, the fragmentation pattern for M + 16 (III) was identical to that of **37**, suggesting that oxygenation had occurred on the cyclopropyl ring. The fragmentation pattern of M + 16 (I) (Figure 5) suggested that it was likely the product of oxygenation on the pyrrole ring. The fragment at m/z 255 likely results from loss of the carboxamide side chain in the absence of dehydration. This is then followed by loss of HF to produce the fragment at m/z 235. Further loss of 28 to produce the fragment at m/z 227 suggests loss of CO from the 2-oxopyrrole, supporting the proposal for oxygenation at the 5 position. The presence of the fragments at m/z 161 and 256 suggests that fragmentation possibly occurred *via* radical cleavage pathways as a result of

https://dx.doi.org/10.1021/acs.jmedchem.0c00311
J. Med. Chem. 2020, 63, 4929−4956

Table 9. Activity of 37 on Drug-Resistant *Pf* and Mammalian Cell Lines[a]

Pf strain	resistance profile	selection agent	EC_{50} **37** (μM)	fold change	EC_{50} **1** (μM)	fold-change
Dd2 (parental)	CQ, Py, SD, MF, CG	na	0.016 ± 0.0070 (6)	NA	0.0048, 0.0046[#]	NA
D10 w/yeast DHODH	genetic insertion	na	>20 ± PG*	>100	>20 ± PG*	>100
1D3	3 copies DHODH	**1**	0.083 ± 0.028 (3)	5.2	0.023 ± 0.0036 (3)	4.8
R10C1B	G181C DHODH	**1**	0.024 ± 0.018 (3)	1.5	0.12, 0.15[#]	25
R1BC1A	L531F DHODH	**1**	0.013 ± 0.0069 (3)	0.81	0.080, 0.11[#]	17
R1AC1B	C276F DHODH	**1**	0.089 ± 0.071 (3)	5.6	0.17, 0.17[#]	35
R2B	R265G DHODH	**1**	0.078 ± 0.024 (3)	4.9	0.074, 0.15[#]	15
			Mammalian Cell Line (CC_{50} μM)			
human HepG2	na	na	>50	na	>50	na
mouse L1210	na	na	>50	na	>50	na
			Human Ion Channel Activity			
hERG	na	na	>33	na	1.6[##], 7.0[##]	na
$Na_V1.5$	na	na	>33	na	nd	na
$Ca_v1.2$	na	na	>33	na	nd	na
$K_V1.5$ K^+	na	na	>11	na	nd	na

[a]See Table 1 footnote for the description of error analysis. *The study was conducted ±3 and 10 μM proguanil (PG) to distinguish between DHODH and bc1 inhibition. CQ, chloroquine; Py, pyrimethamine; SD, sulphadoxine; MF, mefloquine; and CG, cycloguanil. DSM265-resistant clones were previously reported.[22,34,42] For DSM265, an additional set of EC_{50} data was collected in parallel to the **37** data and that value is reported first followed by [#]data taken from ref 34, which was the average of triplicate biological repeats. [##]DSM265 hERG data were taken from ref 22. Ion channel data; hERG was performed using IonWorks patch clamp electrophysiology under contract by AZ UK. Sodium and potassium channel assays were performed by Essen Bioscience using IonWorks patch clamp electrophysiology, and calcium channel (cardiac L-type) data were collected using a Flexstation fluorescence assay by Essen Bioscience. na, not applicable. nd, not determined.

Table 10. Physicochemical Properties and In Vitro Binding and Metabolism[d]

cmpd	**37**	**1**[a]
MW	323	415
log *D* 7.4	2.8[b]	4.0[c]
solubility (μg/mL)		
FaSSGF (pH 1.6)	46.4	6.8
FaSSIF (pH 6.5)	60.1	5.1
FeSSIF (pH 5.8)	115	27.6
PBS (pH 7.4)	45.6	2.0
H/R/M plasma protein binding (% bound)	90.0/88.2/88.9	99.9/97.0/99.7
AlbuMAX binding (% bound)	51.8	83.1
microsome binding (% bound)	29.9	71.7
DMEM/10% FCS binding (% bound)	31.5	78.5
H/R/M CL_{int} (μL/min/mg)	10/14/24	<7/<7/<7

[a]Data from ref 22. [b]Chromatographic. [c]Shake flask. [d]Human (H), rat (R), and mouse (M).

the modified pyrrole. Further structural confirmation of both metabolites M + 16 (I) and (III) would require the synthesis of authentic standards. It is worth noting that each of the metabolites M + 16 (I), (II), and (III) was resistant to reduction by sodium metabisulphite, suggesting the absence of N-oxidation products.

Cytochrome P450 inhibition studies were conducted using a substrate-specific interaction approach and suggested that **37** does not directly inhibit the major CYP isoforms 1A2, 2C9, 2C19, 2D6, or 3A4/5 with IC_{50} values all exceeding 20 μM. Additional time-dependent inhibition studies with **37** were conducted using an "IC_{50} shift" protocol as described previously.[44] There was no evidence of time-dependent inhibition of any isoform except for CYP3A4/5 where the IC_{50} shifted from >20 μM when a 30 min pre-incubation was conducted in the absence of NADPH to ∼5.5 μM when the pre-incubation step included NADPH suggestive of time-dependent inhibition of this isoform.

PK Properties of 37 and Analogues in Mice and Rats. Compound **37** was dosed to mice and rats to assess its *in vivo* PK properties (Tables 11 and 12 and Figures 6 and 7). After intravenous (IV) administration to mice, clearance and volume of distribution were both moderate. Clearance of **37** was approximately threefold higher than that seen for **1** in mice.[22] Following oral (PO) administration to mice, plasma exposure was similar to that observed previously for **1**[22] but bioavailability was greater than 100%, suggesting dose-dependent kinetics. C_{max} and AUC increased to a greater extent than the increase in dose from 20 to 50 mg/kg (4−5-fold increase vs a 2.5-fold increase in dose) (Table 11). The observed exposure of **37** in mice after oral dosing was significantly better than that for **18** and **45** (Figure 6) consistent with the higher CL_{int} observed *in vitro* for these latter compounds (Table 8).

After IV dosing of **37** to rats, plasma clearance was moderate (∼50% of hepatic blood flow in rats) and volume of distribution was high (∼4.7 L/kg) (Figure 7 and Table 12). Compared to **1**, clearance of **37** was nearly fivefold higher in rats. At an oral dose of 3 mg/kg, bioavailability was approximately 90%. Increasing the oral dose to 30 mg/kg resulted in a bioavailability of >100%, suggesting saturation of clearance processes. There was minimal excretion of **37** in urine after either IV or PO administration of **37**, suggesting that metabolism was likely the major route of clearance. At the higher oral dose, the time to reach the maximum plasma concentration was prolonged, possibly suggesting slow dissolution and absorption within the gastrointestinal tract.

SCID Mouse Efficacy Studies. Compound **37** was tested for *in vivo* efficacy in the SCID mouse *Pf* model in two separate studies, the first of which was accompanied by PK analysis of drug concentrations in blood (Figure 8). Oral doses were administered once daily for 4 days starting on day 3 after mice had been inoculated with parasites. Parasitemia was monitored

https://dx.doi.org/10.1021/acs.jmedchem.0c00311
J. Med. Chem. 2020, 63, 4929−4956

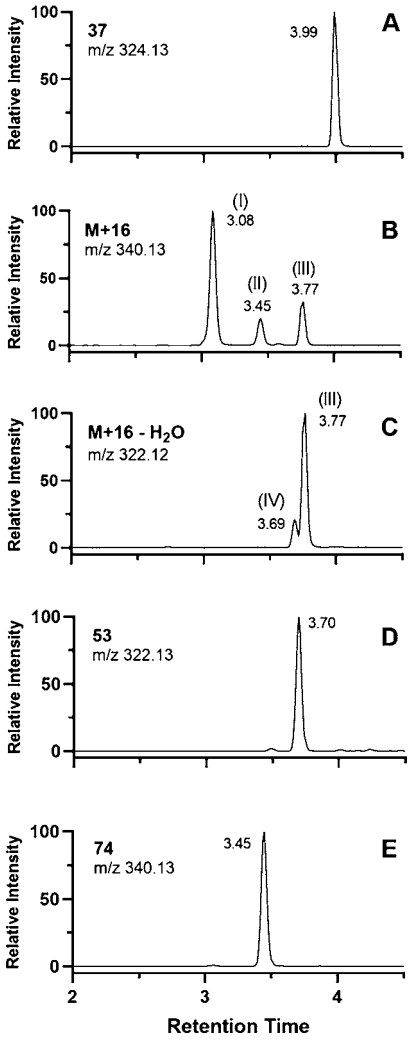

Figure 4. Extracted ion chromatograms obtained by high-resolution MS. (A) Authentic standard for **37**; (B) and (C) M + 16 metabolites and an in-source fragment of an M + 16 metabolite, respectively, formed by incubation of **37** with human liver microsomes in the presence of NADPH. (D,E) Authentic standards for **53** and **74**, respectively.

daily and final parameters were determined 24 h after the last dose. In the first study (conducted by GSK), mice were dosed at both 10 and 50 mg/kg. The 10 mg/kg mouse died on day 5, so a full set of parasitemia data could not be collected. The death was assessed as unlikely to be drug-related, and the compound was well-tolerated at the higher 50 mg/kg dose in both studies. In the GSK study, the ED_{90} (dose that provides 90% reduction in parasitemia 24 h after the last dose) was ~50 mg/kg corresponding to an $AUC_{ED_{90}}$ of 9 μg h/mL (28 μM h), which compares favorably to the $AUC_{ED_{90}}$ observed previously for **1** in a similar study (Tables 13 and 14). The dose required for the ED_{90} was significantly higher for **37** than for **1** (Table 14). Interestingly, the exposure levels for **37** in the SCID mouse were lower than those observed in the normal mice (Figures 6 and 8) where the SCID mouse C_{max} was 4−6-fold lower (10 and 50 mg/kg) and AUC was 7-fold lower (50 mg/kg) (Tables 11 and 13). The basis for these differences in exposure is not yet known. In the second confirmatory SCID study (conducted at Swiss TPH), only a single dose of 50 mg/kg was administered and PK data were not collected. In this study, higher parasitemia levels were observed for the vehicle control, but **37** showed similar to slightly improved efficacy compared to the first study (50 mg/kg dose resulted in 97% parasite clearance compared to 85% clearance in the GSK study) (Figure 8).

DISCUSSION

Malaria remains a serious public health issue to 50% of the world's population, and drug resistance threatens to derail existing therapies. Our group has previously validated DHODH as a drug target for the treatment of malaria through the identification of **1**, which reached clinical development.[23] Herein, we sought to identify a potential backup candidate from a distinct chemical scaffold. The pyrrole scaffold was identified as a hit in our original HTS program to discover *Pf*DHODH inhibitors. We progressed the series to the point of identifying a lead candidate **37** that showed potent and selective *Plasmodium* DHODH inhibition, equivalent activity on *Pf* parasites *in vitro*, and efficacy in the SCID mouse *Pf* mouse model. The pyrrole lead **37** was ~fourfold less potent than **1** in parasite assays but showed efficacy at similar blood exposure as **1** in the SCID mouse model, likely due to the significantly higher unbound concentrations compared to **1**. Compound **37** showed improved species selectivity over **1**; it was not an inhibitor of any of the tested mammalian enzymes and showed equivalent activity on both *Pf* and *Pv* DHODH. Additionally, while some cross-resistance was observed for **37** versus some of the **1**-selected resistant *Pf* cell lines, the magnitude of the EC_{50} shifts was significantly lower and not all **1**-selected point mutations led to **37** resistance. Thus, **37** achieved three of our key milestones for a **1** backup: improved species selectivity, equivalent *Pf* and *Pv* activity, and a different resistance profile.

X-ray structure analysis of *Pf*DHODH bound to both an ester (**4**) and amide (**60**) analogue in the series demonstrated that the pyrroles bind to the enzyme in an overlapping but distinct binding mode when compared to the triazolopyrimidines (e.g., **1**). The pyrrole ring bound between the conserved R265 and H185 making H-bond interactions similar to the triazolopyrimidine ring of **1**. The cyclopropyl amide of **60** also bound in a similar position to CF_2CH_3 in **1**, but the polar amide NH donates a second H bond to the side chain N of H185. In contrast, the benzyl group binds in an alternative pocket compared to the aniline of **1** because of a 180° rotation of F188. This different binding mode also likely explains the equivalent activity on *Pf* and *Pv*DHODH and the differing resistance profiles for the pyrrole series compared to the triazolopyrimidines. None of the tested pyrrole analogues bound to the mammalian enzymes, leading to better overall species selectivity compared to **1**. In contrast, prior crystallographic studies demonstrated that rodent and human DHODHs have a binding pocket that can accommodate compounds from the triazolopyrimidine series with binding affinity dictated by aniline hydrophobicity and facilitated by the addition of meta-fluorines on the aniline ring.[40]

Comparison of the cross-resistance of **37** on multiple **1**-selected *Pf*Dd2 mutant clones demonstrated that the differing binding modes did lead to a different resistance profile. As expected, the strain that harbors a DHODH gene amplification showed ~fivefold higher EC_{50} for both compounds; however, two of the **1**-selected resistance mutants G181C and L531F showed wild-type to slightly improved activity for L531F toward **37**. Parasites harboring C276F or R256G mutations

https://dx.doi.org/10.1021/acs.jmedchem.0c00311
J. Med. Chem. 2020, 63, 4929−4956

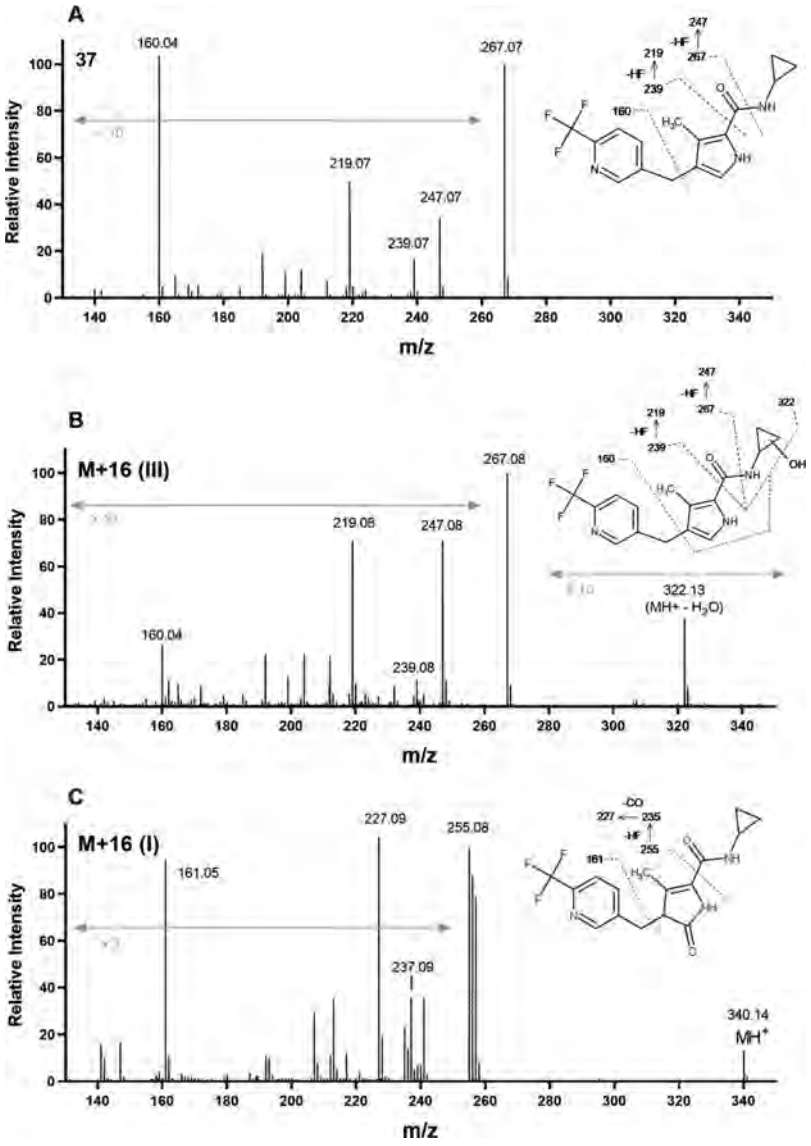

Figure 5. High-resolution MS spectra and proposed fragmentation sites for **37** (A), and the oxygenation metabolites M + 16 (III) (B) and M + 16 (I) (C) formed upon incubation of **37** with human liver microsomes in the presence of NADPH. The molecular ion (m/z 324.13) for **37** was only observed under low energy conditions. For M + 16 (III), the molecular ion (m/z 340.14) was observed as an in-source fragment resulting from loss of water.

Table 11. PK Properties of 37 in Mice after Single IV and PO Doses

cmpd	**37**	**37**	**37**	**37**	**1**
dose and route	2.8 mg/kg IV	10.5 mg/kg PO	18.3 mg/kg PO	50 mg/kg PO	10 mg/kg PO[a]
apparent $t_{1/2}$ (h)	2.8	cnd	2.6	3.6	2.4
IV CL_{plasma} (mL/min/kg)	26.1	na	na	na	na
IV V_{ss} (L/kg)	1.2	na	na	na	na
B/P ratio	0.8	0.8	0.8	0.8	0.7
T_{max} (h)	na	2	0.5	1	1−2
C_{max} (μM)	na	4.6 (3.7)	8.4 (6.7)	42.3 (33.8)	3.94
$AUC_{0-\infty h}$ (μM h)	5.6	cnd	55.6 (44.5)	220 (176)	29.7
bioavailability (%)	na	cnd	>100	>100	61

[a]Data taken from ref 22. Values in parentheses are blood values obtained by multiplying the plasma data by the blood to plasma ratio. cnd, could not determine.

showed some cross-resistance but had a less-pronounced EC_{50} shift when compared to **1** (5-fold for **37** vs 15−25-fold for **1**). These two mutations are of note as C276F was observed in a single patient receiving the 400 mg dose in the phase IIb clinical study[23] and both the C276F and R265G mutations have been observed after *in vivo* selections in SCID mice.[45] The ability of DHODH point mutations to show differential affinity toward inhibitors from different scaffolds has been

https://dx.doi.org/10.1021/acs.jmedchem.0c00311
J. Med. Chem. 2020, 63, 4929−4956

Table 12. Rat Plasma PK Parameters after a Single PO Dose

cmpd	37[a]	1[b]
IV dose (mg/kg)	**3.4**	**2.6**
apparent $t_{1/2}$ (h)	14.6	12.6
CL_{plasma} (mL/min/kg)	28.6	6.5
V_{ss} (L/kg)	4.7	5.9
PO dose (mg/kg)	**3.0**	**2.1**
PO T_{max} (h)	1	3.3
apparent $t_{1/2}$ (h)	3.9	11.6
C_{max} (μM)	1.7	0.75
AUC_{∞} (μM h)	5.1	15.6
bioavailability (%)	91	66
PO dose (mg/kg)	**33**	**18.8**
T_{max} (h)	4	7
apparent $t_{1/2}$ (h)	2.8	15.5
C_{max} (μM)	27	3.95
AUC_{∞} (μM h)	204	122
bioavailability (%)	>100	57

[a]Mean of two animals per dose group. [b]Data taken from ref 22.

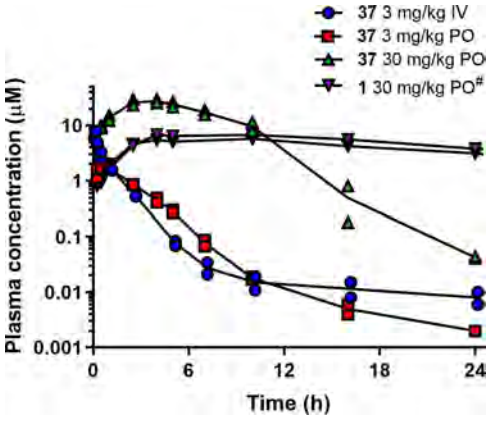

Figure 7. Plasma concentration vs time profiles for **37** in rats (n = 2 animals per dose group). #Data for **1** are based on results obtained at a PO dose of 20 mg/kg[22] which were then scaled to 30 mg/kg for comparison purposes and with the assumption of linear kinetics over this dose range.

previously noted and our data further support the hypothesis that DHODH inhibitors from different structural classes might be able to protect each other from the generation of resistance if dosed together.[46]

During the medicinal chemistry effort to identify **37**, we explored variation in the substituents at all positions of the pyrrole scaffold. The ester linkage of the original HTS hit **3** could be readily replaced with an ethyl amide that yielded good activity and this substitution was also a key to improving metabolic stability. Exploration around the amide showed that small linear or small cyclic alkanes provided the best activity with a cyclopropyl amine as in **37**, showing the best activity. The order of preference for linear alkanes was ethyl > propyl > butyl amide and that for the cyclic alkanes was cyclopropyl > cyclobutyl > azetidine, although di-fluoro-azetidine retained good activity. Larger rings (n = 5 or greater) were inactive. Dimethyl and diethyl amide had poor to no activity. We determined that only a single methyl on the pyrrole at the 3-position contributed to binding, whereas the methyl at the 5-position was detrimental to good binding affinity. The benzyl groups substituted with 4-CF_3 and 3-pyridinyl-4-CF_3 yielded both the best potency and most favorable ADME properties (e.g., solubility and metabolic stability). The addition of fluoro or chloro at the 2-position of the benzyl ring when combined with 4-CF_3 also yielded good activity. The bridging carbon could be hydroxylated with only a 2-fold reduction in activity or replaced with oxygen with a 10-fold reduction.

In vitro ADME data suggested that **37** is marginally more soluble than **1** and it has lower plasma protein binding but a higher intrinsic clearance in liver microsomes from various species. *In vitro* metabolite identification studies suggested the formation of multiple oxygenation products, whereas there was no evidence for direct inhibition of CYP enzymes by **37**. IC_{50} shift experiments highlighted the potential for time-dependent CYP inhibition, possibly as a result of reactive metabolite formation. Although further mechanistic and kinetic studies could shed light on these questions, the observed time-dependent CYP inhibition represents a potential risk for the advancement of **37** and a point of inferiority when compared to triazolopyrimidines including **1**. *In vivo* PK studies in mice and rats indicated that similar to the *in vitro* results, **37** has a higher clearance compared to **1** (3−5-fold). The volume of distribution was found to be similar or marginally higher for **1** than for **37**; however, in general, the data suggested that **37** was unlikely to have a sufficiently long half-life in humans to support a single-dose regimen.

Interestingly, the efficacy studies conducted in SCID mice indicated that the exposure of **37** after oral dosing was considerably lower (by ∼5−7-fold) than that seen in normal mice (similar formulations and dose levels were used for normal and SCID mice) (Tables 11 and 13). This result may possibly reflect increased hepatic metabolic activity in the SCID mice versus normal mice resulting in higher clearance; however, data are currently not available to confirm this

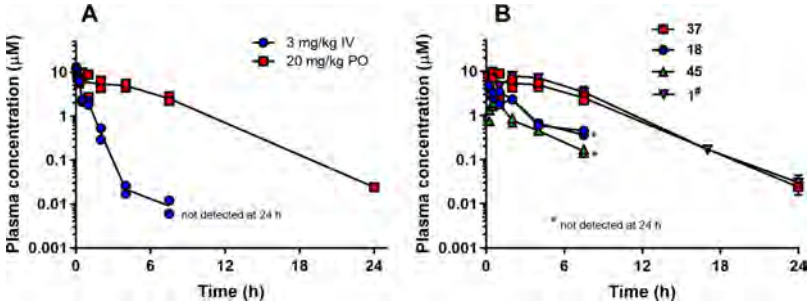

Figure 6. Plasma concentration vs time profiles in mice (n = 2 animals per time point). (A) Data for **37** after IV and PO dosing. (B) Comparative profiles after PO dosing at 20 mg/kg for compounds as indicated in the graph legend. #Data for **1** are based on results obtained at an oral dose of 10 mg/kg[22] which were then scaled to 20 mg/kg for comparison purposes with the assumption of linear kinetics.

https://dx.doi.org/10.1021/acs.jmedchem.0c00311
J. Med. Chem. 2020, 63, 4929−4956

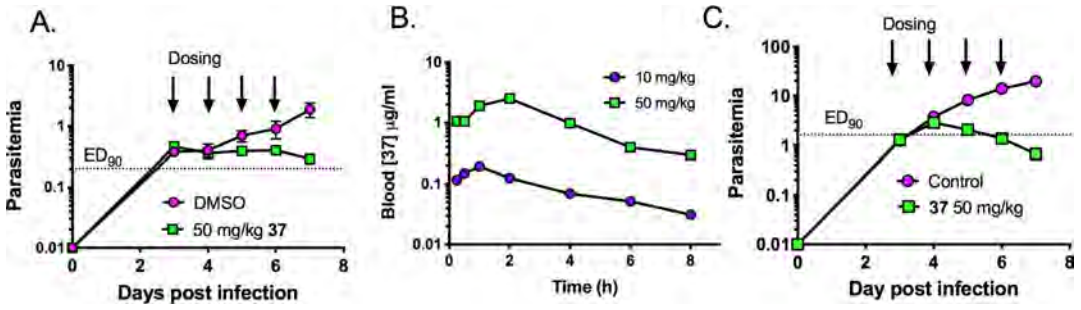

Figure 8. SCID mouse efficacy data. Two separate studies were conducted either at GSK (A,B) or at Swiss TPH (C). (A,C) Parasitemia vs days post infection for the DMSO control (pink circles) and the **37**-treated mice (green squares). (B) Blood levels of **37** for the mice treated in (A). PK data were not collected in the Swiss TPH study (C).

Table 13. Blood Exposure Parameters for 37 Following Oral Dosing to *Pf*-Infected SCID Mice

dose mg/kg	blood C_{max} μg/mL (μM)	blood AUC_{23h} μg h/mL (μM h)
10	0.194 (0.6)	0.680 (2.10)
50	2.52 (7.81)	8.60 (26.7)

hypothesis. The lower than expected exposure in SCID mice meant that the dose required to achieve a 90% reduction in parasitemia (ED_{90} ≈ 50 mg/kg/day for **37**) was considerably higher than for **1** in the QD study (ED_{90} ≈ 8 mg/kg/day[21]); however, the blood exposure levels ($AUC_{ED_{90}}$, Table 14) were similar. Correcting blood exposure for the fraction unbound in blood suggests that a 50-fold higher unbound exposure is required for **37** to reach a 90% reduction in parasitemia compared to **1**. In contrast, the difference in unbound *in vitro* potency (3D7 parasites, Table 14) differed by only 8-fold (EC_{50} of 0.0077 μM for **37**, 0.0010 μM for **1**). These results suggest that the *in vivo* efficacy of **37** is below what would be expected if it performed as well as the triazolopyrimidines. Conducting a similar analysis for DSM421[26] compared to **1** yielded consistent differences between the unbound *in vitro* 3D7 EC_{50} and the unbound AUC_{ED90} (which were 10-fold lower for **1** for both parameters, Table 14). The basis for the discrepancy in efficacy for **37** compared to the triazolopyrimidines is not currently understood.

CONCLUSIONS

Although **37** has many attractive features and improves on some aspects of **1**, it is less metabolically stable and does not show the sustained exposure needed to fulfill the criteria for single dose cure or once weekly chemoprevention, which is the current objective of new antimalarials.[47] Additional improvements in metabolic stability and modifications that would eliminate the time-dependent CYP inhibition could be undertaken to improve the series further. However, **37** may have sufficient potency and plasma exposure to be able to support a therapeutic use if dosed more frequently than once for treatment or once weekly for chemoprevention. Thus, we have demonstrated herein that the pyrrole-based series has the potential to deliver an antimalarial candidate that could advance to preclinical development.

EXPERIMENTAL SECTION

Materials. Routine chemicals were sourced from Sigma or Aldrich unless otherwise stated.

Protein Expression and Purification. BL21-DE3 *Escherichia coli* phage-resistant cells containing His_6-tagged DHODH-pRSETb (N-terminal tag) (*Pf* and *Pv*DHODH), pET22b C-terminal tag (human), or pET-28b C-terminal tag (rat, mouse, and dog) constructs were grown and harvested as described using appropriate antibiotics.[21,22,34] Cells in lysis buffer A [50 mM Tris pH 8.5, 20 mM imidazole pH 8.0, 5 mM 2-mercaptoethanol, 2% Triton X-100, 0.5 mM FMN, 10% glycerol, and 1× Protease Inhibitor Cocktail (Sigma P8849)] were passed through an EmulsiFlex-C5 high-pressure homogenizer (3×), and the lysate was clarified by centrifugation (20,000 rpm at 4 °C). The lysate was loaded onto a 5 mL HisTrap HP column (20 mM Tris pH 8.5, 300 mM NaCl, 10% glycerol, 20 mM imidazole, pH 8.0, and 0.05% Triton X-100), and DHODH was eluted using a linear imidazole gradient (20−400 mM) and then further purified by gel filtration chromatography on a Pharmacia HiLoad 16/600 Superdex 200 column (100 mM HEPES, pH 8.0, 300 mM NaCl, 0.05% Triton X-100 reduced, and 1 mM DTT) to a purity >95% based on sodium dodecyl sulfate-polyacrylamide gel analysis. The purified DHODH concentration was determined based on absorbance at 280 nm with the molar extinction coefficient calculated using ProtParam in ExPASy (*Pf*DHODH—30,830 M^{-1} cm^{-1}, *Pv*DHODH—29,340 M^{-1} cm^{-1}, human DHODH—15,930 M^{-1} cm^{-1}, rat DHODH—11,920 M^{-1} cm^{-1}, mouse DHODH—11,920 M^{-1} cm^{-1}, and dog DHODH—11,920 M^{-1} cm^{-1}).[48]

Table 14. Comparison of In Vitro Potency (3D7 Parasites) and SCID Mouse Efficacy Data for *Pf*DHODH Inhibitors[b]

cmpd	3D7 EC_{50} (μM)	unbound 3D7 EC_{50} (μM)[c]	ED_{90} (mg/kg/day)	blood $AUC_{ED_{90}}$ (μg h/mL)	unbound blood AUC (μg h/mL)[d]
37	0.016	0.0077	∼50* (QD)	∼9	∼1.1
1[a]	0.0060	0.0010	8.1 (QD)	16.7	0.023
1[a]	as above	as above	3.0 (BID)	10.8	0.015
DSM421[a]	0.014	0.0070	2.6 (QD)	12.9	0.25

[a]Data taken from refs.[21,22,26] [b]QD = once daily dosing; BID = twice daily dosing. Studies compared using the standard Peters test with 4 days of consecutive dosing. Parasite levels 1 day after the final dose were used to determine the ED_{90}. *For **37**, the ED_{90} reflects the average from the two studies where 24 h after the last dose, 85% reduction in parasitemia was observed in the GSK study and 97% reduction was observed in the Swiss TPH study, both at the 50 mg/kg dose. [c]Obtained by multiplying the EC_{50} by the fraction unbound in the AlbuMAX medium. [d]Approximated by multiplying the blood $AUC_{ED_{90}}$ by the fraction unbound in blood ($f_{u(blood)}$) where $f_{u(blood)} = f_{u(plasma)}/B/P$.

https://dx.doi.org/10.1021/acs.jmedchem.0c00311
J. Med. Chem. 2020, 63, 4929−4956

DHODH Kinetic Analysis. Steady-state DHODH assays to determine the 50% inhibitory concentration (IC_{50}) of the described compounds were performed using the 2,6-dichloroindophenol (DCIP) assay to monitor the reaction rate at 25 °C in assay buffer (100 mM HEPES, pH 8.0, 150 mM NaCl, 10% glycerol, 0.1% Triton X-100 reduced, 20 μM CoQ_D, 200 μM L-DHO, 120 μM DCIP, and 5−20 nM enzyme) as described.[48] Inhibitor stocks (100 mM) were prepared in dimethyl sulfoxide (DMSO) in amber bottles. Stocks were diluted in DMSO to generate a threefold dilution series and then dispensed into assay buffer *via* a 1/100 dilution to generate a final concentration range of 0.001−100 μM. Triplicate rate data were collected at each inhibitor concentration. To determine the IC_{50}, data were fitted to log (inhibitor) versus response equation Y = Bottom + (Top − Bottom)/(1 + $10^{(X - \text{Log IC}_{50})}$) in GraphPad Prism.

***Pf* Growth and Inhibition Assays.** *Pf*3D7 cells were grown in RPMI media supplemented AlbuMAX (2.5 g/L) and hypoxanthine (50 mg/L) with human red blood cells and plated to achieve a 0.5% hematocrit and 0.5% parasitemia solution. Inhibitor stocks (as mentioned above) were serially diluted in DMSO in two- or threefold steps (final inhibitor concentrations 0.001−30 μM depending on the cell line and a final DMSO concentration of 0.2%). Parasites in the presence of either DMSO controls or DHODH inhibitors were grown at 37 °C for 72 h before growth was assessed using the SYBR green I method (as described[49] with minor modifications[40]), which measures fluorescence (ex./em. 485/535 nm) as the output. Data were collected in triplicate and to determine the 50% effective concentration (EC_{50}) by fitting data to log (inhibitor) versus response equation Y = Bottom + (Top − Bottom)/(1 + $10^{(X - \text{Log IC}_{50})}$) equation in GraphPad Prism.

X-ray Crystallography. *Protein Preparation.* The pET28b-TEV−*Pf*DHOD$_{\Delta 384-413}$ expression construct used for crystallography was previously described.[28,50] In this construct, the N-terminal nonenzymatic domain and membrane spanning domain (residues 1−157) were deleted to allow expression of the soluble enzyme, and the surface loop 384−413 was deleted to improve crystallization such that the expressed protein contains *Pf*DHODH residues 158−383 contiguous with residues 414−569. *Pf*DHOD$_{\Delta 384-413}$ was expressed in *E. coli* BL21 phage-resistant cells (NEB and C252H), and protein was purified with nickel and gel-filtration chromatography as previously described.[50] Protein was concentrated to 20 mg/mL in a buffer with 20 mM Hepes pH 7.8, 20 mM NaCl, 2 mM *n*-dodecyl-*N*,*N*-dimethylamine-*N*-oxide (LDAO, Anatrace), and 10 mM DTT and stored at −80 °C.

*Crystallization and Data Collection of Pf*DHODH$_{\Delta 384-413}$*-**4** and -**60**.* Preliminary crystallization conditions were found using the random crystallization screen Cryos Ssuite (NeXtal), followed by variation in pH, precipitant, and protein concentrations to find optimal conditions. Crystals of *Pf*DHODH$_{\Delta 384-413}$ in complex with **4** or **60** grew from the same condition [reservoir solution = 0.17 M ammonium acetate (Fluka, Ultra), 0.1 M tri-sodium citrate (Sigma, BioUltra), pH 5.6, 25% PEG4000 (Sigma), 16% glycerol (Sigma), and 10 mM DTT (Sigma)]. Crystallizations were set up using hanging drop vapor diffusion at 20 °C from an equal volume mixture of reservoir solution and *Pf*DHODH$_{\Delta 384-413}$ (20 mg/mL) pre-equilibrated with an inhibitor (1 mM) and DHO (2 mM). Crystals of *Pf*DHODH$_{\Delta 384-413}$-**4** typically grew in 1 week, whereas crystals of *Pf*DHODH$_{\Delta 384-413}$-**60** grew slowly (∼5 weeks).

Diffraction data were collected at 100 K on beamline 19ID at Advanced Photon Source (APS) using an ADSC Q315 detector with 240° of data collected for *Pf*DHODH$_{\Delta 384-413}$-**4** and 200° of data collected for *Pf*DHODH$_{\Delta 384-413}$-**60**. The crystal of *Pf*DHODH$_{\Delta 384-413}$-**4** diffracted to 1.8 Å in a space group of $P2_12_12_1$ with the cell dimension of a = 92.1, b = 97.5, and c = 186.3 and four molecules of *Pf*DHODH were found in the asymmetric unit. *Pf*DHODH$_{\Delta 384-413}$-**60** diffracted to 2.3 Å in a space group of $P6_4$ with the cell dimension of a = b = 84.8 and c = 138.0 and one molecule of *Pf*DHODH was found in the asymmetric unit. Diffraction data were integrated, and intensities were scaled with the HKL2000 package.[51]

*Structure Determination and Refinement of Pf*DHODH-**4** *and* -**60** *Cocrystal Structures.* Crystallographic phases for *Pf*DHODH inhibitor complexes were solved by molecular replacement with Phaser[52] using the structure of *Pf*DHODH$_{\Delta 384-413}$ bound to a triazolopyrimidine (PDB ID 3I65)[50] (with the inhibitor removed) as the search model. Structures were rebuilt with COOT[53] and refined with phenix.refine.[54] *Pf*DHODH$_{\Delta 384-413}$-**4** was refined to R and R_{free} of 0.151 and 0.194, respectively. Electron density was observed for the following residues (chain A: 158−377, including 3 amino acids (Ala, Asp, and Pro) from the N-terminal-His tag linker, and 414−566. Chain B: 160−378 and 414−566. Chain C: 166−378 and 414−566. Chain D: 163−377 and 414−566). All residues were within the allowed section of the Ramachandran plot (Table 3). Additionally, water molecules (926) were modeled into the structure using the default setting in phenix.refine. *Pf*DHODH$_{\Delta 384-413}$-**60** was refined with twin operator (h, $-h - k$, $-l$) to R and R_{free} of 0.202 and 0.219, respectively. The refined structure contains amino acid residues 162−383 and 414−566 and 75 waters (Table 3). All amino acid conformations were within the allowed section of the Ramachandran plot. Data collection and refinement statistics are provided in Table 3.

Structure Display and Analysis. Structures were rendered in MacPyMOL: PyMOL v1.8.2.3 Enhanced for Mac OS X (Schrödinger LLC). Structural alignments were conducted using the Align command.

Physicochemical and Binding Properties and In Vitro Metabolism. Methods for assessing solubility in biorelevant media (FaSSIF, FeSSIF, and FaSSGF), binding to plasma proteins, microsomes, and *in vitro* assay media, and whole blood-to-plasma partitioning ratio determination have been described previously.[22]

In Vitro Metabolism. Compound **37** (1 μM) was incubated at 37 °C for up to 60 min with human, rat, or mouse liver microsomes or cryopreserved hepatocytes (all XenoTech LLC, Kansas City, KS) and the samples were analyzed by LC−MS (Waters Xevo G2QTOF coupled to a Waters Acquity UPLC operating in positive electrospray ionization under the MS^E mode). Microsome incubations were conducted at a protein concentration of 0.4 mg/mL and hepatocyte studies at a cell concentration of 7 × 10^5 cells/mL. The degradation half-life and *in vitro* intrinsic clearance in microsomes were calculated from the apparent first-order degradation rate constant.

Metabolite Identification and Reactive Metabolite Trapping. Compound **37** was incubated at 37 °C with human liver microsomes. To maximize the metabolite yield, a high substrate concentration (10 μM) and a high microsomal protein concentration (1 mg/mL) were used. Reactions were initiated by the addition of an NADPH-regenerating system, and the samples were incubated for up to 60 min. Controls containing no NADPH were included in the incubation. The reaction was quenched by protein precipitation with an equal volume of ice-cold acetonitrile (containing 0.15 μg/mL diazepam as the internal standard). Following protein precipitation, samples were vortexed and then centrifuged for 3 min at 10,000 rpm. The supernatant was removed and analyzed by LC−MS. Chromatography and mass spectrometry were conducted using a Waters Acquity UPLC coupled to a Waters Xevo G2 QTOF. The column was an Ascentis Express Amide (50 × 2.1 mm, 2.7 μm), and the mobile phase comprised water and acetonitrile with 0.05% formic acid delivered with a gradient program and 6 min cycle time. The flow rate was 0.4 mL/min, and the injection volume was 5 μL. Mass spectrometry was conducted in positive electrospray ionization under the MS^E mode with metabolites confirmed using accurate mass and MS/MS fragmentation.

Cytochrome P450 Inhibition and Time-Dependent Inhibition Studies. The CYP inhibition assay was performed utilizing a substrate-specific interaction approach which relies on the formation of a metabolite that is mediated by a specific CYP isoform using human liver microsomes. The specific CYP-mediated metabolic pathways included phenacetin *O*-deethylation (CYP1A2), tolbutamide methylhydroxylation (CYP2C9), (*S*)-mephenytoin 4′-hydroxylation (CYP2C19), dextromethorphan *O*-demethylation (CYP2D6), midazolam 1′-hydroxylation (CYP3A4/5), and testosterone 6β-hydroxylation (CYP3A4/5). Multiple concentrations of **37** (0.25−

https://dx.doi.org/10.1021/acs.jmedchem.0c00311
J. Med. Chem. 2020, 63, 4929−4956

20 μM) and positive control inhibitors were incubated at 37 °C concomitantly with each probe substrate in a suspension of human liver microsomes with the total organic solvent concentration being 0.47% (v/v). The microsomal protein concentration was 0.1 mg/mL for all pathways except for CYP2C9 and 2C19 (both 0.2 mg/mL microsomal protein). The reactions were initiated by the addition of an NADPH-regenerating system, and the samples were quenched by the addition of ice-cold acetonitrile containing analytical internal standard (diazepam). Metabolite formation was monitored over variable periods from 10 to 30 min depending on the pathway. Concentrations of the substrate-specific metabolites in quenched samples were determined by UPLC-MS (Waters Xevo TQD triple-quadrupole mass spectrometer) with an Ascentis Express RP Amide column and acetonitrile/water (both containing 0.05% formic acid) gradient. Calibration standards were prepared in the quenched microsomal matrix and analyzed along with the samples. Control samples confirmed that the UPLC-MS assay of the specific metabolites was not affected by the presence of each test compound (and potential metabolites).

Assessment of time-dependent inhibition was conducted using human liver microsomes and the "IC_{50} shift"-method. Multiple concentrations of the inhibitor were incubated in the absence or presence of NADPH at 37 °C with human liver microsomes suspended in 0.1 M phosphate buffer (pH 7.4) for 30 min at 10-fold the final target concentration. The microsomal protein concentration during this pre-incubation period was 1 mg/mL (for CYPs 1A2, 2D6, and 3A4) and 2 mg/mL (for CYPs 2C9 and 2C19), and the total concentration of the organic solvent in the pre-incubation mixture was 1% (v/v). Following the 30 min pre-incubation, aliquots of the mixture were diluted 10-fold in 0.1 M phosphate buffer (pH 7.4) containing the probe substrate for an individual CYP isoform (the same as for the CYP inhibition assay). An NADPH-regenerating cofactor system was added to all samples which were then incubated at 37 °C for 10−40 min. The total concentration of the organic solvent in this incubation mixture was 0.3% (v/v). The incubation was quenched by the addition of ice-cold acetonitrile (containing 0.15 μg/mL diazepam as an internal standard), the samples were centrifuged, and an aliquot of the supernatant was transferred to a fresh 96-well plate for analysis. Concentrations of the probe metabolites were determined by UPLC-MS as described above. IC_{50} values were determined by curve fitting to a four-parameter logistic function following log transformation of the concentration data (GraphPad Prism software, ver 7.01).

Animal Studies. All animal studies were ethically reviewed and carried out in accordance with either the Australian Code of Practice for the Care and Use of Animals for Scientific Purposes (mouse and rat PK studies) or European Directive 2010/63/EEC and the GSK Policy on the Care, Welfare and Treatment of Animals (SCID mouse studies). The human biological samples for the SCID mouse studies were sourced ethically and their research use was in accordance with the terms of the informed consents under an IRB/EC approved protocol. Animal experiments described at the Swiss Tropical and Public Health Institute (Basel, Switzerland) were adhering to local and national regulations of laboratory animal welfare in Switzerland (awarded permission no. 2303). Protocols are regularly reviewed and revised following approval by the local authority (Veterinäramt Basel Stadt).

Mouse and Rat PK Studies. Protocols for the *in vivo* assessment of **37** PKs in male Sprague−Dawley rats and male Swiss outbred mice were reviewed and approved by the Monash University of Pharmaceutical Sciences Animal Ethics Committee. **37** was administered intravenously to rats in a saline vehicle containing 10% (v/v) DMSO and 4% (v/v) Solutol HS 15 (total volume of 1 mL) as a 10 min infusion into the jugular vein *via* a surgically implanted catheter. In mice, the IV dose was administered as a bolus injection into the tail vein in a vehicle comprising 40% (v/v) propylene glycol, 10% (v/v) ethanol, and 0.5% (v/v) Tween 80 in water (2 mL/kg dose volume). Oral doses in both rats and mice were administered by oral gavage in an aqueous suspension vehicle containing 0.5% (w/v) carboxymethyl cellulose, 0.4% (v/v) Tween 80, and 0.5% (v/v) benzyl alcohol (10 mL/kg volume). Blood samples from rats and mice were collected up to 24 h postdose into tubes containing heparin as an anticoagulant and the plasma fraction was transferred to clean tubes following centrifugation. Proteins were precipitated with the addition of two volumes of acetonitrile, and the supernatant was analyzed by LC−MS against calibration standards prepared in blank rat or mouse plasma and extracted in the same way. Diazepam was added to all plasma samples and calibration standards (prior to protein precipitation) as an internal standard. Plasma samples were analyzed on a Waters Xevo TQ mass spectrometer coupled to a Waters Acquity UPLC operating in the positive electrospray ionization multiple-reaction monitoring mode. The column was a Sulpeco Ascentis Express RP Amide column (50 × 2.1 mm, 2.7 μm). The mobile phase consisted of an acetonitrile−water gradient with 0.05% formic acid, a gradient cycle of 4 min, and a flow rate of 0.4 mL/min.

SCID Mouse Efficacy Studies. *In Vivo Antimalarial Efficacy Studies in Pf Conducted at GSK.* The *in vivo* efficacy of **37** was measured against *Pf* 3D70087/N9 growing in the peripheral blood of NOD-scidIL2Rγnull mice (Jackson Laboratory, USA) (23−36 g) engrafted with human erythrocytes as described.[55] The parasites (20×10^6) were inoculated by IV injection, and antimalarial efficacy was assessed using a standard "4-day test". Blood parasitemia was measured by FACS analysis. **37** was administered in a vehicle (0.5% hydroxypropylmethylcellulose, 0.4% Tween 80, and 0.5% benzoyl) by oral gavage for four consecutive days starting on the third day after infection. With the goal to determine PD endpoints the PKs of **37** were evaluated in whole blood in the same animals as part of the efficacy study after dosing 10 and 50 mg/kg. With this goal, peripheral blood samples (25 μL) were taken at different time periods (0.25, 0.5, 1.0, 2.0, 4.0, 6.0, 8.0, and 23 h) at day 1, after first administration of the parent compound. Samples were mixed with 25 μL of Milli-Q water and immediately frozen on dry ice. The frozen samples were stored at −80 °C until analysis. Vehicle-treated mice experienced the same blood-sampling regimen. Blood samples were analyzed for **37** using a method based on protein precipitation, followed by LC−MS/MS analysis (Waters Acquity coupled to a Sciex API4000) (LLOQ = 1 ng/mL). Reversed-phase HPLC separation was achieved with a UPLC HSS T3 column (50 × 2.1 mm 1.8 μm). MS/MS detection was set at mass transitions of 324.193 → 266.2887 m/z for **37** and 326 → 291 m/z for Midazolam, (IS) in the positive mode. PK analysis was performed by noncompartmental methods using WinNonlin Phoenix Version 6.3 (Pharsight Corporation).

In Vivo Antimalarial Efficacy Studies in Pf Conducted at Swiss TPH. Reduction of existing parasitemia *in vivo* was tested in the murine *Pf* SCID model essentially as described.[55] Briefly, **37** was formulated in a vehicle (0.5% hydroxypropylmethylcellulose, 0.4% Tween 80, and 0.5% Benzoyl) and administered to a cohort of age-matched female immunodeficient NOD-scidIL2Rγnull mice (The Jackson Laboratory, Bar Harbor, ME) (20−22 g) previously engrafted for 11 days with human erythrocytes (generously provided by the Blood Bank in Zürich, Switzerland). The mice were intravenously infected with 2×10^7 *P. falciparum Pf*3D70087/N9-infected erythrocytes (day 0). On day 3, after infection, mice ($n = 2$) were randomly allocated to treatments that were administered once a day for 4 consecutive days by oral gavage at 10 mL/kg. Parasitemia was measured by microscopy and flow cytometry using anti-murine erythrocyte TER119 monoclonal antibody (PharMingen, San Diego, CA) in serial 2 μL blood samples taken every 24 h until assay completion.

Chemistry. All reagents and starting materials were obtained from commercial suppliers and used without further purification unless otherwise stated. Reaction progress was monitored by thin layer chromatography (TLC) on preloaded silica gel 60 F_{254} plates. Visualization was achieved with UV light and iodine vapor. Flash chromatography was carried out using prepacked Teledyne ISCO RediSep Rf silica-gel columns as the stationary phase and analytical grade solvents as the eluent unless otherwise stated. Yields were of the purified product and were not optimized. ^{1}H NMR spectra were recorded on a Bruker AVANCE 300 and 500 MHz spectrometer at

https://dx.doi.org/10.1021/acs.jmedchem.0c00311
J. Med. Chem. 2020, 63, 4929−4956

ambient temperature. Chemical shifts are reported in parts per million (δ) and coupling constants in Hz. ^{1}H NMR spectra were referenced to the residual solvent peaks as internal standards (7.26 ppm for $CDCl_3$, 2.50 ppm for DMSO-d_6, and 3.34 ppm for MeOD). Spin multiplicities are described as s (singlet), brs (broad singlet), d (doublet), t (triplet), q (quartet), dd (doublet of doublets), dt (doublet of triplets), and m (multiplet). Total ion current traces were obtained for electrospray positive and negative ionization (ES^+/ES^-) on a Bruker Esquire Liquid Chromatograph−Ion trap mass spectrometer. Analytical chromatographic conditions used for the LC−MS analysis: Column, Zorbax Extend C18 from Agilent Technologies, 2.1 × 100 mm. The stationary phase particle size is 3.5 μM. Solvents were A, aqueous solvent = water + 5% acetonitrile + 1% acetic acid; B, organic solvent = acetonitrile + 1% acetic acid; Methods, 22 min run time (0−10 min 10−60% B, flow rate—0.275 mL/min; 10−20 min 60−100% B, flow rate—0.350 mL/min; 20−22 min 100−10% B, flow rate—0.350 mL/min). The following additional parameters were used: injection volume (10 μL), column temperature (30 °C), and UV wavelength range (254−330 nm). Analytical HPLC analyses were performed on a SUPELCOSIL LC18 column (5 μm, 4.6 mm × 25 cm) with a linear elution gradient ranging from 0 to 100% ACN over 27 min, using a SUPELCOSIL LC18 column (5 μm, 4.6 mm × 25 cm) at a flow rate of 1 mL/min. The purity of all tested compounds was ≥95% using the analytical method (LC−MS) described above unless stated otherwise.

Chemistry Synthetic Methods. The reported pyrrole analogues were synthesized, as shown in Schemes 1−5, using the following methods.

General Procedure for the Intermediate (77a−h). To a solution of acetylacetone (**75**) (10 mmol) in acetone (8 mL) was added solid potassium carbonate (10 mmol), followed by the corresponding aryl bromide (12 mmol). The mixture was heated to 60 °C for 12 h. The solution was allowed to cool to room temperature (RT) and acidified with aq. HCl (10%, 20 mL). The mixture was extracted with ethyl acetate (3 × 25 mL), and the combined organic fractions were washed with brine, dried over Na_2SO_4, and concentrated in vacuo. Flash column chromatography [hexane/ethyl acetate 9:1 v/v] afforded **77a−h** (35−40% yield). Compounds **77c**, **e**, **f**, and **h** were purified as described and then used in the next step without characterization. The NMR data for the remaining intermediates are provided below.

*3-(4-Ethoxy-benzyl)-pentane-2,4-dione (**77a**).* ^{1}H NMR (300 MHz, $CDCl_3$): δ 7.15−6.94 (m, 2H), 6.93−6.71 (m, 2H), 4.09−3.89 (m, 2.6H), 3.61 (s, 1.6H), 3.09 (d, J = 7.6 Hz, 0.8H), 2.14 (s, 1.6H), 2.10 (s, 4.4H), 1.47−1.33 (m, 3H) (Mixture of keto−enol forms) MS (ESI^+) m/z: 235.2.

*3-(4-Trifluoromethyl)-pentane-2,4-dione (**77b**).* ^{1}H NMR (300 MHz, $CDCl_3$): δ 7.52−7.48 (m, 2H), 7.33−7.29 (m, 2H), 4.0 (t, J = 7.6 Hz, 0.5H) 3.8 (s, 1H), 3.2 (d, J = 7.6 Hz, 1H) 2.10 (s, 2.7H), 2.05 (s, 3.3H) (mixture of keto−enol forms) MS (ESI^+) m/z: 259.1.

*3-(4-Methoxy-benzyl)-pentane-2,4-dione (**77d**).* ^{1}H NMR (300 MHz, $CDCl_3$): δ 7.19−7.10 (m, 2H), 6.94−6.73 (m, 2H), 3.99 (t, J = 7.6 Hz, 0.25H), 3.81 (s, 3H), 3.61 (s, 1.5H), 3.1 (d, J = 7.6 Hz, 0.5H) 2.14 (s, 1.6H), 2.10 (s, 4.4H) (mixture of keto−enol forms) MS (ESI^+) m/z: 221.2.

*3-(6-(Trifluoromethyl)pyridin-3-yl)-pentane-2,4-dione (**77g**).* ^{1}H NMR (300 MHz, $CDCl_3$): δ 8.60 (d, J = 7.7 Hz, 1H), 7.77−7.51 (m, 2H), 4.02 (t, J = 7.4 Hz, 0.23H), 3.78 (s, 1.66H), 3.24 (d, J = 7.4 Hz, 0.64H), 2.21 (s, 1.69H), 2.10 (s, 4.31H) (mixture of keto−enol forms) MS (ESI^+) m/z: 260.2.

*Ethyl-2-(hydroxyimino)-3-oxobutanoate **78**.* To a solution of ethyl acetoacetate (**76**) (5 g, 38 mmol) in 6 mL of acetic acid was added a solution of sodium nitrate (3.4 g, 49 mmol) in 6 mL of cold water at −10 °C. The reaction mixture was stirred for 3 h. A saturated aqueous solution of sodium bicarbonate was added to adjust the pH to 7−8 and washed with brine, and the mixture was extracted with diethyl ether. Then, the mixture was dried over anhydrous sodium sulphate, filtered, concentrated, and then purified by flash chromatography on silica gel (hexane/ethyl acetate 10:1 v/v) to give ethyl-2-hydroxyimino-3-oxobutanoate (**78**) as pale yellow oil (4 g, 80% yield).

^{1}H NMR (300 MHz, $CDCl_3$): δ 4.15 (q, J = 7.0 Hz, 2H), 2.30 (s, 3H), 1.92 (brs, 1H), 1.33 (t, J = 7.0 Hz, 3H).

General Procedure for Knorr Pyrrole Synthesis of Pyrroles (3−10). Freshly prepared ethyl-2-(hydroxyimino)-3-oxobutanoate (**78**) (4 mmol) and the corresponding acetylacetone (**77a−h**) (4 mmol) was dissolved in glacial acetic acid (25 mL) at 15 °C. Zn dust (10 mmol) was then slowly added to the mixture and allowed to react at RT with vigorous stirring for 15−20 min. The resulting mixture was heated to 60 °C for 2 h. The mixture was allowed to attain RT and poured into ice water. The aqueous phase was extracted with ethyl acetate (3 × 25 mL), and the combined organic phases were washed with brine, dried (Na_2SO_4), filtered, and concentrated in vacuo. The residue was purified by flash column chromatography on silica gel (eluent: gradient, hexane/EtOAc = 95:5 to 70:30) to afford the corresponding pyrroles **3−10** (60−70% yield).

*Ethyl 4-(4-Ethoxybenzyl)-3,5-dimethyl-1H-pyrrole-2-carboxylate (**3**).* (DSM43, 65% yield, white solid, mp 82−84 °C): ^{1}H NMR (500 MHz, $CDCl_3$): δ 8.61 (brs, 1H), 7.01 (d, J = 8.7 Hz, 2H), 6.80 (d, J = 8.7 Hz, 2H), 4.32 (q, J = 7.1 Hz, 2H), 4.01 (q, J = 7.0 Hz, 2H), 3.70 (s, 2H), 2.23 (s, 3H), 2.19 (s, 3H), 1.39 (dt, J = 12.8 Hz, 7.1 Hz, 6H). MS (ESI^+) m/z: 302.3.

*Ethyl 3,5-Dimethyl-4-(4-(trifluoromethyl)benzyl)-1H-pyrrole-2-carboxylate (**4**).* (DSM483, 60% yield, off white solid): ^{1}H NMR (500 MHz, $CDCl_3$): δ 8.63 (brs, 1H), 7.51 (d, J = 8.1 Hz, 2H), 7.22 (d, J = 8.0 Hz, 2H), 4.32 (q, J = 7.1 Hz, 2H), 3.83 (s, 2H), 2.22 (s, 3H), 2.20 (s, 3H), 1.37 (t, J = 7.1 Hz, 3H). MS (ESI^+) m/z: 326.3.

*Ethyl 4-(3-Ethoxybenzyl)-3,5-dimethyl-1H-pyrrole-2-carboxylate (**5**).* (DSM484, 60% yield, white solid, mp 114−116 °C): ^{1}H NMR (500 MHz, $CDCl_3$): δ 8.60 (brs, 1H), 7.18 (t, J = 7.9 Hz, 1H), 6.72 (dd, J = 7.9, 3 Hz, 2H), 6.66 (s, 1H), 4.33 (q, J = 7.1 Hz, 2H), 3.75 (q, J = 7.0 Hz, 2H), 3.75 (s, 2H), 2.25 (s, 3H), 2.21 (s, 3H), 1.40 (dt, J = 19.0, 7.1 Hz, 6H). MS (ESI^+) m/z: 302.5.

*Ethyl 4-(4-Methoxybenzyl)-3,5-dimethyl-1H-pyrrole-2-carboxylate (**6**).* (DSM485, 70% yield, white solid, mp 129−131 °C): ^{1}H NMR (300 MHz, $CDCl_3$): δ 8.63 (brs, 1H), 7.05 (d, J = 8.7 Hz, 2H), 6.82 (d, J = 8.8 Hz, 2H), 4.33 (q, J = 7.1 Hz, 2H), 3.80 (s, 3H), 3.72 (s, 2H), 2.24 (s, 3H), 2.19 (s, 3H), 1.35 (t, J = 7.3 Hz, 3H). MS (ESI^+) m/z: 288.4.

*Ethyl 4-(3,5-Dimethoxybenzyl)-3,5-dimethyl-1H-pyrrole-2-carboxylate (**7**).* (DSM486, 60% yield, off white solid): ^{1}H NMR (300 MHz, $CDCl_3$): δ 8.50 (brs, 1H), 7.20 (s, 2H), 6.20 (s, 1H), 4.43 (q, J = 7.1 Hz, 2H), 3.68 (s, 6H), 3.62 (s, 2H), 2.15 (s, 3H), 2.11 (s, 3H), 1.38 (t, J = 7.1 Hz, 3H) MS (ESI^-) m/z: 316.7.

*Ethyl 4-(4-Isopropylbenzyl)-3,5-dimethyl-1H-pyrrole-2-carboxylate (**8**).* (DSM487, 70% yield, light yellow solid, mp 113−115 °C): ^{1}H NMR (300 MHz, $CDCl_3$): δ 8.67 (brs, 1H), 7.13 (d, J = 8.0 Hz, 2H), 7.04 (d, J = 8.0 Hz, 2H), 4.33 (q, J = 7.1 Hz, 2H), 3.76 (s, 2H), 2.96−2.79 (m, 1H), 2.25 (s, 3H), 2.21 (s, 3H), 1.37 (t, J = 7.1 Hz, 3H), 1.25 (d, J = 6.9 Hz, 6H). MS (ESI^+) m/z: 300.3.

*Ethyl 3,5-Dimethyl-4-((6-(trifluoromethyl)pyridin-3-yl)methyl)-1H-pyrrole-2-carboxylate (**9**).* (DSM491, 60% yield, off white solid): ^{1}H NMR (300 MHz, $CDCl_3$): δ 8.75 (brs, 1H), 8.56 (s, 1H), 7.68−7.48 (m, 2H), 4.31 (q, J = 7.1 Hz, 2H), 3.84 (s, 2H), 2.81 (s, 3H), 2.21 (s, 3H), 1.37 (t, J = 7.1 Hz, 3H). MS (ESI^+) m/z: 327.3.

*Ethyl 3,5-Dimethyl-4-((5-(trifluoromethyl)pyridin-2-yl)methyl)-1H-pyrrole-2-carboxylate (**10**).* (DSM520, 60% yield, yellow solid): ^{1}H NMR (300 MHz, $CDCl_3$): δ 8.95 (s, 1H), 8.83 (brs, 1H), 8.00 (d, J = 8.2 Hz, 1H), 7.24 (d, J = 8.3 Hz, 1H), 4.34 (q, J = 7.1 Hz, 2H), 4.15 (s, 2H), 2.22 (s, 3H), 2.21 (s, 3H), 1.38 (t, J = 7.1 Hz, 3H). MS (ESI^+) m/z: 327.1.

*Ethyl 1,3,5-Trimethyl-4-(4-(trifluoromethyl)benzyl)-1H-pyrrole-2-carboxylate (**11**).* (DSM490): To a solution of 4 mg (0.015 mmol) of 18-crown-6 in 10 mL of benzene was added 17 mg (0.153 mmol) of potassium *tert*-butoxide and 50 mg (0.15 mmol) of **4**. The reaction mixture was stirred for 15 min. Iodomethane (0.01 mL, 0.169 mmol) dissolved in 1 mL of benzene was added dropwise to the reaction mixture. Stirring was continued for 6 h. The reaction mixture was quenched with water (20 mL), and the mixture was extracted with ethyl acetate. The organic layer was washed with brine, dried over

https://dx.doi.org/10.1021/acs.jmedchem.0c00311
J. Med. Chem. 2020, 63, 4929−4956

anhydrous Na_2SO_4, and evaporated to afford **11** as a white solid (25 mg, 48% yield). ^{1}H NMR (300 MHz, $CDCl_3$): δ 7.51 (d, J = 8.1 Hz, 2H), 7.21 (d, J = 7.9 Hz, 2H), 4.31 (q, J = 7.1 Hz, 2H), 3.83 (s, 2H), 3.82 (s, 3H), 2.22 (s, 3H), 2.14 (s, 3H), 1.38 (t, J = 7.1 Hz, 3H). MS (ESI^+) m/z: 340.4.

General Procedure for the Preparation of 12−25. A solution of pyrrole ester (**3−10**) (1 equiv) and NaOH (4 equiv) in EtOH/water (8:2 mL) was heated to 80 °C for 2−4 h. When the reaction was complete, as determined by TLC, water (10 mL) was added to the residue and neutralized with 1 M aqueous HCl. The precipitate was extracted with EtOAc (3 × 100 mL), the organic extracts were washed with water and brine, dried with Na_2SO_4, and concentrated in vacuo. To this residue (acid, 1 equiv) were added dimethylformamide (DMF) (2.5−5 mL), trimethylamine (4 equiv), EDC (1.25 equiv), and HOBt (1 equiv), and the mixture was stirred for 10 min. To this solution, appropriate amine (1 equiv) was added and stirring continued at RT for 4−6 h. The reaction mixture was poured into sat. aq $NaHCO_3$ and extracted with EtOAc. The organic layer was separated, washed with brine, dried over $MgSO_4$, and concentrated in vacuo. The residue was purified by column chromatography on silica gel (eluted with 20−100% EtOAc in hexane) to afford the title compounds (**12−25**) typically a white or light yellow solid.

*3,5-Dimethyl-4-(4-(trifluoromethyl)benzyl)-1H-pyrrole-2-carboxylic Acid (**12**).* (DSM489, 60% yield, red solid). ^{1}H NMR (300 MHz, $CDCl_3$): δ 8.78 (brs, 1H), 7.53 (d, J = 8.1 Hz, 2H), 7.23 (d, J = 8.0 Hz, 2H), 3.83 (s, 2H) 2.26 (s, 3H), 2.21 (s, 3H). MS (ESI^-) m/z: 296.4.

*N-Ethyl-3,5-dimethyl-4-(4-(trifluoromethyl)benzyl)-1H-pyrrole-2-carboxamide (**13**).* (DSM496, 50% yield, yellow solid, mp 188−190 °C). ^{1}H NMR (300 MHz, $CDCl_3$): δ 9.5 (brs, 1H), 7.49 (d, J = 8.19, Hz, 2H), 7.18 (d, J = 8.19 Hz, 2H), 5.60 (brs, 1H), 3.82 (s, 2H), 3.46 (qd, J = 7.2, 5.8 Hz, 2H), 2.18 (s, 3H), 2.13 (s, 3H), 1.22 (t, J = 7.2 Hz, 3H). MS (ESI^+) m/z: 325.2.

*3,5-Dimethyl-N-propyl-4-(4-(trifluoromethyl)benzyl)-1H-pyrrole-2-carboxamide (**14**).* (DSM495, 50% yield, off white solid). ^{1}H NMR (300 MHz, $CDCl_3$): δ 9.5 (brs, 1H), 7.52 (d, J = 8.1 Hz, 2H), 7.22 (d, J = 7.9 Hz, 2H), 5.68 (t, J = 5.2 Hz, 1H), 3.83 (s, 2H), 3.43 (dd, J = 13.0, 6.9 Hz, 2H), 2.21 (s, 3H), 2.16 (s, 3H), 1.70−1.55 (m, 2H), 0.95 (t, J = 7.4 Hz, 3H). MS (ESI^+) m/z: 339.2.

*N-Butyl-3,5-dimethyl-4-(4-(trifluoromethyl)benzyl)-1H-pyrrole-2-carboxamide (**15**).* (DSM494, 50% yield, off white solid, mp 134−136 °C). ^{1}H NMR (300 MHz, $CDCl_3$): δ 8.96 (brs, 1H), 7.50 (d, J = 8.1, 2H), 7.20 (d, J = 7.6, 2H), 5.63 (t, J = 5.6 Hz, 1H), 3.81 (s, 2H), 3.49−3.38 (m, 2H), 2.18 (s, 3H), 2.12 (s, 3H), 1.63−1.31 (m, 4H), 0.95 (t, J = 7.1, 3H). MS (ESI^+) m/z: 353.4.

*N-Ethyl-3,5-dimethyl-4-((6-(trifluoromethyl)pyridin-3-yl)methyl)-1H-pyrrole-2-carboxamide (**16**).* (DSM497, 60% yield, off white solid, mp 171−173 °C). ^{1}H NMR (300 MHz, $CDCl_3$): δ 9.67 (brs, 1H), 8.58 (s, 1H), 7.71−7.41 (m, 2H), 5.64 (brs, 1H), 3.86 (s, 2H), 3.50 (td, J = 12.8, 7.2 Hz, 2H), 2.23 (s, 3H), 2.15 (s, 3H), 1.25 (t, J = 7.2 Hz, 3H). MS (ESI^+) m/z: 326.3.

*3,5-Dimethyl-N-propyl-4-((6-(trifluoromethyl)pyridin-3-yl)-methyl)-1H-pyrrole-2-carboxamide (**17**).* (DSM498, 55% yield, off white solid, mp 155−157 °C). ^{1}H NMR (300 MHz, $CDCl_3$): δ 9.83 (brs, 1H), 8.58 (s, 1H), 7.55 (dd, J = 17.1, 7.8 Hz, 2H), 5.70 (brs, 1H), 3.85 (s, 2H), 3.43 (dd, J = 13.1, 6.7 Hz, 2H), 2.22 (s, 3H), 2.15 (s, 3H), 1.76−1.53 (m, 2H), 0.98 (t, J = 7.4 Hz, 3H). MS (ESI^+) m/z: 340.3.

*N-Cyclopropyl-3,5-dimethyl-4-((6-(trifluoromethyl)pyridin-3-yl)-methyl)-1H-pyrrole-2-carboxamide (**18**).* (DSM499, 50% yield, off white solid, mp 176−178 °C). ^{1}H NMR (300 MHz, $CDCl_3$): δ 9.03 (brs, 1H), 8.55 (s, 1H), 7.55 (d, J = 8.1 Hz, 1H), 7.48 (d, J = 8.2 Hz, 1H), 5.72 (brs, 1H), 3.82 (s, 2H), 2.84 (td, J = 7.0, 3.0 Hz, 1H), 2.19 (s, 3H), 2.07 (s, 3H), 0.90−0.75 (m, 2H), 0.62−0.52 (m, 2H). MS (ESI^+) m/z: 338.2.

*N-Cyclobutyl-3,5-dimethyl-4-((6-(trifluoromethyl)pyridin-3-yl)-methyl)-1H-pyrrole-2-carboxamide (**19**).* (DSM500, 50% yield, off white solid, mp 177−179 °C). ^{1}H NMR (300 MHz, $CDCl_3$): δ 9.89 (brs, 1H), 8.56 (s, 1H), 7.62−7.44 (m, 2H), 5.82 (d, J = 7.7 Hz, 1H), 4.74−4.44 (m, 1H), 3.85 (s, 2H), 2.52−2.33 (m, 2H), 2.21 (s, 3H), 2.17 (s, 3H), 2.02−1.84 (m, 2H), 1.83−1.66 (m, 2H). MS (ESI^+) m/z: 352.3.

*Azetidin-1-yl(3,5-dimethyl-4-((6-(trifluoromethyl)pyridin-3-yl)-methyl)-1H-pyrrol-2-yl)methanone (**20**).* (DSM508, 35% yield, off white solid). ^{1}H NMR (300 MHz, $CDCl_3$): δ 8.87 (brs, 1H), 8.56 (s, 1H), 7.62−7.49 (m, 2H), 4.23 (t, J = 7.7 Hz, 4H), 3.83 (s, 2H), 2.52−2.27 (m, 2H), 2.20 (s, 3H), 2.06 (s, 3H). MS (ESI^+) m/z: 338.4.

*N,N-Diethyl-3,5-dimethyl-4-((6-(trifluoromethyl)pyridin-3-yl)-methyl)-1H-pyrrole-2-carboxamide (**21**).* (DSM509, 45% yield, red solid). ^{1}H NMR (300 MHz, $CDCl_3$): δ 8.82 (brs, 1H), 8.56 (s, 1H), 7.61−7.50 (m, 2H), 3.82 (s, 2H), 3.52 (q, J = 7.32 Hz, 4H), 2.18 (s, 3H), 2.05 (s, 3H), 1.18 (t, J = 7.32, 6H). MS (ESI^+) m/z: 354.2.

*N,N,3,5-Tetramethyl-4-((6-(trifluoromethyl)pyridin-3-yl)methyl)-1H-pyrrole-2-carboxamide (**22**).* (DSM517, 40% yield, red solid, mp 150−152 °C). ^{1}H NMR (500 MHz, $CDCl_3$): δ 9.23 (brs, 1H), 8.55 (s, 1H), 7.60−7.50 (m, 2H), 3.82 (s, 2H), 3.09 (s, 6H), 2.18 (s, 3H), 1.94 (s, 3H). MS (ESI^+) m/z: 326.2.

*N-Cyclopropyl-3,5-dimethyl-4-((5-(trifluoromethyl)pyridin-2-yl)-methyl)-1H-pyrrole-2-carboxamide (**23**).* (DSM519, 50% yield, light yellow solid, mp 182−184 °C). ^{1}H NMR (300 MHz, $CDCl_3$): δ 9.49 (brs, 1H), 8.80 (s, 1H), 7.80−7.75 (m, 1H), 7.11−7.0 (m, 1H), 5.81 (brs, 1H), 4.02 (s, 2H), 2.88−2.82 (m, 1H), 2.24 (s, 3H), 2.13 (s, 3H), 0.88−0.81 (m, 2H), 0.74−0.69 (m, 2H). MS (ESI^+) m/z: 338.2.

*Azetidin-1-yl(3,5-dimethyl-4-((5-(trifluoromethyl)pyridin-2-yl)-methyl)-1H-pyrrol-2-yl)methanone (**24**).* (DSM521, 40% yield, yellow solid, mp 114−116 °C). ^{1}H NMR (300 MHz, $CDCl_3$): δ 8.83 (brs, 1H), 8.80 (s, 1H), 7.78 (dd, J = 8.2, 1.9 Hz, 1H), 7.08 (d, J = 8.2 Hz, 1H), 4.21 (t, J = 7.45 Hz, 4H), 4.0 (s, 2H), 2.44−2.27 (m, 2H), 2.20 (s, 3H), 2.07 (s, 3H). MS (ESI^+) m/z: 338.3.

*N-Cyclobutyl-3,5-dimethyl-4-((5-(trifluoromethyl)pyridin-2-yl)-methyl)-1H-pyrrole-2-carboxamide (**25**).* (DSM522, 50% yield, light red solid, mp 78−80 °C). ^{1}H NMR (300 MHz, $CDCl_3$): δ 9.60 (brs, 1H), 8.82 (s, 1H), 7.79 (dd, J = 8.2, 1.8 Hz, 1H), 7.08 (d, J = 8.2 Hz, 1H), 5.81 (d, J = 7.5 Hz, 1H), 4.68−4.49 (m, 1H), 4.04 (s, 2H), 2.53−2.32 (m, 2H), 2.23 (s, 3H), 2.21 (s, 3H), 2.02−1.84 (m, 2H), 1.83−1.67 (m, 2H). MS (ESI^+) m/z: 352.4.

*Friedel−Crafts Acetylation of Pyrroles: **82**, **83a**, **b**, **84a**, **b**, **85**, and **86**.* Appropriately substituted ethyl pyrrole-2-carboxylate (**79−81**) (1 equiv) and aroyl chloride (1.5 equiv) were dissolved in anhydrous CH_2Cl_2 (50 mL) under argon and cooled to 0 °C in an ice/water bath. $AlCl_3$ (3 equiv) was added portion wise to the reaction mixture and stirred at RT for 16 h. The completion of the reaction was determined by UPLC. Then, the reaction mixture was poured into ice water (50 mL) slowly. The resulting reaction mixture was extracted with dichloromethane (2 × 150 mL). The combined organic layer was washed with saturated sodium bicarbonate solution, dried (Na_2SO_4), and concentrated. The resulting concentrated product was purified by column chromatography using 10−50% ethyl acetate in petroleum ether to afford **82**, **83a**, **b**, **84a**, **b**, **85**, and **86** (40−50% yield).

*Partial Reduction of Ketone: **87**, **88a**, **b**, **89a**, **b**, **90**, and **91**.* Sodium borohydride (1.5 equiv) was added slowly to a solution of appropriate ketones **82**, **83a**, **b**, **84a**, **b**, **85**, and **86** (1 equiv) in ethanol (6 mL) at 0 °C. The reaction mixture was stirred for 1 h at RT. Then, the reaction mixture was concentrated under reduced pressure, dissolved in water, and extracted with ethyl acetate (2 × 30 mL). The combined organic layers were washed with brine solution, dried over Na_2SO_4, and concentrated to afford compounds **87**, **88a**, **b**, **89a**, **b**, **90**, **and 91**, respectively (80−90% yield). The product was taken for the next step without any purification.

*Silane Reduction in Acidic Media **92**, **93a**, **b**, **94a**, **b**, **95**, and **67**.* To a stirred solution of compounds **87**, **88a**, **b**, **89a**, **b**, **90**, and **91** (1 equiv) in trifluoroacetic acid (TFA) (4 equiv) was added triethylsilane (2 equiv). The reaction mixture was stirred at 85 °C for 1 h. Then, saturated $NaHCO_3$ (10 mL) was added dropwise to the reaction mixture and was extracted with ethyl acetate (3 × 20 mL, with careful venting). The resulting ethyl acetate was dried (Na_2SO_4), filtered, and concentrated to dryness on a rotary evaporator. The resulting concentrated product was triturated with pet ether to afford

https://dx.doi.org/10.1021/acs.jmedchem.0c00311
J. Med. Chem. 2020, 63, 4929−4956

compounds **92**, **93a**, **b**, **94a**, **b**, **95**, and **67** as a white solid (36−50% yield).

*Ester Hydrolysis: Preparation of **96**, **97a**, **b**, **98a**, **b**, and **99**.* Compounds **92**, **93a**, **b**, **94a**, **b** and **95** (300 mg, 1.0 mmol) and NaOH (80 mg, 2.01 mmol) in EtOH/water (8:2 mL) were heated to 80 °C for 2 h. After concentration, water (10 mL) was added to the residue and acidified with 10% citric acid solution. The solid was collected on a filter, washed with water, and dried to afford compounds **96**, **97a**, **b**, **98a**, **b**, and **99** as an off white solid. (60−80% yield).

General Synthetic Method for Amides (26−51, 55, 56, and 68). Pyrrole acid **96**, **97a**, **b**, **98a**, **b**, and **99** (1 equiv) in dichloromethane (2 mL) was added to appropriate amine (1.1 equiv) and triethylamine (2 equiv) and stirred for 5 min. Then, HATU (1.5 equiv) was added to the reaction mixture and stirred for 4 h at RT. After completion of the starting material (monitored by TLC), water was added to the reaction mixture and extracted with dichloromethane (2 × 30 mL). Combined organic layers were dried over Na_2SO_4 and concentrated under reduced pressure. The resulting concentrated product was purified by column chromatography using 10−50% ethyl acetate in pet ether to afford **26−51**, **55**, **56**, and **68**.

*N-Cyclopropyl-4-((6-(trifluoromethyl)pyridin-3-yl)methyl)-1H-pyrrole-2-carboxamide (**26**).* (DSM501). (42% yield, off white solid). ^{1}H NMR (400 MHz, DMSO-d_6): δ 11.26 (s, 1H), 8.65 (s, 1H), 7.81−7.87 (m, 3H), 6.75 (s, 1H), 6.53 (s, 1H), 3.87 (s, 2H), 2.69−2.74 (m, 1H), 0.62−0.65 (m, 2H), 0.46−0.48 (m, 2H). MS (ESI$^+$) m/z: 310.2.

*N-Cyclopropyl-5-methyl-4-((6-(trifluoromethyl)pyridin-3-yl)-methyl)-1H-pyrrole-2-carboxamide (**27**).* (DSM503). (41%, off white solid). ^{1}H NMR (400 MHz, DMSO-d_6): δ (ppm): 11.13 (s, 1H), 8.62 (s, 1H), 7.79−7.83 (m, 2H), 7.73 (d, J = 3.8 Hz, 1H), 6.44 (d, J = 2.2 Hz, 1H), 3.80 (s, 2H), 2.68−2.74 (m, 1H), 2.16 (s, 3H), 0.59−0.63 (m, 2H), 0.44−0.47 (m, 2H). MS (ESI$^+$) m/z: 324.2.

*(5-Methyl-4-((6-(trifluoromethyl)pyridin-3-yl)methyl)-1H-pyrrol-2-yl)(pyrrolidin-1-yl) Methanone (**28**).* (DSM506). (85% yield, off white solid). ^{1}H NMR (400 MHz, DMSO-d_6): δ (ppm) 11.15 (s, 1H), 8.64 (s, 1H), 8.78−7.84 (m, 2H), 6.44 (d, J = 2.4 Hz, 1H), 3.84 (s, 2H), 3.45−3.59 (m, 4H), 2.15 (s, 3H), 1.80−1.90 (m, 4H); MS (ESI$^+$) m/z: 338.2.

*(5-Methyl-4-((6-(trifluoromethyl)pyridin-3-yl)methyl)-1H-pyrrol-2-yl)(piperidin-1-yl) Methanone (**29**).* (DSM507). (61% yield, off white solid). ^{1}H NMR (400 MHz, DMSO-d_6): δ (ppm) 11.11 (s, 1H), 8.62 (s, 1H), 7.78−7.83 (m, 2H), 6.27 (d, J = 2.7 Hz, 1H), 3.81 (s, 2H), 3.58 (t, J = 5.3 Hz, 4H), 2.12 (s, 3H), 1.57−1.62 (m, 2H), 1.45−1.51 (m, 4H): MS (ESI$^+$) m/z: 352.2.

*N-Isopropyl-5-methyl-4-((6-(trifluoromethyl)pyridin-3-yl)-methyl)-1H-pyrrole-2-carboxamide (**30**).* (DSM511). (39% yield, off white solid). ^{1}H NMR (400 MHz, DMSO-d_6): δ (ppm): 11.10 (s, 1H), 8.64 (s, 1H), 7.82 (s, 2H), 7.50 (d, J = 8.0 Hz, 1H), 6.49 (s, 1H), 3.97−4.02 (m, 1H), 3.80 (s, 2H), 2.16 (s, 3H), 1.08 (d, J = 6.4 Hz, 6H): MS (ESI$^+$) m/z: 326.2.

*N-(tert-Butyl)-5-methyl-4-((6-(trifluoromethyl)pyridin-3-yl)-methyl)-1H-pyrrole-2-carboxamide (**31**).* (DSM512). (50% yield, off white solid). ^{1}H NMR (400 MHz, DMSO-d_6): δ (ppm) 11.03 (s, 1H), 8.63 (s, 1H), 7.81 (s, 2H), 7.05 (s, 1H), 6.51 (s, 1H), 3.80 (s, 2H), 2.15 (s, 3H), 1.32 (s, 9H): MS (ESI$^+$) m/z: 340.2.

*5-Methyl-N-(tetrahydro-2H-pyran-4-yl)-4-((6-(trifluoromethyl)-pyridin-3-yl)methyl)-1H-pyrrole-2-carboxamide (**32**).* (DSM513). (39% yield, off white solid). ^{1}H NMR (400 MHz, DMSO-d_6): δ (ppm) 11.14 (s, 1H), 8.64 (s, 1H), 7.82 (s, 2H), 7.61 (d, J = 8.0 Hz, 1H), 6.51 (s, 1H), 3.86−3.90 (m, 7H), 2.16 (s, 3H), 1.67−1.70 (m, 2H), 1.45−1.49 (m, 2H): MS (ESI$^+$) m/z: 368.2.

*5-Methyl-N-(piperidin-4-yl)-4-((6-(trifluoromethyl)pyridin-3-yl)-methyl)-1H-pyrrole-2-carboxamide (**33**).* (DSM514). 1-Boc-4-(amino)piperidine (127 mg, 0.63 mmol) and triethylamine (0.15 mL, 1.05 mmol) were added to compound **97a** (150 mg, 0.52 mmol) in dichloromethane (4 mL) and stirred for 5 min. Then, HATU (301 mg, 0.79 mmol) was added to the reaction mixture and stirred at RT for 4 h. After completion of the reaction (monitored by TLC), water was added to the reaction mixture and extracted with dichloromethane (2 × 40 mL). The combined organic layer was dried over Na_2SO_4 and concentrated. The resulting concentrated product was purified by column chromatography using 10−90% ethyl acetate in petroleum ether to afford the intermediate (100 mg, 41% yield). The obtained intermediate was dissolved in 1,4-dioxane and added HCl in 1,4-dioxane solution (4.5 M) at 0 °C for 2 h. Then, it was concentrated under reduced pressure and washed with acetonitrile and dried to afford 5-methyl-*N*-(piperidin-4-yl)-4-((6-(trifluoromethyl) pyridin-3-yl)methyl)-1*H*-pyrrole-2-carboxamide (**33**) (69%, yield) as an off white solid. ^{1}H NMR (400 MHz, DMSO-d_6): δ (ppm) 11.28 (s, 1H), 8.89 (brs, 2H), 8.63 (s, 1H), 7.87 (d, J = 7.7 Hz, 1H), 7.82 (s, 2H), 6.55 (s, 1H), 3.95−3.97 (m, 1H), 3.81 (s, 2H), 3.25−3.28 (m, 2H), 2.95−2.97 (m, 2H), 2.08 (s, 3H), 1.87−1.90 (m, 2H), 1.70−1.72 (m, 2H); MS (ESI$^+$) m/z: 367.2.

*5-Methyl-N-(1-methylpiperidin-4-yl)-4-((6-(trifluoromethyl)-pyridin-3-yl)methyl)-1H-pyrrole-2-carboxamide (**34**).* (DSM515). (45% yield, off white solid). ^{1}H NMR (400 MHz, DMSO-d_6): δ (ppm) 11.11 (s, 1H), 8.62 (s, 1H), 7.81 (brs, 2H), 7.54 (d, J = 8.0 Hz, 1H), 6.49 (s, 1H), 3.80 (s, 2H), 3.60−3.70 (m, 1H), 2.75−2.85 (m, 2H), 2.15−2.30 (m, 6H), 1.90−2.05 (m, 2H), 1.68−1.71 (m, 2H), 1.47−1.49 (m, 2H); MS (ESI$^+$) m/z: 381.1.

*N-(Azetidin-3-yl)-5-methyl-4-((6-(trifluoromethyl)pyridin-3-yl)-methyl)-1H-pyrrole-2-carboxamide (**35**).* (DSM518). *tert*-Butyl 3-aminoazetidine-1-carboxylate (109 mg, 0.63 mmol) and triethylamine (0.15 mL, 1.05 mmol) were added to compound **97a** (150 mg, 0.53 mmol) in dichloromethane (4 mL) and stirred for 5 min. Then, HATU (301 mg, 0.79 mmol) was added to the reaction mixture and stirred at the same temperature for 4 h. After completion of the reaction (monitored by TLC), water was added to the reaction mixture and extracted with dichloromethane (2 × 40 mL). The combined organic layer was dried over Na_2SO_4 and concentrated. The resulting concentrated product was purified by column chromatography using 10−60% ethyl acetate in petroleum ether to afford the intermediate (120 mg, 51.9%). Then, the resulting obtained intermediate was dissolved in 1,4-dioxane and added HCl in dioxane solution (4.5 M) at 0 °C and stirred for 2 h. Then, it was concentrated under reduced pressure and washed with acetonitrile and dried to afford *N*-(azetidin-3-yl)-5-methyl-4-((6-(trifluoromethyl)pyridin-3-yl)methyl)-1*H*-pyrrole-2-carboxamide (**35**). (52% yield, off white solid). ^{1}H NMR (400 MHz, DMSO-d_6): δ (ppm) 11.32 (s, 1H), 8.79−8.81 (m, 2H), 8.62 (s, 1H), 8.44 (d, J = 7.1 Hz, 1H), 7.83 (s, 1H), 7.81 (d, J = 7.1 Hz, 1H), 6.49 (s, 1H), 4.77−4.71 (m, 1H), 3.95−4.08 (m, 4H), 3.82 (s, 2H), 2.16 (s, 3H); MS (ESI$^+$) m/z: 339.2.

*5-Methyl-N-(1-methylazetidin-3-yl)-4-((6-(trifluoromethyl)-pyridin-3-yl)methyl)-1H-pyrrole-2-carboxamide (**36**).* (DSM524). (16% yield, off white solid) ^{1}H NMR (400 MHz, DMSO-d_6): δ (ppm) 11.16 (s, 1H), 8.64 (s, 1H), 8.04 (d, J = 6.1 Hz, 1H), 7.83 (s, 2H), 6.54 (s, 1H), 4.36−4.38 (m, 1H), 3.81 (s, 2H), 3.51 (brs, 2H), 2.88 (brs, 2H), 2.23 (s, 3H), 2.16 (s, 3H); MS (ESI$^+$) m/z: 353.4.

*Cyclopropyl-3-methyl-4-((6-(trifluoromethyl)pyridin-3-yl)-methyl)-1H-pyrrole-2-carboxamide (**37**).* (DSM502). (44% yield, off white solid) ^{1}H NMR (400 MHz, DMSO-d_6): δ 10.85 (s, 1H), 8.61 (s, 1H), 7.79 (s, 2H), 7.42 (d, J = 7.2 Hz, 1H), 6.66−6.67 (m, 1H), 3.83 (s, 2H), 2.69−2.74 (m, 1H), 2.10 (s, 3H), 0.63−0.68 (m, 2H), 0.43−0.47 (m, 2H); MS (ESI$^+$) m/z: 324.2. See Figure S4 for the LC−MS data demonstrating purity and mass.

*Azetidin-1-yl(3-methyl-4-((6-(trifluoromethyl)pyridin-3-yl)-methyl)-1H-pyrrol-2-yl)methanone (**38**).* (DSM525). (25% yield, off white solid). ^{1}H NMR (300 MHz, $CDCl_3$): δ 8.90 (brs, 1H), 8.60 (s, 1H), 7.75−7.51 (m, 2H), 6.64 (d, J = 2.6 Hz, 1H), 4.25 (t, J = 7.45 Hz, 4H), 3.87 (s, 2H), 2.51−2.27 (m, 2H), 2.10 (s, 3H). MS (ESI$^+$) m/z: 324.8.

*3-Methyl-N-(2,2,2-trifluoroethyl)-4-((6-(trifluoromethyl)pyridin-3-yl)methyl)-1H-pyrrole-2-carboxamide (**39**).* (DSM528). (30% yield, off white solid). ^{1}H NMR (500 MHz, $CDCl_3$): δ 9.30 (brs, 1H), 8.62 (s, 1H), 7.68−7.59 (m, 2H), 6.73 (d, J = 2.93 Hz 1H), 5.92 (t, J = 5.86 Hz, 1H), 4.20−4.09 (m, 2H), 3.92 (s, 2H), 2.24 (s, 3H). MS (ESI$^+$) m/z: 366.4.

*N-Isopropyl-3-methyl-4-((6-(trifluoromethyl)pyridin-3-yl)-methyl)-1H-pyrrole-2-carboxamide (**40**).* (DSM529). (61% yield, off

https://dx.doi.org/10.1021/acs.jmedchem.0c00311
J. Med. Chem. 2020, 63, 4929−4956

white solid). ^{1}H NMR (400 MHz, DMSO-d_6): δ (ppm) 10.93 (s, 1H), 8.62 (s, 1H), 7.79 (s, 2H), 7.13 (d, 1H, J = 7.6 Hz), 6.67 (brs, 1H), 3.96−4.01 (m, 1H), 3.83 (s, 2H), 2.11 (s, 3H), 1.11 (d, 6H, J = 6.4 Hz); MS (ESI$^+$) m/z: 326.2.

*N-(tert-Butyl)-3-methyl-4-((6-(trifluoromethyl)pyridin-3-yl)-methyl)-1H-pyrrole-2-carboxamide (**41**).* (DSM530). (34% yield, white solid). ^{1}H NMR (400 MHz, DMSO-d_6): δ (ppm) 11.01 (s, 1H), 8.62 (s, 1H), 7.79 (s, 2H), 6.78 (brs, 1H), 6.67 (s, 1H), 3.83 (s, 2H), 2.10 (s, 3H), 1.33 (s, 9H); MS (ESI$^+$) m/z: 340.2.

*(3-Methyl-4-((6-(trifluoromethyl)pyridin-3-yl)methyl)-1H-pyrrol-2-yl)(pyrrolidin-1-yl) Methanone (**42**).* (DSM531). (64% yield, off white solid). ^{1}H NMR (400 MHz, DMSO-d_6): δ (ppm) 10.82 (s, 1H), 8.64 (s, 1H), 7.82 (brs, 2H), 6.62 (brs, 1H), 3.84 (s, 2H), 3.42 (t, J = 6.8 Hz, 4H), 1.97 (s, 3H), 1.79−1.82 (m, 4H); MS (ESI$^+$) m/z: 338.2.

*1-(3-Methyl-4-((6-(trifluoromethyl)pyridin-3-yl)methyl)-1H-pyrrol-2-yl)butan-1-one (**43**).* (DSM532) (Scheme S1): **Step 1**: A mixture of pyrrole ester (**93b**, 200 mg, 0.64 mmol) and sodiumhydroxide (50 mg, 1.28 mmol) in 10 mL of ethylene glycol was slowly heated to 200 °C over a 2 h period, while the distillate was collected. The mixture was then cooled to 20 °C, 10 mL of water was added, and the aqueous mixture was extracted with 3 × 20 mL of chloroform. The pooled extracts were dried over Na_2S0_4. Evaporation of the solvent under reduced pressure afforded 111 mg (73%) of 3-methylpyrrole as colorless oil that was directly used in the next step without further purification.

Step 2: To a stirred suspension of anhydrous $AlC1_3$ (1.5 equiv) in 20 mL of 1,2-dichloroethane at 0 °C was added slowly propionyl chloride (1 equiv). The resulting solution was stirred at 25 °C for 10 min, a solution of 3-methylpyrrole (0.8 equiv) in 10 mL of 1,2-dichloroethane was added slowly, and the mixture was stirred at 25 °C for 4 h. The reaction mixture was poured into ice/water, and the aqueous layer was extracted with dichloromethane (3 × 50 mL). The combined organic layer was washed with brine, dried over anhydrous Na_2SO_4, and filtered, and the solvent was removed under reduced pressure. The crude product was chromatographed on silica gel using 20% ethyl acetate in hexane to afford 1-(3-methyl-4-((6-(trifluoromethyl)pyridin-3-yl)methyl)-1*H*-pyrrol-2-yl)butan-1-one (**43**). (30% yield, off white solid).

^{1}H NMR (300 MHz, $CDCl_3$): δ 9.17 (brs, 1H), 8.62 (s, 1H), 7.69−7.55 (m, 2H), 6.73 (d, J = 3.0 Hz, 1H), 3.91 (s, 2H), 2.75 (t, J = 7.3 Hz, 2H), 2.28 (s, 3H), 1.87−1.70 (m, 2H), 1.02 (t, J = 7.45 Hz, 3H). MS (ESI$^+$) m/z: 311.3.

*Cyclopropyl(3-methyl-4-((6-(trifluoromethyl)pyridin-3-yl)-methyl)-1H-pyrrol-2-yl)methanone **44**.* (DSM536). (20% yield, off white solid). **44** was prepared according to the procedure reported for compound **43**, treating 3-methyl pyrrole intermediate with cyclopropane carbonylchloride and $AlCl_3$ afforded **44**. ^{1}H NMR (300 MHz, $CDCl_3$): δ 9.14 (brs, 1H), 8.63 (s, 1H), 7.73−7.54 (m, 2H), 6.72 (s, 1H), 3.92 (s, 2H), 2.51−2.39 (m, 1H), 2.37 (s, 3H), 1.32−1.15 (m, 2H), 1.08−0.94 (m, 2H). MS (ESI$^+$) m/z: 309.3.

*(3,3-Difluoroazetidin-1-yl)(3-methyl-4-((6-(trifluoromethyl)-pyridin-3-yl)methyl)-1H-pyrrol-2-yl)methanone (**45**).* (DSM538). (35% yield, off white solid, mp 130−132 °C). ^{1}H NMR (300 MHz, $CDCl_3$): δ 9.21 (brs, 1H), 8.59 (s, 1H), 7.68−7.58 (m, 2H), 6.68 (d, J = 3.06 Hz, 1H), 4.48 (t, J = 12.27 Hz, 4H), 3.87 (s, 2H), 2.12 (s, 3H). MS (ESI$^+$) m/z: 360.3.

*3-Methyl-N-(methylsulfonyl)-4-((6-(trifluoromethyl)pyridin-3-yl)-methyl)-1H-pyrrole-2-carboxamide (**46**).* (DSM539). (30% yield, off white solid). ^{1}H NMR (500 MHz, $CDCl_3$): δ 9.53 (brs, 1H), 8.61 (s, 1H), 8.28 (brs, 1H), 7.65−7.60 (m, 2H), 6.85 (s, 1H), 3.92 (s, 2H), 3.44 (s, 3H), 2.32 (s, 3H). MS (ESI$^+$) m/z: 362.5.

*(3-Fluoroazetidin-1-yl)(3-methyl-4-((6-(trifluoromethyl)pyridin-3-yl)methyl)-1H-pyrrol-2-yl)methanone (**47**).* (DSM546). (40% yield, off white solid, mp 108−110 °C). ^{1}H NMR (300 MHz, $CDCl_3$): δ 9.71 (brs, 1H), 8.57 (s, 1H), 7.67−7.53 (m, 2H), 6.63 (d, J = 2.9 Hz, 1H), 5.54−5.14 (m, 1H), 4.60−4.17 (m, 4H), 3.85 (s, 2H), 2.09 (s, 3H). MS (ESI$^+$) m/z: 342.2.

*N-(3,3-Difluorocyclobutyl)-3-methyl-4-((6-(trifluoromethyl)-pyridin-3-yl)methyl)-1H-pyrrole-2-carboxamide (**48**).* (DSM552). (40% yield, off white solid). ^{1}H NMR (300 MHz, $CDCl_3$): δ 9.64 (brs, 1H), 9.19 (s, 1H), 7.71−7.56 (m, 2H), 6.69 (d, J = 2.9 Hz, 1H), 3.89 (s, 2H), 3.17−3.01 (m, 2H), 2.73−2.48 (m, 2H), 2.21 (s, 3H). MS (ESI$^+$) m/z: 374.0.

*N-(3-Fluorocyclobutyl)-3-methyl-4-((6-(trifluoromethyl)pyridin-3-yl)methyl)-1H-pyrrole-2-carboxamide (**49**).* (DSM553). (60% yield, off white solid, mp 174−176 °C). ^{1}H NMR (500 MHz, $CDCl_3$): δ 9.49 (brs, 1H), 8.60 (s, 1H), 7.75−7.47 (m, 2H), 6.67 (d, J = 2.8 Hz, 1H), 5.84 (d, J = 5.8 Hz, 1H), 5.46−5.07 (m, 1H), 4.90−4.55 (m, 1H), 3.90 (s, 2H), 2.96−2.61 (m, 2H), 2.50−2.32 (m, 2H), 2.20 (s, 3H). MS (ESI$^+$) m/z: 356.2.

*3-Methyl-N-(1-(trifluoromethyl)cyclopropyl)-4-((6-(trifluoromethyl)pyridin-3-yl)methyl)-1H-pyrrole-2-carboxamide (**50**).* (DSM559). (40% yield, off white solid). ^{1}H NMR (500 MHz, $CDCl_3$): δ 9.20 (brs, 1H), 8.62 (s, 1H), 7.65−7.58 (m, 2H), 6.72 (d, J = 2.8 Hz, 1H), 6.11 (brs, 1H), 3.91 (s, 2H), 2.23 (s, 3H), 1.51−1.38 (m, 2H), 1.28−1.20 (m, 2H). MS (ESI$^+$) m/z: 392.2.

*N-Cyclobutyl-3-methyl-4-((6-(trifluoromethyl)pyridin-3-yl)-methyl)-1H-pyrrole-2-carboxamide (**51**).* (DSM560). (60% yield, off white solid). ^{1}H NMR (500 MHz, $CDCl_3$): δ 9.82 (brs, 1H), 8.59 (s, 1H), 7.68−7.49 (m, 2H), 6.62 (d, J = 2.9 Hz, 1H), 6.01 (d, J = 7.6 Hz, 1H), 4.67−4.44 (m, 1H), 3.88 (s, 2H), 2.51−2.35 (m, 2H), 2.20 (s, 3H), 1.99−1.85 (m, 2H), 1.80−1.69 (m, 2H). MS (ESI$^+$) m/z: 338.3.

*4-Methoxy-1-(6-(trifluoromethyl)pyridin-3-yl)but-2-yn-1-one (**101**).* To a solution of methyl propargyl ether **100** (4 g, 57.14 mmol) in THF (60 mL) was added *n*-BuLi (1.6 M in hexane) (25 mL, 62.85 mmol) at −78 °C and stirred for 40 min at −78 °C. Then, *N*-methoxy-*N*-methyl-6-(trifluoromethyl)nicotinamide (10.7 g, 45.7 mmol) was added to the reaction mixture at −78 °C and was stirred for 30 min at the same temperature. The reaction mixture was quenched with saturated NH_4Cl solution and extracted with ethyl acetate (2 × 300 mL) and washed with brine solution, dried over Na_2SO_4, and concentrated. The resulting concentrated product was purified by column chromatography using 20−50% ethyl acetate in pet ether to afford 4-methoxy-1-(6-(trifluoromethyl)pyridin-3-yl)but-2-yn-1-one (**101**; 6 g, 43% yield) as brown oil.

*3-(Methoxymethyl)-4-(6-(trifluoromethyl)nicotinoyl)-1H-pyrrole-2-carboxylate **102**.* To a stirred solution of compound **101** (6 g, 24.69 mmol) in NMP (30 mL) were added silver carbonate (0.68 g, 2.47 mmol) and ethyl isocyanoacetate (4.2 g, 37.04 mmol) at RT. It was stirred for 2 h at 85 °C. The reaction mixture was taken in water and extracted with ethyl acetate (2 × 200 mL). The resulting organic layer was washed with brine solution, dried over Na_2SO_4, and concentrated under reduced pressure. The resulting concentrated product was purified by column chromatography using 5−40% ethyl acetate in pet ether to afford ethyl 3-(methoxymethyl)-4-(6-(trifluoromethyl)nicotinoyl)-1*H*-pyrrole-2-carboxylate (**102**; 4.7 g, 54% yield).

*Ethyl 4-(Hydroxy(6-(trifluoromethyl)pyridin-3-yl)methyl)-3-(methoxymethyl)-1H-pyrrole-2-carboxylate (**103**).* Sodium borohydride (0.76 g, 19.8 mmol) was added to a stirred solution of compound **102** (4.7 g, 13.20 mmol) in ethanol (25 mL) and stirred for 1 h at RT. The reaction mixture was concentrated under reduced pressure, taken in water, and extracted with ethyl acetate (2 × 30 mL). The resulting organic layer was washed with brine solution, dried over Na_2SO_4, and concentrated to afford ethyl 4-(hydroxy(6-(trifluoromethyl)pyridin-3-yl)methyl)-3-(methoxymethyl)-1*H*-pyrrole-2-carboxylate (**103**; 4.5 g, 95% yield).

*Ethyl 3-(Methoxymethyl)-4-((6-(trifluoromethyl)pyrimidi-3-yl)-methyl)-1H-pyrrole-2-carboxylate (**104**).* To a stirred solution of **103** (4.5 g, 12.57 mmol) in TFA (9 mL, 75.4 mmol) was added triethylsilane (3.2 mL, 25.13 mmol). The reaction mixture was stirred at 85 °C for 1 h. The reaction mixture was quenched with saturated $NaHCO_3$ solution and extracted with ethyl acetate. The combined organic layers were dried (Na_2SO_4), filtered, and concentrated to dryness on a rotary evaporator. The resulting concentrated product was purified by column chromatography using 5−20% ethyl acetate in pet ether to afford **104** (3.6 g, 84% yield).

*3-(Methoxymethyl)-4-((6-(trifluoromethyl)pyridin-3-yl)methyl)-1H-pyrrole-2-carboxylic Acid (**105**).* NaOH (0.84 g, 11.04 mmol) was added to a stirred solution of compound **104** (3.6 g, 10.52 mmol)

https://dx.doi.org/10.1021/acs.jmedchem.0c00311
J. Med. Chem. 2020, 63, 4929−4956

and EtOH/water (18:2 mL) and the reaction mixture was heated to 80 °C for 2 h. After concentration, water (10 mL) was added and acidified with 10% citric acid solution. The solid obtained was filtered, washed with water, and dried to afford 3-(methoxymethyl)-4-((6-(trifluoromethyl)pyridin-3-yl)methyl)-1*H*-pyrrole-2-carboxylic acid, (**105**; 2.5 g, 75% yield) as an off white solid.

*N-Cyclopropyl-3-(methoxymethyl)-4-((6-(trifluoromethyl)-pyridin-3-yl)methyl)-1H-pyrrole-2-carboxamide (**52**).* (DSM534). Cyclopropyl amine (0.5 g, 9.55 mmol) was added to a solution of **105** (2.5 g, 7.96 mmol) and triethylamine (3 mL, 15.92 mmol) in dichloromethane (20 mL). Then, HATU (4.5 g, 11.94 mmol) was added to the reaction mixture and stirred for 4 h at RT. After completion of starting (monitored by TLC), water was added to the reaction mixture and extracted with dichloromethane (2 × 30 mL). The combined organic layers were dried over Na_2SO_4 and concentrated under reduced pressure. The resulting concentrated product was purified by column chromatography using 20−50% ethyl acetate in pet ether to afford *N*-cyclopropyl-3-(methoxymethyl)-4-((6-(trifluoromethyl)pyridin-3-yl)methyl)-1*H*-pyrrole-2-carboxamide (**52**, 2.1 g, 73% yield) as an off white solid. ^{1}H NMR (400 MHz, DMSO-d_6): δ (ppm) 11.33 (s, 1H), 8.62 (s, 1H), 7.75−7.84 (m, 3H), 6.70 (d, 1H, J = 3.0 Hz), 4.39 (s, 2H), 3.90 (s, 2H), 3.14 (s, 3H), 2.73−2.77 (m, 1H), 0.67−0.72 (m, 2H), 0.40−0.44 (m, 2H); MS (ESI$^+$) m/z: 354.2.

*N-Cyclopropyl-3-(hydroxymethyl)-4-((6-(trifluoromethyl)pyridin-3-yl)methyl)-1H-pyrrole-2-carboxamide (**53**).* (DSM535). 1 M BBr_3 solution (0.5 g, 9.55 mmol) was added to a stirred solution of **52** (2.0 g, 7.96 mmol) in dichloromethane (20 mL) at 0 °C and it was stirred for 1 h at the same temperature. After completion of starting material (monitored by TLC), water was added to the reaction mixture and extracted with dichloromethane (2 × 30 mL). The combined organic layers were dried over Na_2SO_4 and concentrated under reduced pressure to afford *N*-cyclopropyl-3-(hydroxymethyl)-4-((6-(trifluoromethyl)pyridin-3-yl)methyl)-1*H*-pyrrole-2-carboxamide. (**53**, 150 mg, 8%). ^{1}H NMR (400 MHz, DMSO-d_6): δ (ppm) 11.26 (s, 1H), 8.26 (s, 1H), 8.43 (d, 1H, J = 3.6 Hz), 7.79 (s, 2H), 6.65 (s, 1H), 5.62 (t, 1H, J = 4.4 Hz), 4.43 (d, 2H, J = 4.4 Hz), 3.89 (s, 2H), 2.76−2.67 (m, 1H), 0.71−0.69 (m, 2H), 0.44−0.42 (m, 2H). MS (ESI$^+$) m/z: 340.2.

*Perfluorophenyl 3-Methyl-4-((6-(trifluoromethyl) pyridin-3-yl)-methyl)-1H-pyrrole-2-carboxylate (**106**).* Pentafluorophenol (0.15 mg, 0.845 mmol) was added to a stirred solution of 3-methyl-4-((6-(trifluoromethyl)pyridin-3-yl)methyl)-1*H*-pyrrole-2-carboxylic acid **98b** (0.2 g, 1.53 mmol) and DCC (0.17 g, 0.84) in THF (5 mL) at RT. It was stirred for 1 h. The reaction mixture was filtered through and the filtrate was concentrated under reduced pressure. The concentrated product was purified by flash chromatography (silica gel, eluting with hexane/EtOAc mixtures from 100 to 80:20%) to afford perfluorophenyl 3-methyl-4-((6-(trifluoromethyl)pyridin-3-yl)-methyl)-1*H*-pyrrole-2-carboxylate (**106**; 0.16 mg, 48% yield) as a white solid.

*Perfluorophenyl 5-Iodo-3-methyl-4-((6-(trifluoromethyl)pyridin-3-yl)methyl)-1H-pyrrole-2-carboxylate (**107**).* *N*-Iodosuccinimide (82 mg, 0.366 mmol) was added to a stirred solution of **106** (0.15 mg, 0.33 mmol) in DMF (1 mL) at 0 °C. The reaction mixture was stirred at RT for 1 h. After stirring for 1 h, the reaction mixture was poured into water and filtered and dried to afford perfluorophenyl 5-iodo-3-methyl-4-((6-(trifluoromethyl)pyridin-3-yl)methyl)-1*H*-pyrrole-2-carboxylate (**107**; 0.15 g, 79% yield) as an off white solid.

*Perfluorophenyl 3-Methyl-5-(trifluoromethyl)-4-((6-(trifluoromethyl)pyridin-3-yl)methyl)-1H-pyrrole-2-carboxylate (**108**).* Methyl 2,2-difluoro-2-(fluorosulfonyl)acetate (100 mg, 0.52 mmol) was added to a solution of **107** (0.15 g, 0.26 mmol) and CuI (15 mg, 0.08 mmol) in NMP (2 mL) at RT and it was heated to 120 °C for 16 h. The reaction mixture was cooled to RT and water (10 mL) was added. It was extracted with ethyl acetate (2 × 30 mL), washed with brine solution, dried over Na_2SO_4, and concentrated. The resulting concentrated product was purified by column chromatography using 0−5% ethyl acetate in pet ether to afford perfluorophenyl 3-methyl-5-(trifluoromethyl)-4-((6-(trifluoromethyl)pyridin-3-yl)methyl)-1*H*-pyrrole-2-carboxylate (**108**); (15 mg, 11% yield) as a white solid.

*N-Cyclopropyl-3-methyl-5-(trifluoromethyl)-4-((6-(trifluoromethyl)pyridin-3-yl)methyl)-1H-pyrrole-2carboxamide (**54**).* (DSM526). Cyclopropyl amine (13 mg, 0.23 mmol) was added to a solution of **108** (60 mg, 0.12 mmol) in THF (1 mL) and stirred for 30 min. After 30 min, the reaction mixture was concentrated and triturated with pet ether to afford *N*-cyclopropyl-3-methyl-5-(trifluoromethyl)-4-((6-(trifluoromethyl)pyridin-3-yl)methyl)-1*H*-pyrrole-2-carboxamide (**54**, 6 mg, 55% yield) as a white solid. ^{1}H NMR (400 MHz, CD_3OD): δ (ppm); 8.50 (s, 1H), 7.73 (s, 2H), 4.09 (s, 2H), 2.79−2.85 (m, 1H), 2.17 (s, 3H), 0.79−0.89 (m, 2H), 0.62−0.63 (m, 2H). MS (ESI$^+$) m/z: 392.4.

*N-Cyclopropyl-5-methyl-4-((2-(trifluoromethyl)pyrimidin-5-yl)-methyl)-1H-pyrrole-2-carboxamide (**55**).* (DSM527). (50% yield, off white solid). ^{1}H NMR (400 MHz, DMSO-d_6): δ (ppm) 11.16 (s, 1H), 8.88 (s, 2H), 7.72 (s, 1H), 6.41 (brs, 1H), 3.81 (s, 2H), 2.66−2.72 (m, 1H), 2.17 (s, 3H), 0.58−0.63 (m, 2H), 0.41−0.45 (m, 2H). MS (ESI$^+$) m/z: 325.2.

*N-Cyclopropyl-3-methyl-4-((2-(trifluoromethyl)pyrimidin-5-yl)-methyl)-1H-pyrrole-2-carboxamide (**56**).* (DSM533). (50% yield, off white solid). ^{1}HNMR (400 MHz, DMSO-d_6): δ (ppm) 10.90 (s, 1H), 8.89 (s, 2H), 7.44 (s, 1H), 6.68 (s, 1H), 3.86 (s, 2H), 2.68−2.73 (m, 1H), 2.13 (s, 3H), 0.64−0.68 (m, 2H), 0.44−0.48 (m, 2H). MS (ESI$^+$) m/z: 325.2.

Compounds (114−118). 1-Propynylmagnesium bromide (0.5 M in THF) (1.1 equiv) was added to the corresponding aryl aldehyde **109−113** (1 equiv) in THF (150 mL) at 0 °C and stirred for 2 h at RT. The reaction mixture was quenched with 1.5 N HCl solution and extracted with ethyl acetate (2 × 30 mL). The resulting organic layer was washed with brine, dried over Na_2SO_4, and concentrated to afford compounds **114−118** (11.2 g, 80−94% yield) as a colorless liquid.

Compounds (119−123). Dess−Martin (1.5 equiv) was added to a stirred solution of compounds **114−118** (1 equiv) in CH_2Cl_2 (15 mL) at RT and stirred for 2 h. The reaction mixture was quenched with saturated sodium bicarbonate solution and extracted with CH_2Cl_2. The combined organic layers were dried (Na_2SO_4), filtered, and concentrated. The concentrated product was purified by flash chromatography (silica gel, eluting with hexane/EtOAc mixtures from 100 to 80:20%) to afford the title compounds **119−123** (72−82% yield) as an off white solid.

Compounds (124−128). Compounds (**119−123**) (1 equiv) were added to a stirred solution of silver carbonate (0.1 equiv) in NMP (10 mL) at RT. Ethyl isocyanoacetate (1.5 equiv) was added at RT and stirred for 2 h at 80 °C. The reaction mixture was cooled to RT, quenched with water (800 mL), and extracted with ethyl acetate (2 × 40 mL). The combined organic layers were dried (Na_2SO_4), filtered, and concentrated. The concentrated product was purified by flash chromatography (silica gel, eluting with hexane/EtOAc mixtures from 100 to 70:30%) to afford compounds **124−128**; (35−41%, as an off white solid).

*Ethyl 4-(2,6-Difluoro-4-(trifluoromethyl)benzoyl)-3-methyl-1H-pyrrole-2-carboxylate (**129**).* Methyl 2,2-difluoro-2-(fluorosulfonyl)-acetate (1.3 g, 6.44 mmol) was added to a solution of **126** (1.2 g, 3.22 mmol), KI (53 mg, 0.32 mmol), and CuI (29 mg, 0.32 mmol) in NMP (2 mL) at RT. It was heated to 120 °C for 16 h. The reaction mixture was cooled to RT and water (20 mL) was added and extracted with ethyl acetate (2 × 30 mL). The resulting organic layer was washed with brine solution, dried over Na_2SO_4, and concentrated. The resulting concentrated product was purified by preparative HPLC to afford ethyl 4-(2,6-difluoro-4-(trifluoromethyl)benzoyl)-3-methyl-1*H*-pyrrole-2-carboxylate (**129**) (200 mg, 17% yield) as a white solid. ^{1}H NMR (400 MHz, DMSO-d_6): δ (ppm) 12.51 (s, 1H), 7.79 (s, 1H), 7.78 (s, 1H), 7.49 (s, 1H), 4.30 (q, J = 7.1 Hz, 2H), 3.78 (s, 2H), 2.67 (s, 3H), 1.26 (t, J = 7.1 Hz, 3H).

Compounds **130−134** were prepared according to the reported procedure for **87**, reducing **124**, **125**, **127**, **128**, and **129** with sodium borohydride (60−75% yield).

https://dx.doi.org/10.1021/acs.jmedchem.0c00311
J. Med. Chem. 2020, 63, 4929−4956

Compounds **57**, **59**, **61**, **63**, and **65** were prepared according to the procedure reported for compound **92**, treating with triethylsilane–TFA.

*Ethyl 3-Methyl-4-((6-(trifluoromethyl)pyridin-3-yl)methyl)-1H-pyrrole-2-carboxylate (**57**).* (DSM561) (0.1 g, 70%, white solid). ^{1}H NMR (300 MHz, DMSO-d_6): δ (ppm) 11.36 (s, 1H), 7.63 (d, J = 8.0 Hz, 2H), 7.38 (d, J = 8.0 Hz, 2H), 6.77 (s, 1H), 4.21 (q, J = 7.2 Hz, 2H), 3.87 (s, 2H), 2.13 (s, 3H), 1.27 (t, J = 7.2 Hz, 3H); MS (ESI$^+$) m/z: 312.2.

*N-Cyclopropyl-3-methyl-4-(4-(trifluoromethyl)benzyl)-1H-pyrrole-2-carboxamide (**58**).* (DSM562) (53% yield, off white solid). ^{1}H NMR (400 MHz, DMSO-d_6): δ (ppm) 10.80 (s, 1H), 7.61 (d, J = 8.0 Hz, 2H), 7.35–7.41 (m, 3H), 6.64 (s, 1H), 3.78 (s, 2H), 2.70–2.73 (m, 1H), 2.08 (s, 3H), 0.63–0.67 (m, 2H), 0.45–0.47 (m, 2H); MS (ESI$^+$) m/z: 323.2.

*Ethyl 4-(2-Fluoro-4-(trifluoromethyl)benzyl)-3-methyl-1H-pyrrole-2-carboxylate (**59**).* (DSM556) (47% yield, white solid). ^{1}H NMR (400 MHz, $CDCl_3$): δ 8.85 (s, 1H), 7.30–7.33 (m, 2H), 7.19–7.23 (m, 1H), 6.68 (s, 1H), 4.33 (q, J = 7.1 Hz, 2H), 3.86 (s, 2H), 2.27 (s, 3H), 1.38 (t, J = 7.1 Hz, 3H). MS (ESI$^+$) m/z: 330.2.

*N-Cyclopropyl-4-(2-fluoro-4-(trifluoromethyl)benzyl)-3-methyl-1H-pyrrole-2-carboxamide (**60**).* (DSM557) (36% yield, off white solid). ^{1}H NMR (400 MHz, $CDCl_3$): δ 9.13 (s, 1H), 7.30–7.32 (m, 2H), 7.16–7.20 (m, 1H), 6.68 (s, 1H), 5.84 (s, 1H), 3.85 (s, 2H), 2.85–2.87 (m, 1H), 2.16 (s, 3H), 0.86–0.90 (m, 2H), 0.60–0.62 (m, 2H). MS (ESI$^+$) m/z: 341.0.

*Ethyl 4-(2,6-Difluoro-4-(trifluoromethyl)benzyl)-3-methyl-1H-pyrrole-2-carboxylate **61**.* (DSM563) (77% yield, white solid). ^{1}H NMR (400 MHz, DMSO-d_6): δ (ppm) 10.37 (s, 1H), 7.61 (s, 1H), 7.60 (s, 1H), 6.57 (s, 1H), 4.20 (q, J = 7.2 Hz, 2H), 3.78 (s, 2H), 2.24 (s, 3H), 1.26 (t, J = 7.2 Hz, 3H); MS (ESI$^+$) m/z: 348.2.

*N-Cyclopropyl-4-(2,6-difluoro-4-(trifluoromethyl)benzyl)-3-methyl-1H-pyrrole-2-carboxamide (**62**).* (DSM564) (51% yield, off white solid). ^{1}H NMR (400 MHz, DMSO-d_6): δ (ppm) 10.82 (s, 1H), 7.62 (s, 1H), 7.60 (s, 1H), 7.45 (s, 1H), 6.47 (s, 1H), 3.75 (s, 2H), 2.71–2.72 (m, 1H), 2.21 (s, 3H), 0.64–0.66 (m, 2H), 0.44–0.46 (m, 2H); MS (ESI$^+$) m/z: 359.0.

*Ethyl 4-(2-Methoxy-4-(trifluoromethyl)benzyl)-3-methyl-1H-pyrrole-2-carboxylate (**63**).* (DSM566) (73% yield, white solid). ^{1}H NMR (400 MHz, $CDCl_3$): δ (ppm) 8.79 (s, 1H), 7.07–7.14 (m, 3H), 6.64 (s, 1H), 4.34 (q, J = 7.2 Hz, 2H), 3.91 (s, 3H), 3.79 (s, 2H), 2.27 (s, 3H), 1.38 (t, J = 7.2 Hz, 3H); MS (ESI$^+$) m/z: 342.2.

*N-Cyclopropyl-4-(2-methoxy-4-(trifluoromethyl)benzyl)-3-methyl-1H-pyrrole-2-carboxamide (**64**).* (DSM567) (64% yield, off white solid). ^{1}H NMR (400 MHz, DMSO-d_6): δ (ppm) 10.79 (s, 1H), 7.42 (d, J = 3.6 Hz, 1H), 7.19–7.21 (m, 2H), 7.10–7.12 (d, J = 7.7 Hz, 1H), 6.57 (s, 1H), 3.89 (s, 3H), 3.68 (s, 2H), 2.68–2.74 (m, 1H), 2.09 (s, 3H), 0.64–0.69 (m, 2H), 0.45–0.48 (m, 2H); MS (ESI$^+$) m/z: 353.0.

*Ethyl 4-(2-Chloro-4-(trifluoromethyl)benzyl)-3-methyl-1H-pyrrole-2-carboxylate (**65**).* (DSM570) (75% yield, white solid). ^{1}H NMR (400 MHz, $CDCl_3$): δ (ppm) 8.85 (s, 1H), 7.66 (s, 1H), 7.42 (d, J = 8.0 Hz, 1H), 7.20 (d, J = 8.0 Hz, 1H), 6.64 (s, 1H), 4.35 (q, J = 7.2 Hz, 2H), 3.93 (s, 2H), 2.26 (s, 3H), 1.38 (t, J = 7.2 Hz, 3H): MS (ESI$^+$) m/z: 346.2.

*4-(2-Chloro-4-(trifluoromethyl)benzyl)-N-cyclopropyl-3-methyl-1H-pyrrole-2-carboxamide (**66**).* (DSM571) (55% yield, off white solid). ^{1}H NMR (400 MHz, DMSO-d_6): δ (ppm) 10.86 (s, 1H), 7.82 (s, 1H), 7.63 (d, 1H, J = 7.2 Hz), 7.45 (s, 1H), 7.32 (d, 1H, J = 7.2 Hz), 6.58 (s, 1H), 3.84 (s, 2H), 2.66–2.74 (m, 1H), 2.10 (s, 3H), 0.64–0.68 (m, 2H), 0.44–0.48 (m, 2H); ESI MS m/z: 357.0.

*Ethyl 4-((6-Cyanopyridin-3-yl)methyl)-3-methyl-1H-pyrrole-2-carboxylate (**67**).* (DSM584) (50% yield, off white solid). ^{1}H NMR (500 MHz, $CDCl_3$): δ 9.06 (s, 1H), 8.60 (s, 1H), 7.68–7.48 (m, 2H), 6.68 (d, J = 3.0 Hz, 1H), 4.34 (q, J = 7.1 Hz, 2H), 3.89 (s, 2H), 2.22 (s, 3H), 1.38 (t, J = 7.1 Hz, 3H). MS (ESI$^+$) m/z: 270.2.

*N-Cyclopropyl-3-methyl-4-(pyridin-3-ylmethyl)-1H-pyrrole-2-carboxamide (**68**).* (DSM585) (45% yield, light brown solid). ^{1}H NMR (500 MHz, $CDCl_3$): δ 8.40 (s, 1H), 8.13 (m, 3H), 7.64 (d, J = 8.2 Hz, 1H), 6.57 (s, 1H), 6.43 (s, 1H), 3.85 (s, 2H), 2.99–2.90 (m, 1H), 1.99 (s, 3H), 0.92–0.80 (m, 2H), 0.69–0.51 (m, 2H). MS (ESI$^+$) m/z: 256.3.

*3-(6-(Trifluoromethyl)pyridin-3-yloxy)pentane-2,4-dione (**137**).* A mixture of commercially available 3-chloroacetylacetone (135) (0.2 mL, 1.84 mmol), 5-hydroxy-2-trifluoromethyl pyridine (**136**) (250 mg, 1.5 mmol), caesium carbonate (599 mg, 1.84 mmol), and acetone (10 mL) was heated under reflux for 5 h. After cooling, a solid was removed by filtration and it was washed with dichloromethane (25 mL), and the combined filtrates were concentrated under reduced pressure. The remaining oil was diluted with dichloromethane (25 mL), washed with 1 M hydrochloric acid (20 mL) and brine (20 mL), dried over sodium sulphate, filtered, and finally concentrated under reduced pressure. The crude product was purified by flash chromatography on silica gel eluting with 0–10% ethyl acetate in hexane to provide the titled compound (180 mg, 45%) as a white solid (**137**).

*Ethyl 3,5-Dimethyl-4-(6-(trifluoromethyl)pyridine-3yloxy)-1H-pyrrole-2-carboxylate (**138**).* Freshly prepared ethyl-2-(hydroxyimino)-3-oxobutanoate (**78**) (4 mmol) and the corresponding acetylacetone (**137**) (4 mmol) were dissolved in glacial acetic acid (25 mL) at 15 °C. Zn dust (10 mmol) was then slowly added to the mixture and allowed to react at RT with vigorous stirring for 15–20 min. The resulting mixture was heated to 60 °C for 2 h. The mixture was allowed to attain RT and was then poured into ice water. The aqueous phase was extracted with ethylacetate (3 × 25 mL), and the combined organic phases were washed with brine, dried (Na_2SO_4), filtered, and concentrated in vacuo. The residue was purified by flash column chromatography on silica gel (eluent: gradient, hexane/EtOAc = 95:5 to 70:30) to give the pyrrole ester **138** (60% yield).

*N-Cyclopropyl-3,5-dimethyl-4-(5-(trifluoromethyl)pyridin-2-yloxy)-1H-pyrrole-2-carboxamide (**74**).* (DSM537): NaOH (24 mg, 0.6 mmol) was added to a stirred solution of compound **138** (200 mg, 0.3 mmol) and EtOH/water (18:2 mL) and the reaction mixture was heated to 80 °C for 2 h. After concentration, water (10 mL) was added and acidified with 10% citric acid solution. The solid obtained was filtered, washed with water, and dried to afford a carboxylic acid intermediate which was directly used in the next step without further purification (80% yield).

Cyclopropyl amine (20 mg, 0.36 mmol) was added to a solution of carboxylic acid intermediate (100 mg, 0.33 mmol) and triethylamine (66 μL, 0.66 mmol) in dichloromethane (5 mL). Then, HATU (188 mg, 0.5 mmol) was added to the reaction mixture and stirred for 4 h at RT. After completion of starting material (monitored by TLC), water was added to the reaction mixture and extracted with dichloromethane (2 × 30 mL). The combined organic layers were dried over Na_2SO_4 and concentrated under reduced pressure. The resulting concentrated product was purified by column chromatography using 20–50% ethyl acetate in pet ether to afford compound **74**. (60% yield, off white solid, mp 124–126 °C). ^{1}H NMR (300 MHz, $CDCl_3$): δ 10.32 (brs, 1H), 8.47 (s, 1H), 7.59 (d, J = 8.7 Hz, 1H), 7.22 (dd, J = 8.7, 2.8 Hz, 1H), 5.82 (s, 1H), 2.94–2.81 (m, 1H), 2.18 (s, 3H), 2.07 (s, 3H), 0.92–0.81 (m, 2H), 0.68–0.55 (m, 2H). MS (ESI$^+$) m/z: 340.3.

Compounds **69**, **71**, and **73** were synthesized as shown in Scheme S2. Friedel–Crafts acetylation of appropriate aryl acid chloride on the corresponding pyrrole afforded compounds **69** and **70**. Further hydrolysis of ester and amide coupling with cyclopropyl amine gave aryl-pyrrole amides **71** and **72**. Partial reduction of **72** with $NaBH_4$ in ethanol afforded the hydroxy derivative **73**.

*Ethyl 3,5-Dimethyl-4-(5-(trifluoromethyl)picolinoyl)-1H-pyrrole-2-carboxylate (**69**).* (DSM504, 45% yield, off white solid): ^{1}H NMR (300 MHz, $CDCl_3$): δ 9.12 (brs, 1H), 8.94 (s, 1H), 8.14 (d, J = 8.2 Hz, 1H), 8.00 (d, J = 8.2 Hz, 1H), 4.34 (q, J = 7.1 Hz, 2H), 2.31 (s, 3H), 2.21 (s, 3H), 1.37 (t, J = 7.1 Hz, 3H). MS (ESI$^+$): 341.2.

*N-Cyclopropyl-3,5-dimethyl-4-(5-(trifluoromethyl)picolinoyl)-1H-pyrrole-2-carboxamide (**71**).* (DSM505) (55% yield, light yellow solid). ^{1}H NMR (300 MHz, $CDCl_3$): δ 10.53 (brs, 1H), 8.92 (s, 1H), 8.13 (dd, J = 8.2, 1.7 Hz, 1H), 7.99 (d, J = 8.1 Hz, 1H), 5.94 (brs, 1H), 3.02–2.71 (m, 1H), 2.24 (s, 3H), 2.20 (s, 3H), 0.96–0.77 (m, 2H), 0.72–0.48 (m, 2H). MS (ESI$^+$): 352.4.

https://dx.doi.org/10.1021/acs.jmedchem.0c00311
J. Med. Chem. 2020, 63, 4929–4956

*N-Cyclopropyl-4-(hydroxy(6-(trifluoromethyl)pyridin-3-yl)-methyl)-3-methyl-1H-pyrrole-2-carboxamide (**73**).* (DSM558) (70% yield, light red liquid). ^{1}H NMR (300 MHz, $CDCl_3$): δ 9.44 (brs, 1H), 8.74 (s, 1H), 7.95 (d, J = 8.1 Hz, 1H), 7.69 (d, J = 8.1 Hz, 1H), 6.61 (d, J = 3.0 Hz, 1H), 5.95 (s, 1H), 5.89 (brs, 1H), 2.86 (qd, J = 7.1, 3.9 Hz, 1H), 2.23 (s, 3H), 0.96−0.81 (m, 2H), 0.66−0.54 (m, 2H). MS (ESI$^+$) m/z: 340.1.

■ ASSOCIATED CONTENT

Supporting Information

The Supporting Information is available free of charge at https://pubs.acs.org/doi/10.1021/acs.jmedchem.0c00311.

Synthesis of **43** and **44**; synthesis of **69**−**73**; high-resolution MS spectra and proposed fragmentation sites for metabolite M + 16 (II) and the authentic standard for **74**; high-resolution MS spectrum and proposed fragmentation sites for the authentic standard for **53**; and MRM chromatograms for metabolite M + 16 (IV) and the authentic standard for **53** (PDF)

Molecular formula strings excel spread sheet (CSV)

LC−MS chromatograms demonstrating purity for the lead compound **37** (DSM502) and two similarly potent analogues **60** (DSM557) and **66** (DSM571) (PDF)

Accession Codes

The coordinates for the structure of *Pf*DHODH bound to **4** and **60** have been submitted to the Protein Data Bank (PDB 6VTY and 6VTN, respectively). Authors will release the atomic coordinates and experimental data upon article publication.

■ AUTHOR INFORMATION

Corresponding Author

Margaret A. Phillips − *Departments of Biochemistry, University of Texas Southwestern Medical Center at Dallas, Dallas, Texas 75390-9135, United States;* orcid.org/0000-0001-5250-5578; Email: margaret.phillips@utsouthwestern.edu

Authors

Sreekanth Kokkonda − *Departments of Chemistry and Global Health, University of Washington, Seattle, Washington 98195, United States*

Xiaoyi Deng − *Departments of Biochemistry, University of Texas Southwestern Medical Center at Dallas, Dallas, Texas 75390-9135, United States*

Karen L. White − *Centre for Drug Candidate Optimisation, Monash Institute of Pharmaceutical Sciences, Monash University, Parkville, Victoria 3052, Australia*

Farah El Mazouni − *Departments of Biochemistry, University of Texas Southwestern Medical Center at Dallas, Dallas, Texas 75390-9135, United States*

John White − *Departments of Chemistry and Global Health, University of Washington, Seattle, Washington 98195, United States*

David M. Shackleford − *Centre for Drug Candidate Optimisation, Monash Institute of Pharmaceutical Sciences, Monash University, Parkville, Victoria 3052, Australia*

Kasiram Katneni − *Centre for Drug Candidate Optimisation, Monash Institute of Pharmaceutical Sciences, Monash University, Parkville, Victoria 3052, Australia*

Francis C. K. Chiu − *Centre for Drug Candidate Optimisation, Monash Institute of Pharmaceutical Sciences, Monash University, Parkville, Victoria 3052, Australia*

Helena Barker − *Centre for Drug Candidate Optimisation, Monash Institute of Pharmaceutical Sciences, Monash University, Parkville, Victoria 3052, Australia*

Jenna McLaren − *Centre for Drug Candidate Optimisation, Monash Institute of Pharmaceutical Sciences, Monash University, Parkville, Victoria 3052, Australia*

Elly Crighton − *Centre for Drug Candidate Optimisation, Monash Institute of Pharmaceutical Sciences, Monash University, Parkville, Victoria 3052, Australia*

Gong Chen − *Centre for Drug Candidate Optimisation, Monash Institute of Pharmaceutical Sciences, Monash University, Parkville, Victoria 3052, Australia*

Inigo Angulo-Barturen − *GSK, Madrid 28760, Spain*

Maria Belen Jimenez-Diaz − *GSK, Madrid 28760, Spain*

Santiago Ferrer − *GSK, Madrid 28760, Spain*

Leticia Huertas-Valentin − *GSK, Madrid 28760, Spain*

Maria Santos Martinez-Martinez − *GSK, Madrid 28760, Spain*

Maria Jose Lafuente-Monasterio − *GSK, Madrid 28760, Spain*

Rajesh Chittimalla − *Syngene International Ltd, Bangalore 560 099, India*

Shatrughan P. Shahi − *Syngene International Ltd, Bangalore 560 099, India*

Sergio Wittlin − *Swiss Tropical and Public Health Institute, 4002 Basel, Switzerland; University of Basel, 4002 Basel, Switzerland*

David Waterson − *Medicines for Malaria Venture, 1215 Geneva, Switzerland*

Jeremy N. Burrows − *Medicines for Malaria Venture, 1215 Geneva, Switzerland*

Dave Matthews − *Medicines for Malaria Venture, 1215 Geneva, Switzerland*

Diana Tomchick − *Department of Biophysics, University of Texas Southwestern Medical Center at Dallas, Dallas, Texas 75390-9135, United States*

Pradipsinh K. Rathod − *Departments of Chemistry and Global Health, University of Washington, Seattle, Washington 98195, United States*

Michael J. Palmer − *Medicines for Malaria Venture, 1215 Geneva, Switzerland*

Susan A. Charman − *Centre for Drug Candidate Optimisation, Monash Institute of Pharmaceutical Sciences, Monash University, Parkville, Victoria 3052, Australia*

Complete contact information is available at: https://pubs.acs.org/10.1021/acs.jmedchem.0c00311

Notes

The authors declare no competing financial interest.

■ ACKNOWLEDGMENTS

The authors thank Sibylle Sax (Swiss TPH) for technical assistance with the SCID mouse model. Results shown in this report are derived from work performed at the Argonne National Laboratory, Structural Biology Center at the Advanced Photon Source. This work was supported by funds from the United States National Institutes of Health grant, R01AI103947 (to MAP and PKR), and from Medicines for Malaria Venture (MMV). MAP acknowledges the support of the Welch Foundation (I-1257). MAP holds the Sam G. Winstead and F. Andrew Bell Distinguished Chair in Biochemistry.

■ ABBREVIATIONS

DHODH, dihydroorotate dehydrogenase; *Pf*, *Plasmodium* falciparum; *Pv*, *Plasmodium vivax*; *h*DHODH, human DHODH; *m*DHODH, mouse DHODH; *r*DHODH, rat DHODH; *d*DHODH, dog DHODH; *Pf*3D7, *P. falciparum* 3D7 parasites; *Pf*Dd2, *P. falciparum* Dd2 parasites; PG, proguanil; CQ, chloroquine; Py, pyrimethamine; SD, sulphadoxine; MF, mefloquine; CG, cycloguanil

■ REFERENCES

(1) World Health Organization. Leading Causes of Death. https://www.who.int/news-room/fact-sheets/detail/the-top-10-causes-of-death (accessed Feb 27, 2020).

(2) World Health Organization. *World Malaria Report 2019*. ISBN: 978-92-4-156572-1, Geneva, Switzerland, 2019.

(3) Miller, L. H.; Ackerman, H. C.; Su, X.-z.; Wellems, T. E. Malaria biology and disease pathogenesis: insights for new treatments. *Nat. Med.* **2013**, *19*, 156−167.

(4) Phillips, M. A.; Burrows, J. N.; Manyando, C.; van Huijsduijnen, R. H.; Van Voorhis, W. C.; Wells, T. N. C. Malaria. *Nat. Rev. Dis. Primers* **2017**, *3*, 17050.

(5) White, N. J.; Pukrittayakamee, S.; Hien, T. T.; Faiz, M. A.; Mokuolu, O. A.; Dondorp, A. M. Malaria. *Lancet* **2014**, *383*, 723−735.

(6) Schuerman, L. RTS,S malaria vaccine could provide major public health benefits. *Lancet* **2019**, *394*, 735−736.

(7) Adepoju, P. RTS,S malaria vaccine pilots in three African countries. *Lancet* **2019**, *393*, 1685.

(8) Haldar, K.; Bhattacharjee, S.; Safeukui, I. Drug resistance in Plasmodium. *Nat. Rev. Microbiol.* **2018**, *16*, 156−170.

(9) Goldberg, D. E.; Siliciano, R. F.; Jacobs, W. R., Jr. Outwitting evolution: fighting drug-resistant TB, malaria, and HIV. *Cell* **2012**, *148*, 1271−1283.

(10) Tilley, L.; Straimer, J.; Gnädig, N. F.; Ralph, S. A.; Fidock, D. A. Artemisinin action and resistance in Plasmodium falciparum. *Trends Parasitol.* **2016**, *32*, 682−696.

(11) Plewes, K.; Leopold, S. J.; Kingston, H. W. F.; Dondorp, A. M. Malaria: What's new in the management of malaria? *Infect. Dis. Clin.* **2019**, *33*, 39−60.

(12) Menard, D.; Dondorp, A. Antimalarial drug resistance: a threat to malaria elimination. *Cold Spring Harbor Perspect. Med.* **2017**, *7*, a025619.

(13) Hooft van Huijsduijnen, R.; Wells, T. N. The antimalarial pipeline. *Curr. Opin. Pharmacol.* **2018**, *42*, 1−6.

(14) Charman, S. A.; Arbe-Barnes, S.; Bathurst, I. C.; Brun, R.; Campbell, M.; Charman, W. N.; Chiu, F. C. K.; Chollet, J.; Craft, J. C.; Creek, D. J.; Dong, Y.; Matile, H.; Maurer, M.; Morizzi, J.; Nguyen, T.; Papastogiannidis, P.; Scheurer, C.; Shackleford, D. M.; Sriraghavan, K.; Stingelin, L.; Tang, Y.; Urwyler, H.; Wang, X.; White, K. L.; Wittlin, S.; Zhou, L.; Vennerstrom, J. L. Synthetic ozonide drug candidate OZ439 offers new hope for a single-dose cure of uncomplicated malaria. *Proc. Natl. Acad. Sci. U.S.A.* **2011**, *108*, 4400−4405.

(15) Moehrle, J. J.; Duparc, S.; Siethoff, C.; van Giersbergen, P. L.; Craft, J. C.; Arbe-Barnes, S.; Charman, S. A.; Gutierrez, M.; Wittlin, S.; Vennerstrom, J. L. First-in-man safety and pharmacokinetics of synthetic ozonide OZ439 demonstrates an improved exposure profile relative to other peroxide antimalarials. *Br. J. Clin. Pharmacol.* **2013**, *75*, 535−548.

(16) Kuhen, K. L.; Chatterjee, A. K.; Rottmann, M.; Gagaring, K.; Borboa, R.; Buenviaje, J.; Chen, Z.; Francek, C.; Wu, T.; Nagle, A.; Barnes, S. W.; Plouffe, D.; Lee, M. C. S.; Fidock, D. A.; Graumans, W.; van de Vegte-Bolmer, M.; van Gemert, G. J.; Wirjanata, G.; Sebayang, B.; Marfurt, J.; Russell, B.; Suwanarusk, R.; Price, R. N.; Nosten, F.; Tungtaeng, A.; Gettayacamin, M.; Sattabongkot, J.; Taylor, J.; Walker, J. R.; Tully, D.; Patra, K. P.; Flannery, E. L.; Vinetz, J. M.; Renia, L.; Sauerwein, R. W.; Winzeler, E. A.; Glynne, R. J.; Diagana, T. T. KAF156 is an antimalarial clinical candidate with potential for use in prophylaxis, treatment, and prevention of disease transmission. *Antimicrob. Agents Chemother.* **2014**, *58*, 5060−5067.

(17) White, N. J.; Duong, T. T.; Uthaisin, C.; Nosten, F.; Phyo, A. P.; Hanboonkunupakarn, B.; Pukrittayakamee, S.; Jittamala, P.; Chuthasmit, K.; Cheung, M. S.; Feng, Y.; Li, R.; Magnusson, B.; Sultan, M.; Wieser, D.; Xun, X.; Zhao, R.; Diagana, T. T.; Pertel, P.; Leong, F. J. Antimalarial activity of KAF156 in falciparum and vivax malaria. *N. Engl. J. Med.* **2016**, *375*, 1152−1160.

(18) Rottmann, M.; McNamara, C.; Yeung, B. K. S.; Lee, M. C. S.; Zou, B.; Russell, B.; Seitz, P.; Plouffe, D. M.; Dharia, N. V.; Tan, J.; Cohen, S. B.; Spencer, K. R.; Gonzalez-Paez, G. E.; Lakshminarayana, S. B.; Goh, A.; Suwanarusk, R.; Jegla, T.; Schmitt, E. K.; Beck, H.-P.; Brun, R.; Nosten, F.; Renia, L.; Dartois, V.; Keller, T. H.; Fidock, D. A.; Winzeler, E. A.; Diagana, T. T. Spiroindolones, a potent compound class for the treatment of malaria. *Science* **2010**, *329*, 1175−1180.

(19) White, N. J.; Pukrittayakamee, S.; Phyo, A. P.; Rueangweerayut, R.; Nosten, F.; Jittamala, P.; Jeeyapant, A.; Jain, J. P.; Lefèvre, G.; Li, R.; Magnusson, B.; Diagana, T. T.; Leong, F. J. Spiroindolone KAE609 for falciparum and vivax malaria. *N. Engl. J. Med.* **2014**, *371*, 403−410.

(20) Phillips, M. A.; Gujjar, R.; Malmquist, N. A.; White, J.; El Mazouni, F.; Baldwin, J.; Rathod, P. K. Triazolopyrimidine-based dihydroorotate dehydrogenase inhibitors with potent and selective activity against the malaria parasite, Plasmodium falciparum. *J. Med. Chem.* **2008**, *51*, 3649−3653.

(21) Coteron, J. M.; Marco, M.; Esquivias, J.; Deng, X.; White, K. L.; White, J.; Koltun, M.; El Mazouni, F.; Kokkonda, S.; Katneni, K.; Bhamidipati, R.; Shackleford, D. M.; Angulo-Barturen, I.; Ferrer, S. B.; Jiménez-Díaz, M. B.; Gamo, F.-J.; Goldsmith, E. J.; Charman, W. N.; Bathurst, I.; Floyd, D.; Matthews, D.; Burrows, J. N.; Rathod, P. K.; Charman, S. A.; Phillips, M. A. Structure-guided lead optimization of triazolopyrimidine-ring substituents identifies potent Plasmodium falciparum dihydroorotate dehydrogenase inhibitors with clinical candidate potential. *J. Med. Chem.* **2011**, *54*, 5540−5561.

(22) Phillips, M. A.; Lotharius, J.; Marsh, K.; White, J.; Dayan, A.; White, K. L.; Njoroge, J. W.; El Mazouni, F.; Lao, Y.; Kokkonda, S.; Tomchick, D. R.; Deng, X.; Laird, T.; Bhatia, S. N.; March, S.; Ng, C. L.; Fidock, D. A.; Wittlin, S.; Lafuente-Monasterio, M.; Benito, F. J. G.; Alonso, L. M. S.; Martinez, M. S.; Jimenez-Diaz, M. B.; Bazaga, S. F.; Angulo-Barturen, I.; Haselden, J. N.; Louttit, J.; Cui, Y.; Sridhar, A.; Zeeman, A.-M.; Kocken, C.; Sauerwein, R.; Dechering, K.; Avery, V. M.; Duffy, S.; Delves, M.; Sinden, R.; Ruecker, A.; Wickham, K. S.; Rochford, R.; Gahagen, J.; Iyer, L.; Riccio, E.; Mirsalis, J.; Bathhurst, I.; Rueckle, T.; Ding, X.; Campo, B.; Leroy, D.; Rogers, M. J.; Rathod, P. K.; Burrows, J. N.; Charman, S. A. A long-duration dihydroorotate dehydrogenase inhibitor (DSM265) for prevention and treatment of malaria. *Sci. Transl. Med.* **2015**, *7*, 296ra111.

(23) Llanos-Cuentas, A.; Casapia, M.; Chuquiyauri, R.; Hinojosa, J.-C.; Kerr, N.; Rosario, M.; Toovey, S.; Arch, R. H.; Phillips, M. A.; Rozenberg, F. D.; Bath, J.; Ng, C. L.; Cowell, A. N.; Winzeler, E. A.; Fidock, D. A.; Baker, M.; Möhrle, J. J.; Hooft van Huijsduijnen, R.; Gobeau, N.; Araeipour, N.; Andenmatten, N.; Rückle, T.; Duparc, S. Antimalarial activity of single-dose DSM265, a novel plasmodium dihydroorotate dehydrogenase inhibitor, in patients with uncomplicated Plasmodium falciparum or Plasmodium vivax malaria infection: a proof-of-concept, open-label, phase 2a study. *Lancet Infect. Dis.* **2018**, *18*, 874−883.

(24) McCarthy, J. S.; Lotharius, J.; Rückle, T.; Chalon, S.; Phillips, M. A.; Elliott, S.; Sekuloski, S.; Griffin, P.; Ng, C. L.; Fidock, D. A.; Marquart, L.; Williams, N. S.; Gobeau, N.; Bebrevska, L.; Rosario, M.; Marsh, K.; Möhrle, J. J. Safety, tolerability, pharmacokinetics, and activity of the novel long-acting antimalarial DSM265: a two-part first-in-human phase 1a/1b randomised study. *Lancet Infect. Dis.* **2017**, *17*, 626−635.

(25) Collins, K. A.; Ruckle, T.; Elliott, S.; Marquart, L.; Ballard, E.; Chalon, S.; Griffin, P.; Mohrle, J. J.; McCarthy, J. S. DSM265 at 400 milligrams clears asexual stage parasites but not mature gametocytes from the blood of healthy subjects experimentally infected with

https://dx.doi.org/10.1021/acs.jmedchem.0c00311
J. Med. Chem. 2020, 63, 4929−4956

Plasmodium falciparum. *Antimicrob. Agents Chemother.* **2019**, *63*, No. e01837-18.
(26) Phillips, M. A.; White, K. L.; Kokkonda, S.; Deng, X.; White, J.; El Mazouni, F.; Marsh, K.; Tomchick, D. R.; Manjalanagara, K.; Rudra, K. R.; Wirjanata, G.; Noviyanti, R.; Price, R. N.; Marfurt, J.; Shackleford, D. M.; Chiu, F. C. K.; Campbell, M.; Jimenez-Diaz, M. B.; Bazaga, S. F.; Angulo-Barturen, I.; Martinez, M. S.; Lafuente-Monasterio, M.; Kaminsky, W.; Silue, K.; Zeeman, A.-M.; Kocken, C.; Leroy, D.; Blasco, B.; Rossignol, E.; Rueckle, T.; Matthews, D.; Burrows, J. N.; Waterson, D.; Palmer, M. J.; Rathod, P. K.; Charman, S. A. A Triazolopyrimidine-Based Dihydroorotate Dehydrogenase Inhibitor with Improved Drug-like Properties for Treatment and Prevention of Malaria. *ACS Infect. Dis.* **2016**, *2*, 945−957.
(27) Lynch, J. J., 3rd; Rossignol, E.; Moehrle, J. J.; Van Vleet, T. R.; Marsh, K. C.; Parman, T.; Mirsalis, J.; Ottinger, S. E.; Segreti, J. A.; Rao, M.; Mittelstadt, S. W. Increased stress associated with head-out plethysmography testing can exacerbate respiratory effects and lead to mortality in rats. *J. Pharmacol. Toxicol. Methods* **2019**, *99*, 106580.
(28) Booker, M. L.; Bastos, C. M.; Kramer, M. L.; Barker, R. H., Jr.; Skerlj, R.; Sidhu, A. B.; Deng, X.; Celatka, C.; Cortese, J. F.; Guerrero Bravo, J. E.; Crespo Llado, K. N.; Serrano, A. E.; Angulo-Barturen, I.; Jiménez-Díaz, M. B.; Viera, S.; Garuti, H.; Wittlin, S.; Papastogiannidis, P.; Lin, J.-w.; Janse, C. J.; Khan, S. M.; Duraisingh, M.; Coleman, B.; Goldsmith, E. J.; Phillips, M. A.; Munoz, B.; Wirth, D. F.; Klinger, J. D.; Wiegand, R.; Sybertz, E. Novel inhibitors of Plasmodium falciparum dihydroorotate dehydrogenase with anti-malarial activity in the mouse model. *J. Biol. Chem.* **2010**, *285*, 33054−33064.
(29) Phillips, M. A. Antimalarial agents targeting nucleotide synthesis and electron transport: insight from structural biology. In *Neglected Diseases and Drug Discovery*; Palmer, M., Wells, T. N. C., Eds.; RCS Publishing: Cambridge, U.K., 2011; pp 65−87.
(30) Phillips, M. A.; Rathod, P. K. Plasmodium dihydroorotate dehydrogenase: a promising target for novel anti-malarial chemotherapy. *Infect. Disord.: Drug Targets* **2010**, *10*, 226−239.
(31) Flannery, E. L.; Foquet, L.; Chuenchob, V.; Fishbaugher, M.; Billman, Z.; Navarro, M. J.; Betz, W.; Olsen, T. M.; Lee, J.; Camargo, N.; Nguyen, T.; Schafer, C.; Sack, B. K.; Wilson, E. M.; Saunders, J.; Bial, J.; Campo, B.; Charman, S. A.; Murphy, S. C.; Phillips, M. A.; Kappe, S. H.; Mikolajczak, S. A. Assessing drug efficacy against Plasmodium falciparum liver stages in vivo. *JCI Insight* **2018**, *3*, No. e92587.
(32) Murphy, S. C.; Duke, E. R.; Shipman, K. J.; Jensen, R. L.; Fong, Y.; Ferguson, S.; Janes, H. E.; Gillespie, K.; Seilie, A. M.; Hanron, A. E.; Rinn, L.; Fishbaugher, M.; VonGoedert, T.; Fritzen, E.; Kappe, S. H.; Chang, M.; Sousa, J. C.; Marcsisin, S. R.; Chalon, S.; Duparc, S.; Kerr, N.; Möhrle, J. J.; Andenmatten, N.; Rueckle, T.; Kublin, J. G. A Randomized trial evaluating the prophylactic activity of dsm265 against preerythrocytic Plasmodium falciparum infection during controlled human malarial infection by mosquito bites and direct venous inoculation. *J. Infect. Dis.* **2018**, *217*, 693−702.
(33) Sulyok, M.; Rückle, T.; Roth, A.; Mürbeth, R. E.; Chalon, S.; Kerr, N.; Samec, S. S.; Gobeau, N.; Calle, C. L.; Ibáñez, J.; Sulyok, Z.; Held, J.; Gebru, T.; Granados, P.; Brückner, S.; Nguetse, C.; Mengue, J.; Lalremruata, A.; Sim, B. K. L.; Hoffman, S. L.; Möhrle, J. J.; Kremsner, P. G.; Mordmüller, B. DSM265 for Plasmodium falciparum chemoprophylaxis: a randomised, double blinded, phase 1 trial with controlled human malaria infection. *Lancet Infect. Dis.* **2017**, *17*, 636−644.
(34) White, J.; Dhingra, S. K.; Deng, X.; El Mazouni, F.; Lee, M. C. S.; Afanador, G. A.; Lawong, A.; Tomchick, D. R.; Ng, C. L.; Bath, J.; Rathod, P. K.; Fidock, D. A.; Phillips, M. A. Identification and mechanistic Understanding of dihydroorotate dehydrogenase point mutations in Plasmodium falciparum that confer in vitro resistance to the clinical candidate DSM265. *ACS Infect. Dis.* **2019**, *5*, 90−101.
(35) Baldwin, J.; Michnoff, C. H.; Malmquist, N. A.; White, J.; Roth, M. G.; Rathod, P. K.; Phillips, M. A. High-throughput screening for potent and selective inhibitors of Plasmodium falciparum dihydroorotate dehydrogenase. *J. Biol. Chem.* **2005**, *280*, 21847−21853.
(36) Patel, V.; Booker, M.; Kramer, M.; Ross, L.; Celatka, C. A.; Kennedy, L. M.; Dvorin, J. D.; Duraisingh, M. T.; Sliz, P.; Wirth, D. F.; Clardy, J. Identification and characterization of small molecule inhibitors of Plasmodium falciparum dihydroorotate dehydrogenase. *J. Biol. Chem.* **2008**, *283*, 35078−35085.
(37) Liu, J.; Fang, Z.; Zhang, Q.; Liu, Q.; Bi, X. Silver-catalyzed isocyanide-alkyne cycloaddition: a general and practical method to oligosubstituted pyrroles. *Angew. Chem., Int. Ed. Engl.* **2013**, *52*, 6953−6957.
(38) Eusterwiemann, S.; Martinez, H.; Dolbier, W. R., Jr. Methyl 2,2-difluoro-2-(fluorosulfonyl)acetate, a difluorocarbene reagent with reactivity comparable to that of trimethylsilyl 2,2-difluoro-2-(fluorosulfonyl)acetate (TFDA). *J. Org. Chem.* **2012**, *77*, 5461−5464.
(39) Falck, J. R.; Barma, D. K.; Mioskowski, C.; Schlama, T. α-chlorovinylation: Synthesis of 2-chloropropenyl and propargyl alcohols. *Tetrahedron Lett.* **1999**, *40*, 2091−2094.
(40) Deng, X.; Kokkonda, S.; El Mazouni, F.; White, J.; Burrows, J. N.; Kaminsky, W.; Charman, S. A.; Matthews, D.; Rathod, P. K.; Phillips, M. A. Fluorine modulates species selectivity in the triazolopyrimidine class of Plasmodium falciparum dihydroorotate dehydrogenase inhibitors. *J. Med. Chem.* **2014**, *57*, 5381−5394.
(41) Chen, V. B.; Arendall, W. B.; Headd, J. J.; Keedy, D. A.; Immormino, R. M.; Kapral, G. J.; Murray, L. W.; Richardson, J. S.; Richardson, D. C. MolProbity: all-atom structure validation for macromolecular crystallography. *Acta Crystallogr., Sect. D: Biol. Crystallogr.* **2010**, *66*, 12−21.
(42) Ganesan, S. M.; Morrisey, J. M.; Ke, H.; Painter, H. J.; Laroiya, K.; Phillips, M. A.; Rathod, P. K.; Mather, M. W.; Vaidya, A. B. Yeast dihydroorotate dehydrogenase as a new selectable marker for Plasmodium falciparum transfection. *Mol. Biochem. Parasitol.* **2011**, *177*, 29−34.
(43) Painter, H. J.; Morrisey, J. M.; Mather, M. W.; Vaidya, A. B. Specific role of mitochondrial electron transport in blood-stage Plasmodium falciparum. *Nature* **2007**, *446*, 88−91.
(44) Obach, R. S.; Walsky, R. L.; Venkatakrishnan, K. Mechanism-based inactivation of human cytochrome p450 enzymes and the prediction of drug-drug interactions. *Drug Metab. Dispos.* **2007**, *35*, 246−255.
(45) Mandt, R. E. K.; Lafuente-Monasterio, M. J.; Sakata-Kato, T.; Luth, M. R.; Segura, D.; Pablos-Tanarro, A.; Viera, S.; Magan, N.; Ottilie, S.; Winzeler, E. A.; Lukens, A. K.; Gamo, F. J.; Wirth, D. F. In vitro selection predicts malaria parasite resistance to dihydroorotate dehydrogenase inhibitors in a mouse infection model. *Sci. Transl. Med.* **2019**, *11*, No. eaav1636.
(46) Ross, L. S.; Lafuente-Monasterio, M. J.; Sakata-Kato, T.; Mandt, R. E. K.; Gamo, F. J.; Wirth, D. F.; Lukens, A. K. Identification of collateral sensitivity to dihydroorotate dehydrogenase inhibitors in Plasmodium falciparum. *ACS Infect. Dis.* **2018**, *4*, 508−515.
(47) Burrows, J. N.; Duparc, S.; Gutteridge, W. E.; Hooft van Huijsduijnen, R.; Kaszubska, W.; Macintyre, F.; Mazzuri, S.; Mohrle, J. J.; Wells, T. N. C. New developments in anti-malarial target candidate and product profiles. *Malar. J.* **2017**, *16*, 26.
(48) Malmquist, N. A.; Gujjar, R.; Rathod, P. K.; Phillips, M. A. Analysis of flavin oxidation and electron-transfer inhibition in Plasmodium falciparum dihydroorotate dehydrogenase. *Biochemistry* **2008**, *47*, 2466−2475.
(49) Bennett, T. N.; Paguio, M.; Gligorijevic, B.; Seudieu, C.; Kosar, A. D.; Davidson, E.; Roepe, P. D. Novel, rapid, and inexpensive cell-based quantification of antimalarial drug efficacy. *Antimicrob. Agents Chemother.* **2004**, *48*, 1807−1810.
(50) Deng, X.; Gujjar, R.; El Mazouni, F.; Kaminsky, W.; Malmquist, N. A.; Goldsmith, E. J.; Rathod, P. K.; Phillips, M. A. Structural plasticity of malaria dihydroorotate dehydrogenase allows selective binding of diverse chemical scaffolds. *J. Biol. Chem.* **2009**, *284*, 26999−27009.
(51) Otwinowski, Z.; Minor, W. Processing of X-ray diffraction data collected in oscillation mode. *Methods Enzymol.* **1997**, *276*, 307−326.

https://dx.doi.org/10.1021/acs.jmedchem.0c00311
J. Med. Chem. 2020, 63, 4929−4956

(52) McCoy, A. J.; Grosse-Kunstleve, R. W.; Adams, P. D.; Winn, M. D.; Storoni, L. C.; Read, R. J. Phaser crystallographic software. *J. Appl. Crystallogr.* **2007**, *40*, 658−674.
(53) Emsley, P.; Lohkamp, B.; Scott, W. G.; Cowtan, K. Features and development of Coot. *Acta Crystallogr., Sect. D: Biol. Crystallogr.* **2010**, *66*, 486−501.
(54) Adams, P. D.; Afonine, P. V.; Bunkóczi, G.; Chen, V. B.; Davis, I. W.; Echols, N.; Headd, J. J.; Hung, L.-W.; Kapral, G. J.; Grosse-Kunstleve, R. W.; McCoy, A. J.; Moriarty, N. W.; Oeffner, R.; Read, R. J.; Richardson, D. C.; Richardson, J. S.; Terwilliger, T. C.; Zwart, P. H. PHENIX: a comprehensive Python-based system for macromolecular structure solution. *Acta Crystallogr., Sect. D: Biol. Crystallogr.* **2010**, *66*, 213−221.
(55) Jiménez-Díaz, M. B.; Mulet, T.; Viera, S.; Gómez, V.; Garuti, H.; Ibáñez, J.; Alvarez-Doval, A.; Shultz, L. D.; Martínez, A.; Gargallo-Viola, D.; Angulo-Barturen, I. Improved murine model of malaria using Plasmodium falciparum competent strains and non-myelodepleted NOD-scid IL2Rgammanull mice engrafted with human erythrocytes. *Antimicrob. Agents Chemother.* **2009**, *53*, 4533−4536.

https://dx.doi.org/10.1021/acs.jmedchem.0c00311
J. Med. Chem. 2020, 63, 4929−4956